Journal of Chemistry

Synthesis, Characterization, and Applications of Green Nanotechnology

Lead Guest Editor: Amr Mohamed Elsayed Nassar
Guest Editors: Ahmed Alshahrani, Ahmed Mourtada Elseman, and Wael Abdelgayed Ahmed Arafa

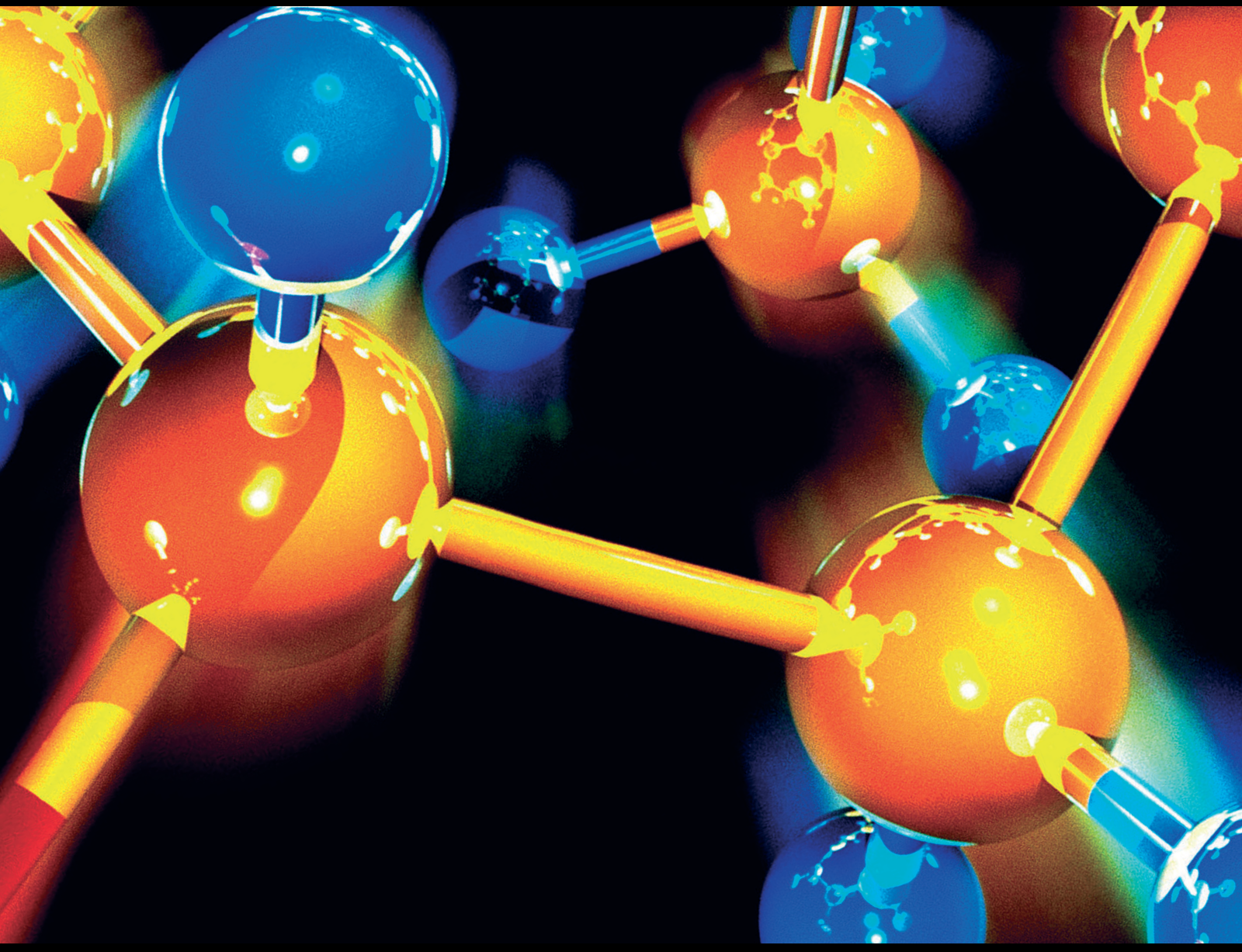

Synthesis, Characterization, and Applications of Green Nanotechnology

Journal of Chemistry

Synthesis, Characterization, and Applications of Green Nanotechnology

Lead Guest Editor: Amr Mohamed Elsayed Nassar
Guest Editors: Ahmed Alshahrani, Ahmed Mourtada Elseman, and Wael Abdelgayed Ahmed Arafa

Contents

Hindawi
Journal of Chemistry
Volume 2022, Article ID 4593086, 14 pages
https://doi.org/10.1155/2022/4593086

Research Article

Green Synthesis of Trimetallic Nanocomposite (Ru/Ag/Pd)-Np and Its In Vitro Antimicrobial and Anticancer Activities

Shaimaa Hussein,[1] **Ayman M. Mahmoud**,[2] **Hassan A. Elgebaly**,[3] **Omnia Magdy Hendawy**,[1] **Emad H. M. Hassanein**,[4] **Shaima M. N. Moustafa**,[5] **Nasser F. Alotaibi**,[6] **and Amr M. Nassar**[6]

[1]*Department of Pharmacology, College of Pharmacy, Jouf University, Sakaka 72341, Aljouf, Saudi Arabia*
[2]*Physiology Division, Zoology Department, Faculty of Science, Beni-Suef University, Beni-Suef, Egypt*
[3]*Department of Biology, College of Science, Jouf University, Sakaka, Saudi Arabia*
[4]*Department of Pharmacology and Toxicology, Faculty of Pharmacy, Al-Azhar University, Assiut, Egypt*
[5]*Biology.Department College of Science, Jouf University, P.O. Box 2014, Sakaka, Saudi Arabia*
[6]*Chemistry Department, College of Science, Jouf University, Sakaka, Saudi Arabia*

Correspondence should be addressed to Amr M. Nassar; amnassar@ju.edu.sa

Received 2 June 2022; Revised 9 July 2022; Accepted 22 August 2022; Published 15 September 2022

Academic Editor: Ashanul Haque

In this study, we used the aqueous extract of garlic tunicate leaf to reduce a mixture of equal amounts of ruthenium chloride, silver nitrate, and palladium acetate for the biosynthesis of ruthenium/silver/palladium trimetallic nanocomposite (Ru/Ag/Pd)-Np. Some physicochemical tools were used for nanocomposite characterization, including Fourier-transform infrared spectroscopy (FT-IR), X-ray diffraction (XRD), thermal gravimetric analysis (TGA), UV-Vis spectroscopy (UV-Vis), scanning electron microscope (SEM), and transmittance electron microscope (TEM). XRD revealed that the crystal size of the nanocomposite is 15.67 nm. The TEM images showed that the particle size ranged 50–90 nm. The antimicrobial efficacy of the nanocomposite was examined against *Aspergillus flavus, Aspergillus niger*, *Candida albicans*, *Candida glabrata*, *Escherichia coli*, and *Bacillus cereus*. The results showed a potent antimicrobial activity toward all tested microorganisms. (Ru/Ag/Pd)-Np showed antiproliferative activity against Caco-2, HepG2, and K562 cell lines. The antiproliferative potential of (Ru/Ag/Pd)-Np was significantly improved following UV irradiation.

1. Introduction

Nanomedicine involves the use of the knowledge and tools of nanotechnology in the diagnosis, treatment, and prevention of disease and represents one of the most metamorphose ways in the future [1]. Nanometals have displayed a great interest in several innovative research fields. The activity, chemical, biological, physical, optical, and electrical properties of metal nanoparticles such as palladium (Pd), ruthenium (Ru), silver (Ag), platinum (Pt), and gold (Au) nanoparticles (NPs) depend on their particle shape and size [2].

Pd is a metal with fewer side effects and greater potential in biological applications than many other metals [3, 4]. Pd-NPs have been used as drug carriers, prodrug activators, and antibacterial, anticancer, antifungal, and antioxidant agents [5–8]. Pd-NPs showed promising therapeutic effects against cancer cells and multidrug-resistant bacteria and strong antibacterial/antibiofilm activities [9]. In addition, Pd (0) exhibited high efficacy as a therapeutic agent for human ovarian cancer [10]. Ag-NPs exhibited great success in several biological applications due to the large surface area of their particles [11]. Ag-NPs displayed antimicrobial, cytotoxic, and antiproliferative properties effects as previously reported [12–14]. Ru is a 4 d transition metal widely used in

industrial and biological applications. Ru-NPs have a high surface area (1–3 m^2/g) and hence could be used in catalysis and photocatalysis [15].

Some inorganic composites have emerged as attractive candidates in medicine due to their enormous surface area, conductivity, and high biological activity [16]. The green synthesis of Ag@Pd core-shell composite with enhanced anticancer activities using plant extracts was studied. When compared to WISH normal cells and the standard drug doxorubicin (DOX), the composite showed a significant antiproliferative activity against MCF7 and HEPG2 [17]. A nanoplate (Pd@Ag) core@silica shell composite was loaded with DOX and showed more potent antiproliferative activity by releasing DOX in response to heat and pH through the responsive coordination bonds [18]. A trimetallic Ti-Ag-Pd alloy with $\alpha+\beta$-Ti structure has been synthesized and characterized. The $Ti_{94}Ag_3Pd_3$ alloy has great potential as a biomedical implant metallic composite [19]. Pd-Ag-decorated reduced graphene oxide (rGO) nanostructures were synthesized using a green chemical technique involving stevia extract and showed antibacterial potential under light irradiation. The biosynthesized Pd Ag-decorated rGO nanostructures had good antibacterial action, inactivating 96% of *Escherichia coli* cells after 150 minutes of visible light irradiation. The study recommended that the nanostructured composite could be used for alternative nanomaterial-based medication development [20].

The citrate approach was used to make colloidal Ag@Pd core-shell nanoparticles (NPs) in aqueous media [21]. The antibacterial activity of Ag@Pd core-shell NPs was assessed qualitatively and quantitatively against model microbial species using the disc diffusion method to calculate the lowest inhibitory concentration. The inhibitory efficacy against bacteria and fungi was increased as the core-shell NPs concentration was raised to 25 mg/ml, demonstrating broad-spectrum actions.

Over the last few decades, the concept of green nanotechnology has grown, and sustainable methods of synthesis of nanoparticles were developed. The basic objectives of these methods include the synthesis of NPs using phytochemicals as simple, safe, ecofriendly, and cost-effective alternatives to toxic chemicals frequently used as reducing or capping agents [22]. Several bioresources have been used to create NPs of different sizes and forms, including plants, bacteria, fungi, yeasts, and algae [23]. Garlic (*Allium sativum* L.) possesses a wide antibiotic action against both Gram-positive and Gram-negative bacteria as well as antioxidant, anti-inflammatory, and anticancer activities. These beneficial effects were attributed to its rich content of bioactive molecules, including polysaccharides, organosulfur compounds, saponins, and phenolics [24].

This investigation aimed to synthesize and characterize a new trimetallic (Ru/Ag/Pd)-Np composite using *A. sativum* extract and to explore its antimicrobial and antiproliferative activities. In addition, the effect of UV irradiation on the antiproliferative activity of this nanocomposite was investigated.

2. Experimental

2.1. Instruments. Thermo Scientific Quattro S was used for scanning electron microscope (SEM) photodetection. An IRTracer-100 SHIMADZU spectrophotometer was used for Fourier-transform infrared (FT-IR) measurements. X-ray diffraction (XRD) patterns were determined by XRD-7000 SHIMADZU via a copper radiation source. Thermal gravimetric analysis (TGA) was detected using TGA-51SHIMADZU with a heating rate of 10°C/min. A flow cytometer (BD FACSCalibur, USA) was used for cell cycle analysis. Japan's Shimadzu A LABOMED-Spectro 99 UV-Vis double beam-3200 was used to detect electronic spectra in the 200–800 nm range. A JEOL GEM-1010 transmission electron microscope operating at 80 kV was used to get the transmittance electron microscope (TEM) images.

2.2. Materials. The white tunicate leaf of *A. sativum* was collected from a local market in Sakaka, Saudi Arabia. The chemicals used in this study, namely, palladium acetate, ruthenium chloride, silver nitrate, 3-(4,5 dimethylthiazol-2-yl)-2,5-diphenyl tetrazolium bromide (MTT), and Annexin V-FITC apoptosis detection kit were supplied by Sigma-Aldrich (USA). All aqueous solutions were prepared using MilliQ water. Dulbecco's modified Eagle's medium (DMEM) and propidium iodide (PI) were purchased from Cambrex (New Jersey, USA) and Tianjin Dingsheng Xin (China), respectively. Human colon cancer (Caco-2), human hepatocellular carcinoma (HepG2), and human leukemia (K562) cells were supplied by VACSERA (Egypt). The antimicrobial activity of the prepared materials was tested against *Aspergillus flavus* (MT550030), *Aspergillus niger* (MW596373), *Candida albicans* (MW534712), *Candida glabrata* (MW865705), *Escherichia coli* (MW534699), and *Bacillus cereus* (MW830387). These isolates were obtained from the Biology Department, College of Science, Jouf University.

2.3. Green Synthesis of (Ru/Ag/Pd)-Np. The tunicate leaf of *A. sativum* (garlic) was collected and washed several times with tap and distilled water to remove debris and other contaminated contents and then dried at room temperature in the shade. Then, in 100 mL of distilled water, 3 g of the outer tunicate garlic leaves was boiled for 1 h to make the aqueous extract. The extract was filtered and mixed with 0.25 mmol of metal precursor (0.042 g of $AgNO_3$, 0.052 g of $RuCl_3$, and 0.056 g of Pd $(CH_3COO)_2$) in an aqueous solution. The color of the solution turned brown immediately, and the mixture was heated for 1 h at 50°C with stirring to allow the formation of a precipitate. To synthesize each nanometal, the extract was mixed separately with 0.042 g of $AgNO_3$, 0.052 g of $RuCl_3$, and 0.056 g of Pd $(CH_3COO)_2$, followed by the same steps. All precipitates were filtered through Whatman's No. 1 filter paper, then washed with hot distilled water, and dried in the air. The dried precipitates were preserved for all further characterization and biological studies.

2.4. Assessment of Cytotoxicity for (Ru/Ag/Pd)-Np before and after UV Exposure. Caco-2, HepG2, and K562 cells were cultured in DMEM supplemented with 10% fetal bovine

serum. The cells were trypsinized, seeded in 96-well plates, and treated with different concentrations of (Ru/Ag/Pd)-NP, nonirradiated or exposed to UV for 20 min, for 24 h. The MTT cell viability assay was used to determine the half-maximal inhibitory concentration (IC50) in comparison to control cell growth. The optical density was measured at a wavelength of 570 nm [25].

2.5. Apoptosis Induction and Cell Cycle Analysis Assessment. Flow cytometry was used to assess cell cycle analysis and apoptosis [26]. Caco-2 cells were seeded and incubated in a CO_2 incubator at 37°C. The cells were then treated with (Ru/Ag/Pd)-NP before and after being exposed to UV light. The cells were collected, washed, fixed with cold alcohol, and incubated at 4°C for 2 h. After washing, the cells were stained with PI for 30 min at room temperature and protected from light. DNA content was determined by BD FACSCalibur, and cell cycle phase distribution was determined using Cell Quest Pro software (BD Biosciences, USA).

2.6. Annexin V-FITC Assay. Using fluorescently labeled Annexin V, the degree of apoptosis was also determined [26]. Briefly, Caco-2 cells were treated with the IC50 of (Ru/Ag/Pd)-NP, before and after photoactivation, for 24 h. Then, the treated cells were harvested and washed in phosphate-buffered saline, and the degree of apoptosis was determined using a commercial kit.

2.7. Evaluation of Antimicrobial Activity of Metallic Np. The antimicrobial activity of the prepared NPs was tested against *A. flavus*, *A. niger*, *C. albicans*, *C. glabrata*, *E. coli*, and *B. cereus*. By using a 3 mm cork borer, 100 μl of garlic leaf water extract and metallic nanoparticles Ag-NP, Ru-NP, Pd-NP, and (Ru/Ag/Pd)-NP composite were added to wells formed in the solid media (nutrient agar for bacteria and potato dextrose agar for fungi) which have been previously inoculated by spreading a freshly prepared inoculum over the entire agar). The fungal plates were incubated for 6 days at 26°C [27], whereas yeast and bacterial plates were cultured for 48 h at 30°C [28]. The percentage of inhibition rate was calculated using the following equation [29, 30]:

$$\text{Inhibition growth percentage} = \frac{\text{MC} - \text{MT}}{\text{MC} \times 100}, \quad (1)$$

where MC is the diameter of the inhibition zone around the control, MT is the diameter of the inhibition zone around the treated material, and minimum inhibitory concentrations (MICs) were determined. All the experiments were repeated three times.

3. Results and Discussion

In this study, a trimetallic (Ru/Ag/Pd)-NP composite was synthesized using an aqueous extract of *A. sativum* leaf, demonstrating how environmentally sustainable bio-resources may function as efficient reducing agents for the ecofriendly synthesis of NPs. The entire green synthesis, characterization, and biological applications of bio-synthesized nanocomposite are shown in Scheme 1.

3.1. IR Spectra. The FT-IR spectra of solid garlic leaf and the synthesized composite in the spectral range of 500–4000 cm^{-1} are depicted in Figure 1. The spectrum of solid garlic leaf revealed several bands at 3350, 2900, 1710, 1660, and 1160 cm^{-1}, which are attributed to stretching bonds of O-H, C-H, C=O, C=C, and C-O, respectively, found in bioorganic molecules such as phenolics, amino acids, and carboxylic acid compounds [31]. Allicin is the principal organosulfur compound in garlic [32]. Therefore, additional distinct bands associated with allicin were found at 800 cm^{-1} (vC-S), 1050 cm^{-1} (vS = O), and 1215 cm^{-1} (vSS) [33]. On the other hand, the spectrum of the nanocomposite showed all of these vibrations with higher intensity due to weak van der Waals interactions between biochemical and metallic NPs [34]. New strong bands in the 550–600 cm^{-1} range were observed, which are attributed to metal-metal interaction in the nanocomposite [35]. The new bands at 1610 and 1475 cm^{-1} are often associated with the stretching and bending vibrations of the carboxylate anion (-COO), respectively, which is most likely caused by the oxidation of -C-OH in phytochemicals during the reduction of metal ions [36].

3.2. XRD. Figure 2 shows XRD patterns of the trimetallic nanocomposite. The positions of high-intensity peaks refer to the formation of pure (Ru/Ag/Pd) trimetallic NP. Peaks appeared at $2\theta = 40.11$, 47.75, and 68.31, which correspond to (111), (200), and (220), respectively, and are consistent with a conventional Pd-NP phase pattern (JCPDS: 87–0641) [37,38]. Ag-NP had typical peaks corresponding to the (111), (200), (220), and (311) planes at 2θ values of 38.45, 44.85, 67.55, and 77.5, respectively (JCPDS: 04–0783) [39]. For the hexagonal structure of Ru-NP, five different diffraction peaks were found and indexed with the planes (100), (002), (101), (102), and (110) at 38.42°, 43.82°, 46.12°, 58.32°, and 69.42° (JCPDS: 06–0663) [40]. No further impurity peaks were seen, indicating the presence of exclusively crystalline trimetallic NP. The size of the crystals was determined using the Scherrer equation [41, 42].

$$D = \frac{0.9.\lambda}{\beta.\,\text{Cos}\,\theta}, \quad (2)$$

where $\lambda = 1.5418$ Å is the wavelength of X-ray (for Cu Kα1), and θ is the XRD angle. β is the half-maximum width. The crystal size of the nanocomposite was calculated to be 15.67 nm.

3.3. TGA. TGA was used to assess the purity and thermal stability of composite NP (Figure 3). The weight of the nanocomposite decreased throughout the temperature range of 25–400°C, according to the TGA curve, showing that at higher temperatures, the organic compounds from the garlic leaf extract that served as the reducing agents in the formation of NP were completely decomposed (1.60% of the

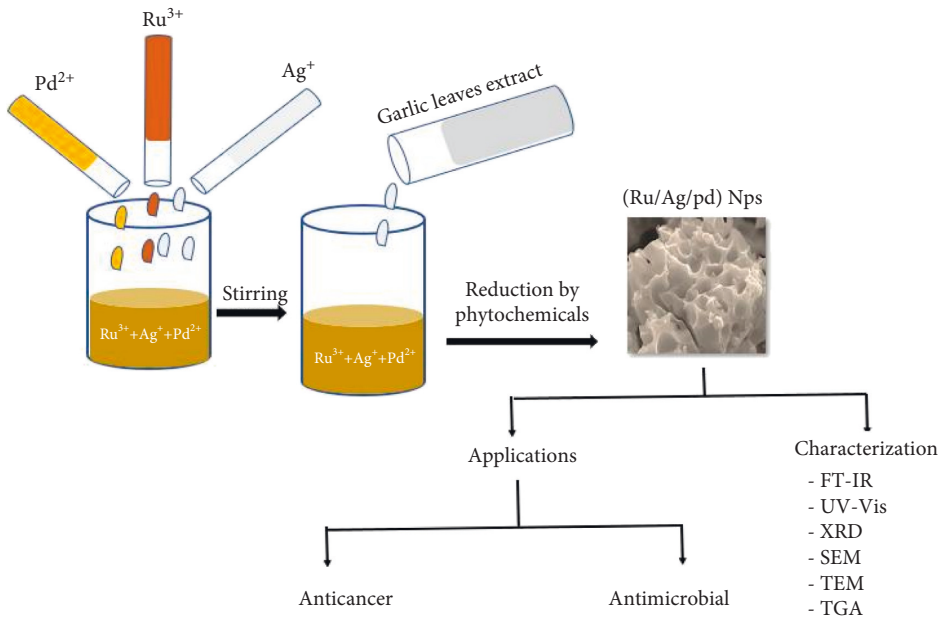

Scheme 1: Overall representation of synthesis, characterization, and bioapplications of (Ru/Ag/Pd)-Np.

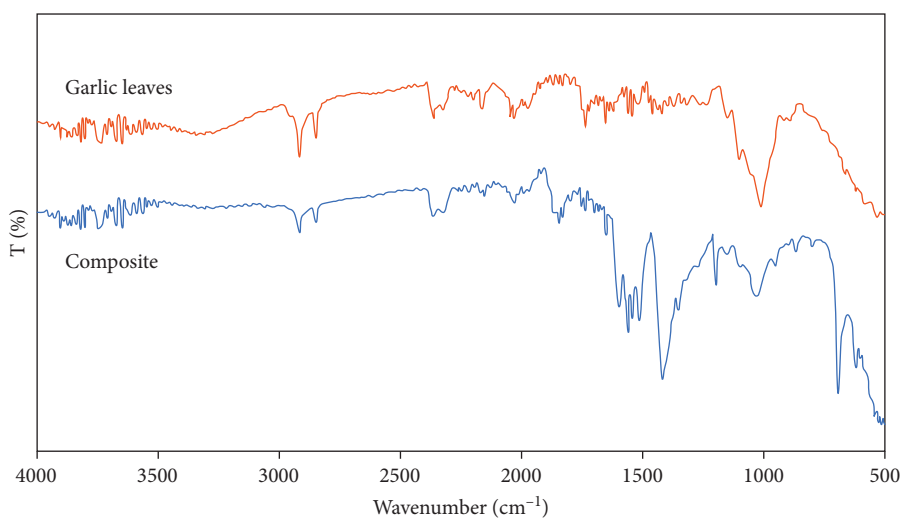

Figure 1: IR spectra of solid garlic leaf and (Ru/Ag/Pd)-Np.

original sample weight). Above 400°C, there was almost no deprivation, which accounts for the pure weight of the NP (98.40% of the original sample weight) [43].

3.4. Morphological Study. Using SEM imaging, the morphology of a nanocomposite was studied. SEM images were recorded and are shown in Figure 4. The trimetallic composite structure showed an irregular crystalline porous structure which is typical for metallic nanocomposites due to the strong interparticle contact imposed by the high surface energy. The bigger molecules of mixed nanostructures are formed when smaller nanostructures combine to form them. This may be seen in the SEM photos and is an indication of nanocomposite formation [44]. TEM images show the spherical shape of nanoparticles with a particle size of 50–90 nm (Figure 5).

3.5. Absorption Spectra. The formation of metal NP is confirmed by absorption spectroscopy. Figure 6 shows the electronic spectra for both water *A. sativum* leaf extract and nanocomposite. Phytochemicals found in *A. sativum* leaf water extract are abundant and play a crucial function in the reduction methods used to produce metal NP [45]. A band at 280 nm in the absorption spectrum of the extract could be attributed to electronic transitions in the extracted phytochemicals [46]. The absorption spectrum of the

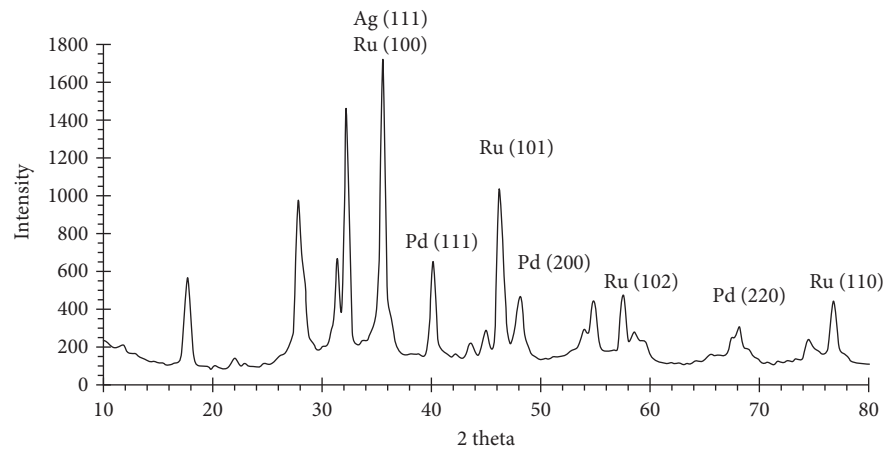

Figure 2: XRD of (Ru/Ag/Pd)-Np.

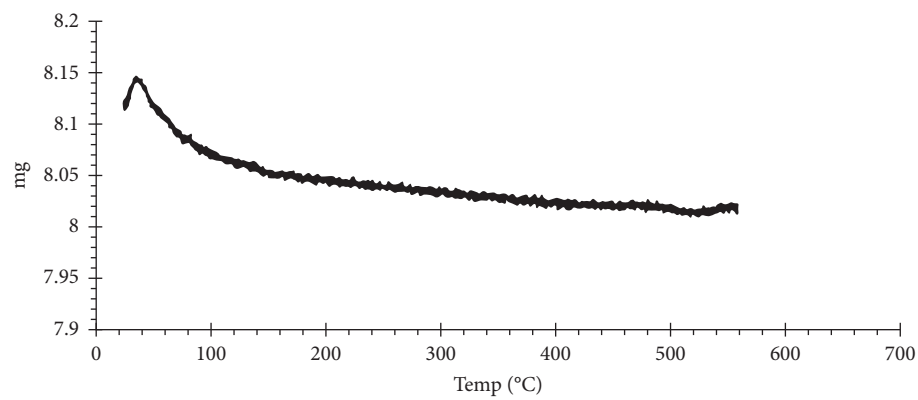

Figure 3: TGA of (Ru/Ag/Pd)-Np.

nanocomposite showed a distinct surface plasmon resonance, which is assigned by the appearance of the maximum absorption peak at 265 nm [47]. The absence of the bands assigned to Ag+, Pd2+, and Ru3+ in Figure S1 from the composite spectrum suggests that the nanocomposite formation follows precursor metal ion reduction.

3.6. In Vitro Anticancer Activity of (Ru/Ag/Pd)-Np before and after UV Exposure. The cytotoxic activity of (Ru/Ag/Pd)-NP before and after UV exposure was evaluated using Caco-2, HepG2, and K562 cells. Our data revealed that photoactivation markedly enhanced the anticancer efficacy of (Ru/Ag/Pd)-NP as represented in Table 1 and Figure 7.

Cell cycle arrest is a crucial mechanism through which anticancer drugs produce their antiproliferative effects [48, 49]. As a result, we investigated how (Ru/Ag/Pd)-NP, before and after UV exposure, affected the distribution of Caco-2 cells throughout the cell cycle. The purpose of the current study was to examine the cell cycle distribution and proliferation potential of Caco-2 cells following treatment with (Ru/Ag/Pd)-NP before and after UV exposure. To ascertain the total population distribution in the various phases (G0/G1, S, and G2/M), asynchronously growing Caco-2 cells were exposed to (Ru/Ag/Pd)-NP before and after UV exposure for 24 h. The cells were then stained with PI and subjected to flow cytometry analysis.

Herein, Caco-2 cells were treated with the IC50 of (Ru/Ag/Pd)-NP before photoactivation (47.35 μg/ml) and (Ru/Ag/Pd)-NP after photoactivation (9.32 μg/ml). (Ru/Ag/Pd)-NP before and after photoactivation induced apoptosis as indicated by an increase in the G2/M phase of 19.3% and 31.06%, respectively, in comparison with that of control Caco-2 cells (5.87%). Moreover, in the pre-G1 phase, (Ru/Ag/Pd)-NP before photoactivation resulted in apoptosis induction by 17.03%, while the photoactivated (Ru/Ag/Pd)-NP produced marked cells apoptosis by 32.41%, in comparison with that of control Caco-2 cells (2.23%) as represented in Figure 8. As a result, treatment with (Ru/Ag/Pd)-NP before and after UV exposure can encourage the transition of colon cancer cells from the G1 to the S phase and subsequently induce cycle arrest in the S phase, thereby weakening their ability to proliferate and decreasing their viability.

Apoptosis can be induced by arresting the cell cycle. The anticancer activities of NP synthesized by green synthesis have been proved in several investigations [50] showing that the cytotoxic activity was mediated by different mechanisms, including blocking cell cycle in G0/G1 [51] or G2/M [52] phases. In this study, we explored the impact of (Ru/Ag/Pd)-

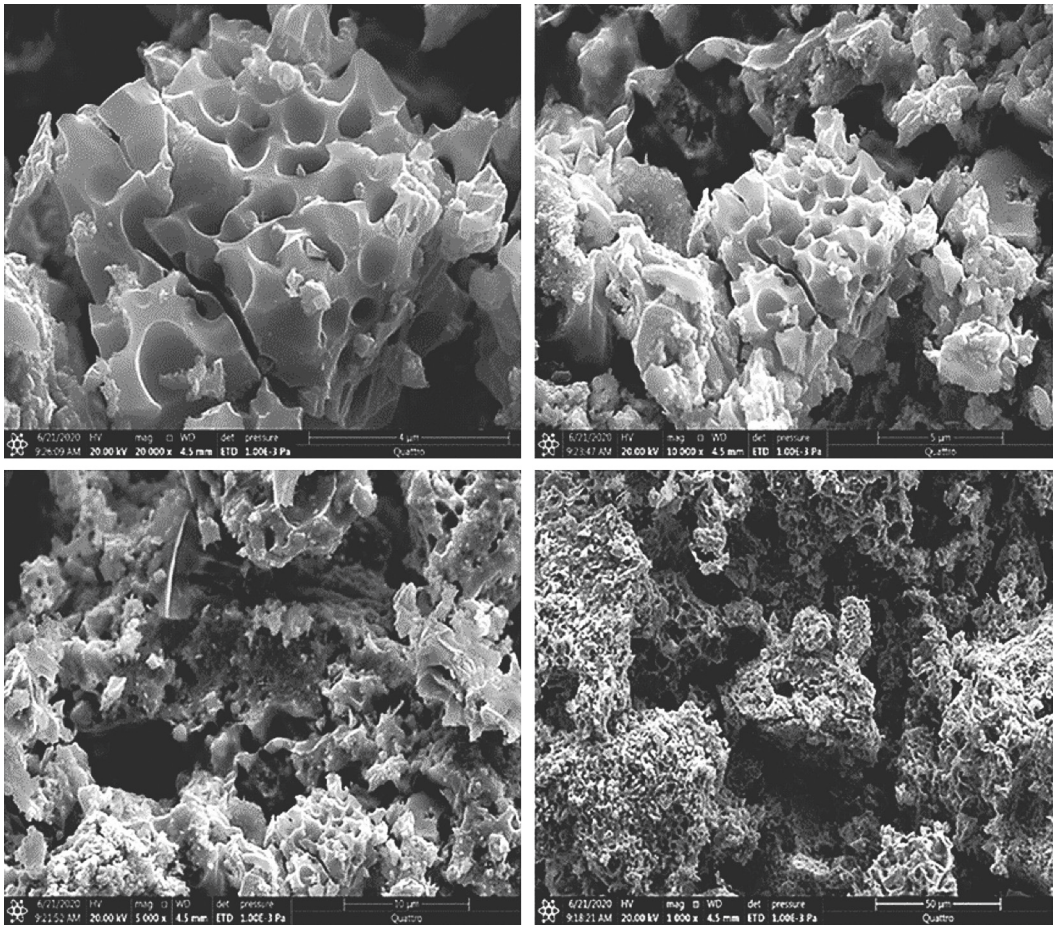

Figure 4: SEM images of (Ru/Ag/Pd)-Np.

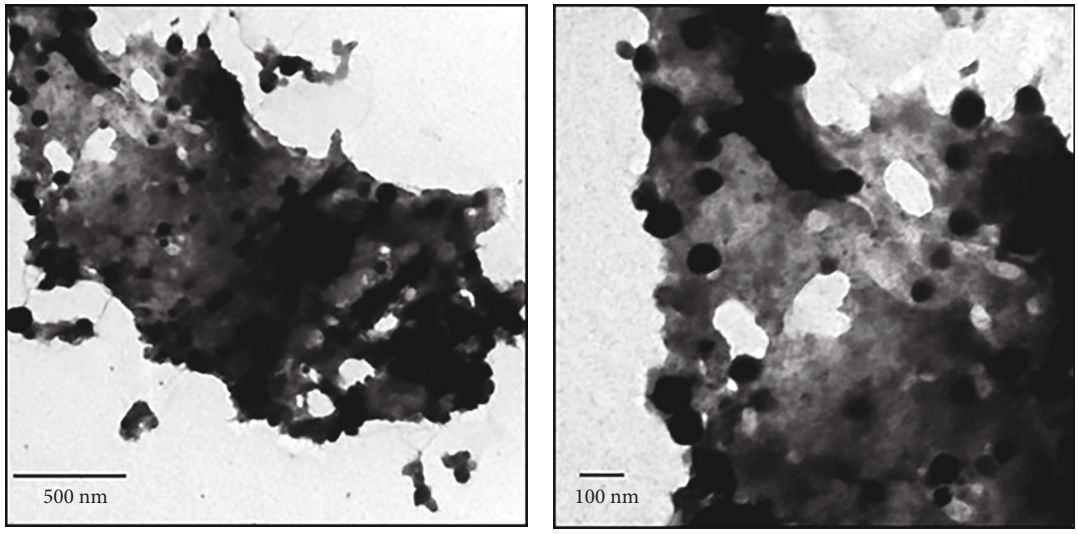

(a) (b)

Figure 5: TEM images of (Ru/Ag/Pd)-Np.

NP on the ability of Caco-2 cells to undergo apoptosis before and after exposure to UV light. The presence of phosphatidylserine (PS) residues on the surface of the cell, which are typically concealed by the plasma membrane, is used for the identification and quantification of apoptosis. One of the distinctive cues for macrophages to recognize and remove apoptotic cells is the presence of PS on the cell surface. Annexin V has demonstrated a high affinity for binding to

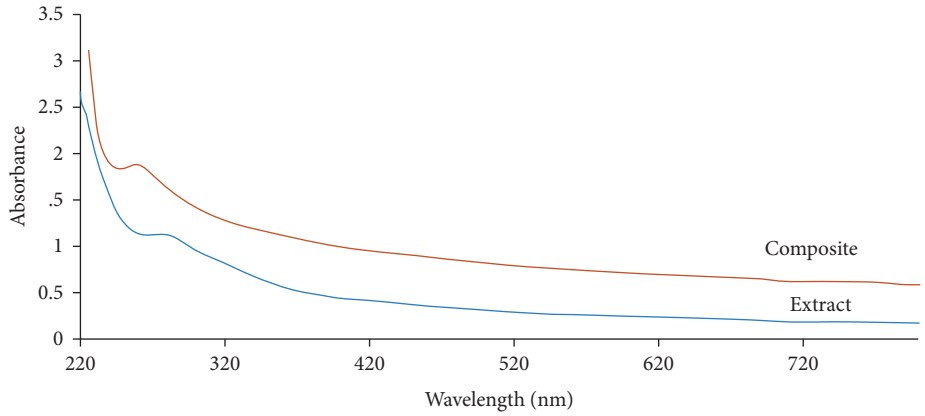

Figure 6: Electronic spectra of *A. sativum* extract and (Ru/Ag/Pd)-Np.

Table 1: IC50 values of (Ru/Ag/Pd)-Np against different cancer cell lines.

Tumor cell lines	IC50 before UV exposure (μg/ml)	IC50 after UV exposure (μg/ml)
Caco-2	47.35 ± 2.7	9.32 ± 0.52
HepG2	68.8 ± 3.9	46.77 ± 2.6
K562	35.87 ± 2.0	28.32 ± 1.6

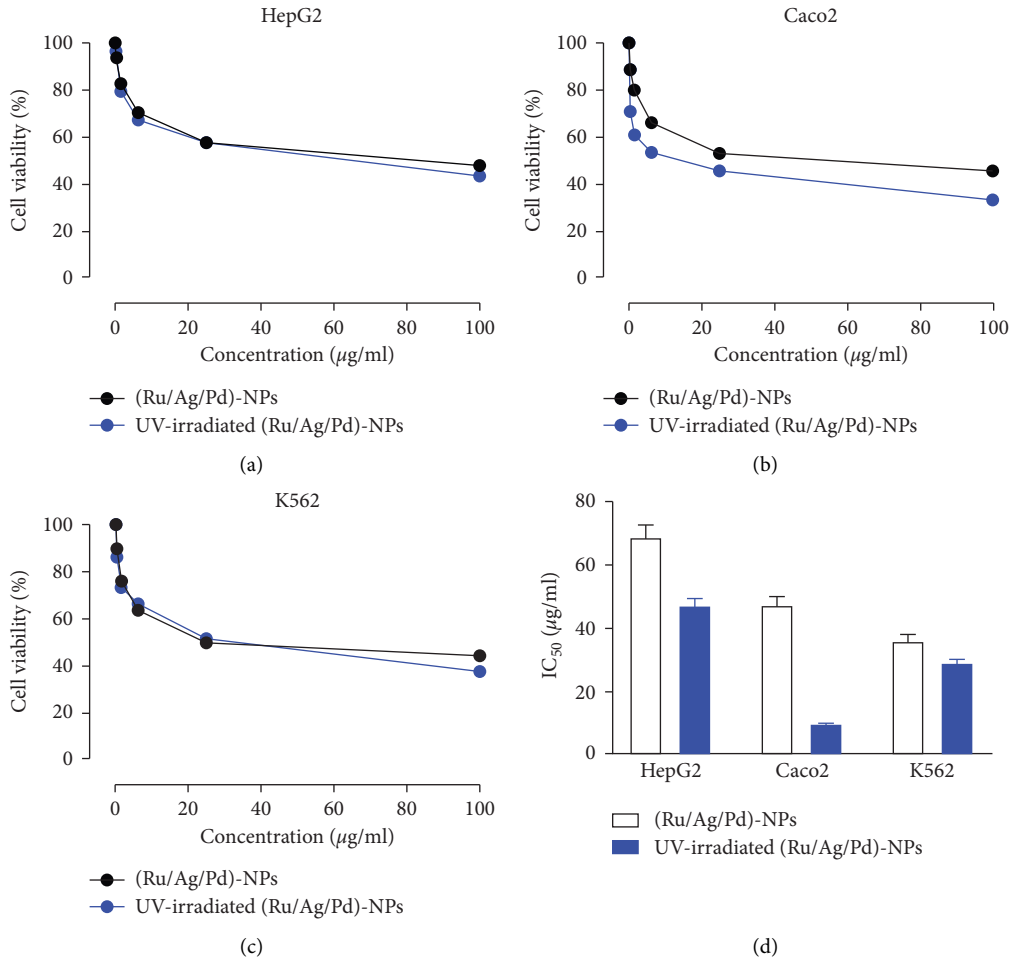

Figure 7: UV exposure increases the cytotoxic activity of (Ru/Ag/Pd)-NP against (a) HepG2, (b) Caco-2, and (c) K562 cancer cell lines. (d) IC50 values of the antiproliferative activity of (Ru/Ag/Pd)-NP on HepG2, Caco-2, and K562 cell lines. Data are mean ± SD. The experiment was repeated three times ($N = 3$).

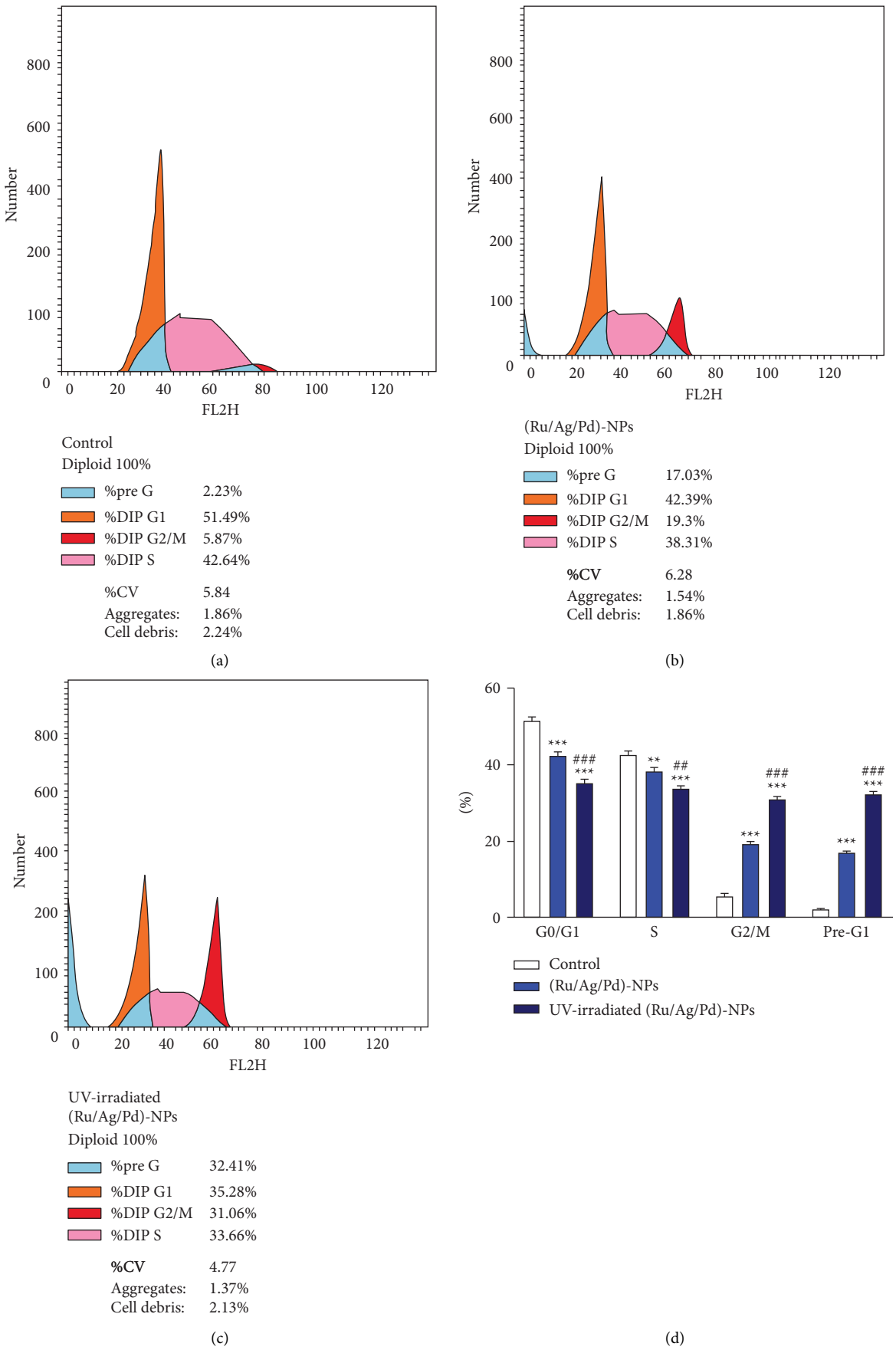

Figure 8: Representative histograms of DNA content distribution of cell cycle phases of control (a) and Caco-2 cancer cell line treated with (Ru/Ag/Pd)-NP before (b) and after UV exposure (c). (d) Percentage of the Caco-2 cells at different phases of the cell cycle. Data are mean ± SD, $N = 3$. $^{**}P < 0.01$ and $^{***}P < 0.001$ versus control. $^{\#\#}P < 0.01$ and $^{\#\#\#}P < 0.001$ versus (Ru/Ag/Pd)-NP before UV exposure.

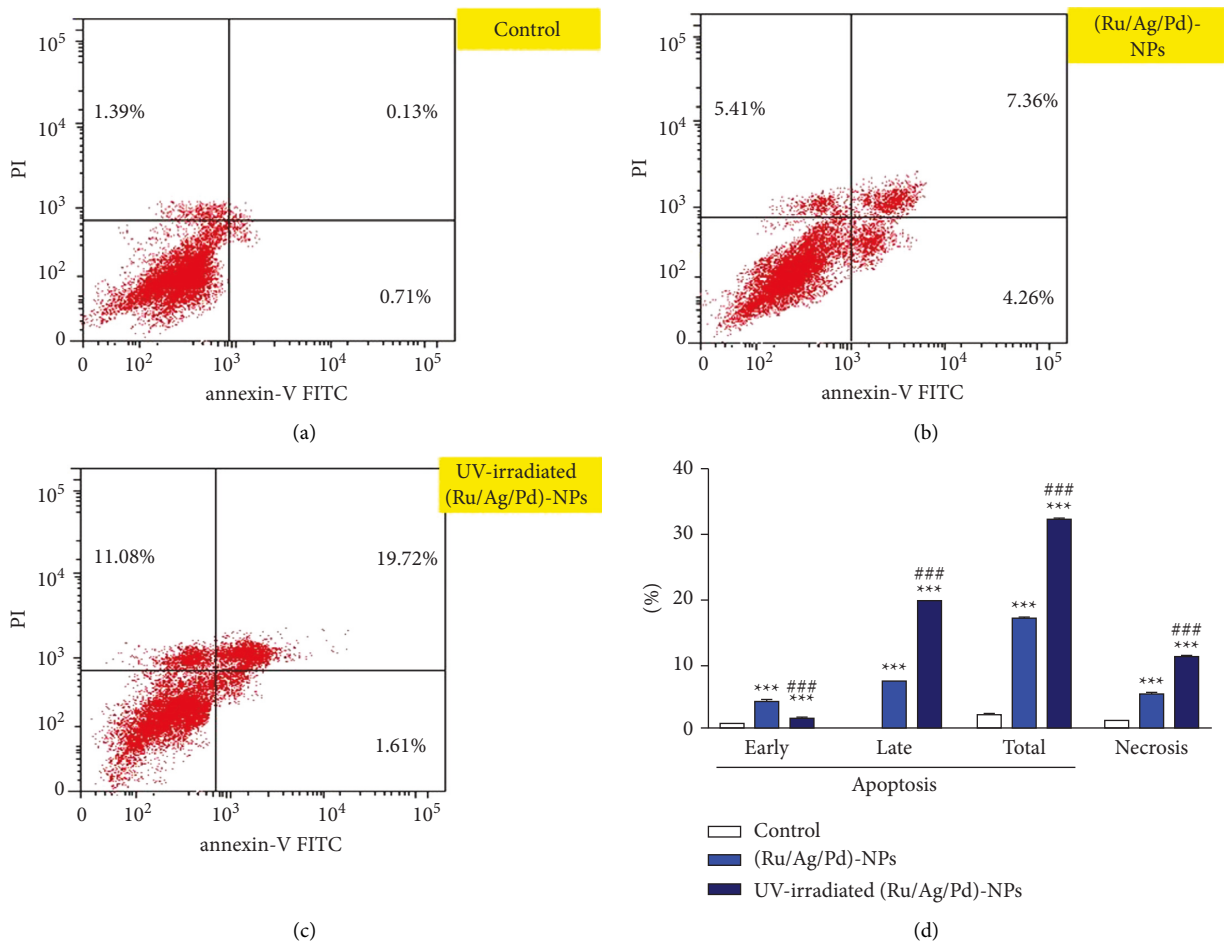

Figure 9: Representative blots of Annexin V/PI-stained control (a) and Caco-2 cancer cell line treated with (Ru/Ag/Pd)-NP before (b) and after UV exposure (c). (d) Percentage of Caco-2 cells exhibiting early and late apoptosis and necrosis following treatment with (Ru/Ag/Pd)-NP exposed to UV. Data are mean ± SD, $N = 3$. $^{***}P < 0.001$ versus control and $^{###}P < 0.001$ versus (Ru/Ag/Pd)-Np before UV exposure.

PS and hence could be used to check the integrity of the cell membrane, which is compromised as the apoptotic process develops. It is feasible to discriminate between early and late apoptotic cells as well as dead cells using DNA-specific viability dyes such as PI [53].

Cell cycle analysis of the Caco-2 after treatment with (Ru/Ag/Pd)-NP either before or after photoactivation showed a preG1 peak that proved apoptosis (Figure 9). To confirm the effect of both (Ru/Ag/Pd)-NP on apoptosis induction and the impact of photoactivation, Caco-2 cells were stained with Annexin V/PI, incubated for 24 h, and analyzed. The results proved that both (Ru/Ag/Pd)-NP and its photoactivation potently induced apoptosis in Caco-2 cells by 17.03% and 32.41%, respectively, in comparison with that of Caco-2 control cells (2.23%). These results indicated that photoactivation of the (Ru/Ag/Pd)-NP resulted in a 1.9-fold increase in its ability to induce apoptosis.

3.7. Antimicrobial Activity of (Ru/Ag/Pd)-NP. Six isolates of microbial strains, *A. flavus*, *A. niger*, *C. albicans*, *C. glabrata*, *E. coli*, and *B. cereus* were selected to evaluate the antimicrobial activity of the trimetallic NPs composite. MICs were determined using four different dosages of nanomaterials (0.0125, 0.025, 0.05, and 0.1 mg/mL) (Figure 10). Table 2 shows the MIC experimental results. The nanocomposite's MIC value against the investigated microbes was 0.0125 mg/mL.

For comparison, antimicrobial experiments were carried out for every single metal as represented in Table 3 and Figure 11. The findings indicated that all tested materials demonstrated high antibacterial activity and followed the sequence (Ru/Ag/Pd)-NP > Pd-NP = Ag-NP = Ru-NP > *A. sativum* extract in comparison to different isolate species of bacteria and fungus. Microbial growth inhibition was best with the composite (Ru/Ag/Pd)-NP.

To compare our findings with those of other studies, Table 4 displays the biological applications, synthesis techniques, and other characteristics of mono-, bi-, and trimetallic nanoparticles.

3.8. Mechanism of Bioactivity of NP. In this study, the high biological activity of (Ru/Ag/Pd)-NP could be attributed to its capacity to disrupt membranes, damage DNA, produce reactive oxygen species (ROS) such as peroxides and

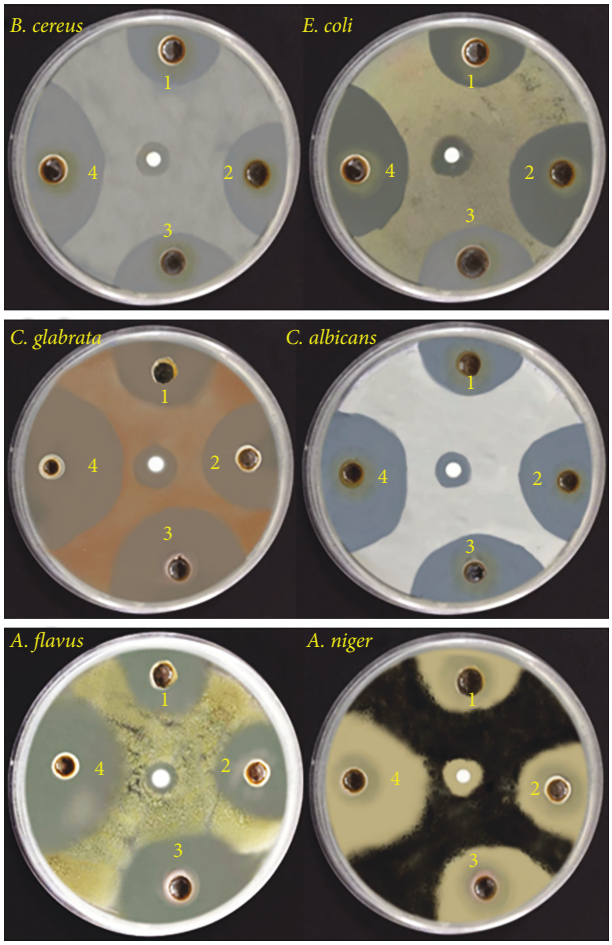

Figure 10: MICs results of (Ru/Ag/Pd)-NP (1) 0.0125 mg/mL, (2) 0.025 mg/mL, (3) 0.05 mg/mL, and (4) 0.1 mg/mL.

Table 2: MIC values in (mg/mL) of composite (Ru/Ag/Pd)-Np against different microbes.

Conc. of composite	Inhibition %					
	A. flavus	*A. niger*	*C. albicans*	*C. glabrata*	*E. coli*	*B. cereus*
(0.0125 mg/mL)	37.1	39.4	34.2	38.5	32.9	31.6
(0.025 mg/mL)	55.3	59.4	50	52.8	59.2	54.8
(0.05 mg/mL)	60.7	62.8	65.7	69.3	60.2	60.4
(0.1 mg/mL)	94.8	91.6	89.3	91.6	88.8	87.1

Table 3: Effect of different treatments of NPs at 0.0125 mg/mL concentration on growth %.

	% inhibition mycelia growth					
	A. flavus	*A. niger*	*C. albicans*	*C. glabrata*	*E. coli*	*B. cereus*
Control positive (miconazole)	32.7				—	—
Control positive (amikacin 30)	—	—	—	—	30.6	
Garlic extract	19.7	15.5	20	14	20	19
Ag-NP	26.2	31.4	25	30	32.9	29.8
Pd-NP	24.9	29.7	32.4	29.5	25	27.4
Ru-NP	28.7	26.4	21.5	26.3	28.5	29.3
(Ru/Ag/Pd)-NP	37.1	39.4	34.2	38.5	32.9	31.6

superoxide, denaturant proteins, and inactivate enzymes. They can either stop bacterial growth or eliminate it. Similar to this, NP can saturate and adhere to fungal hyphae and create insoluble compounds that damage the membrane, bind lipids and enzymes, and induce cell lysis by inactivating the sulfhydryl groups of the fungal cell wall [58, 59].

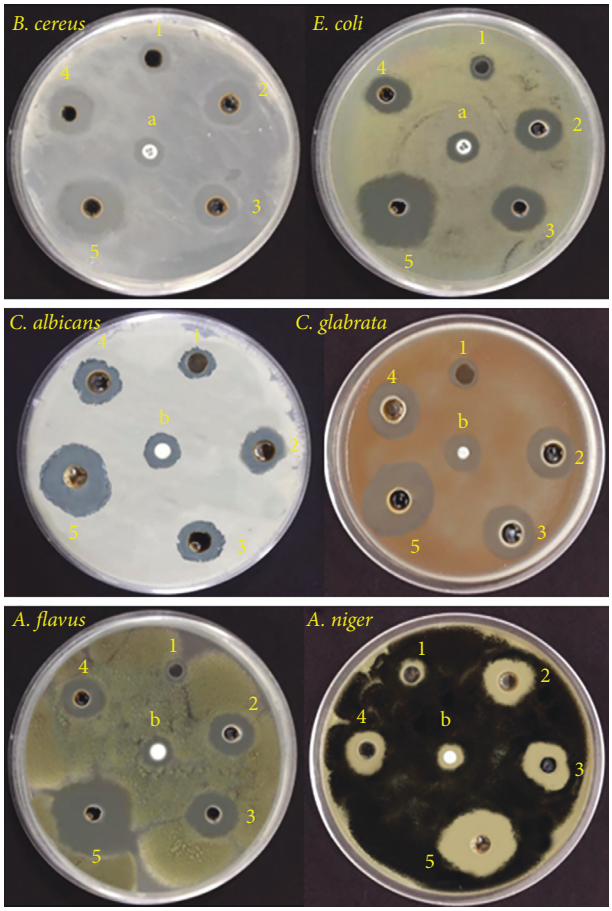

Figure 11: Effect of scale leaf of garlic (1), Ag-NP (2), Ru-NP (3), Pd-NPsp (4), and (Ru/Ag/Pd)-NP (5) on the growth of tested microbes, amikacin 30 (a) and miconazole (b).

Table 4: Comparison between biological activity using similar NPs.

NPs	Synthesis method	Particles size (nm)	Bio application	Average diameter inhibition zones (mm) against microorganisms tested	Reference
Ag	Green method via garlic leaf extract	20–70	Antimicrobial	11–24	[54]
Pd	Green method via brown alga, *Padina boryana*	11.16	Antimicrobial and anticancer	18–23	[9]
Ru	Green method via *Gloriosa superba* extract	25–90	Antibacterial	2.67–6.67	[55]
Ag/Pd	Chemical method via citrate reduction	9.8	Antimicrobial	1.4–1.9	[21]
Ag/Ru@GO	Chemical method via sodium borohydride	10–15	Antibacterial	0.5–9	[56]
Au/Pt/Ag	Microwave	20–40	Antimicrobial	14–17	[57]
(Ru/Ag/Pd)-NP	Green method via garlic leaf extract	15.67	Antimicrobial Anticancer	31.6–39.4 High anticancer activity	The current study

4. Conclusion

(Ru/Ag/Pd)-NP was synthesized using a green method. The nanocomposite was characterized with different physico-chemical techniques and its antiproliferative activity, before and after UV exposure, was studied against HepG2, Caco-2, and K562 cancer cell lines. UV irradiation greatly improved the antiproliferative efficacy of the nanocomposite against all cancer cell types. In Caco-2 cells, (Ru/Ag/Pd)-NP caused cell cycle arrest, apoptosis, and necrosis, all of which were

enhanced by UV exposure. The antimicrobial activity of each single metal NP and the composite was determined against different bacterial and fungal strains. The highest activity appeared for the (Ru/Ag/Pd)-NP with a MIC value of 0.0125 mg/mL.

Data Availability

The data supporting the findings of this study are included within the article and its supplementary materials.

Disclosure

Some of the data included in the article were previously deposited as a preprint (https://www.researchsquare.com/article/rs-1819275/v1 2.).

Conflicts of Interest

The authors declare that they have no conflicts of interest.

Acknowledgments

The authors would like to thank the Deanship of Scientific Research at Jouf University for funding this research (grant number DSR 2020-04-438).

Supplementary Materials

Additional data in this work are stated in the supplementary file. In the supplementary file, Figure S1 depicts the absorption spectra of metal precursors used in this work. (*Supplementary Materials*)

References

[1] M. M. Rahman, F. Islam, S. Afsana Mim et al., "Multifunctional therapeutic approach of nanomedicines against inflammation in cancer and aging," *Journal of Nanomaterials*, vol. 2022, Article ID 4217529, 19 pages, 2022.

[2] A. M. Abu-Dief, L. H. Abdel-Rahman, M. A. Abd-El Sayed, M. M. Zikry, and A. Nafady, "Green synthesis of AgNPs ultilizing Delonix Regia extract as anticancer and antimicrobial agents," *ChemistrySelect*, vol. 5, no. 42, pp. 13263–13268, 2020.

[3] A. M. Nassar, "Bioactive palladium azomethine chelates, a review of recent research," *Synthesis and Reactivity in Inorganic, Metal-Organic, and Nano-Metal Chemistry*, vol. 46, no. 9, pp. 1349–1366, 2016.

[4] A. M. Nassar, A. M. Hassan, and S. S. Alabd, "Antitumor and antimicrobial activities of novel palladacycles with abnormal aliphatic CH activation of Schiff Base 2-[(3-phenylallylidene) amino] phenol," *Synthesis and Reactivity in Inorganic, Metal-Organic, and Nano-Metal Chemistry*, vol. 45, no. 2, pp. 256–270, 2015.

[5] S. Azizi, M. Mahdavi Shahri, H. S. Rahman, R. Abdul Rahim, A. Rasedee, and R. Mohamad, "Green synthesis palladium nanoparticles mediated by white tea (Camellia sinensis) extract with antioxidant, antibacterial, and antiproliferative activities toward the human leukemia (MOLT-4) cell line," *International Journal of Nanomedicine*, vol. 12, pp. 8841–8853, 2017.

[6] S. A. Fahmy, E. Preis, U. Bakowsky, and H. M. E.-S. Azzazy, "Palladium nanoparticles fabricated by green chemistry: promising chemotherapeutic, antioxidant and antimicrobial agents," *Materials*, vol. 13, no. 17, p. 3661, 2020.

[7] Y. Liu, D.-D. Wang, L. Zhao et al., "Polypyrrole-coated flower-like Pd nanoparticles (Pd NPs@ PPy) with enhanced stability and heat conversion efficiency for cancer photothermal therapy," *RSC Advances*, vol. 6, no. 19, pp. 15854–15860, 2016.

[8] I. Saldan, Y. Semenyuk, I. Marchuk, and O. Reshetnyak, "Chemical synthesis and application of palladium nanoparticles," *Journal of Materials Science*, vol. 50, no. 6, pp. 2337–2354, 2015.

[9] H. Sonbol, F. Ameen, S. Alyahya, A. Almansob, and S. Alwakeel, "Padina boryana mediated green synthesis of crystalline palladium nanoparticles as potential nanodrug against multidrug resistant bacteria and cancer cells," *Scientific Reports*, vol. 11, no. 1, pp. 5444–5519, 2021.

[10] S. Gurunathan, E. Kim, J. W. Han, J. H. Park, and J.-H. Kim, "Green chemistry approach for synthesis of effective anticancer palladium nanoparticles," *Molecules*, vol. 20, no. 12, pp. 22476–22498, 2015.

[11] N. S. Al-Radadi and A. M. Abu-Dief, "Silver nanoparticles (AgNPs) as a metal nano-therapy: possible mechanisms of antiviral action against COVID-19," *Inorganic and Nano-Metal Chemistry*, pp. 1–19, 2022.

[12] C. Greulich, J. Diendorf, T. Simon, G. Eggeler, M. Epple, and M. Köller, "Uptake and intracellular distribution of silver nanoparticles in human mesenchymal stem cells," *Acta Biomaterialia*, vol. 7, no. 1, pp. 347–354, 2011.

[13] C. Krishnaraj, E. Jagan, S. Rajasekar, P. Selvakumar, P. Kalaichelvan, and N. Mohan, "Synthesis of silver nanoparticles using Acalypha indica leaf extracts and its antibacterial activity against water borne pathogens," *Colloids and Surfaces B: Biointerfaces*, vol. 76, no. 1, pp. 50–56, 2010.

[14] K. Venugopal, H. A. Rather, K. Rajagopal et al., "Synthesis of silver nanoparticles (Ag NPs) for anticancer activities (MCF 7 breast and A549 lung cell lines) of the crude extract of Syzygium aromaticum," *Journal of Photochemistry and Photobiology B: Biology*, vol. 167, pp. 282–289, 2017.

[15] M. Y. S. Ali, V. Anuradha, R. Abishek, N. Yogananth, and H. Sheeba, "In vitro anticancer activity of green synthesis ruthenium nanoparticle from Dictyota dichotoma marine algae," *NanoWorld Journal*, vol. 03, no. 04, pp. 66–71, 2017.

[16] M. Venu, S. Venkateswarlu, Y. V. M. Reddy et al., "Highly sensitive electrochemical sensor for anticancer drug by a zirconia nanoparticle-decorated reduced graphene oxide nanocomposite," *ACS Omega*, vol. 3, no. 11, pp. 14597–14605, 2018.

[17] W. I. Abdel-Fattah, M. Eid, S. I. Abd El-Moez, E. Mohamed, and G. W. Ali, "Synthesis of biogenic Ag@ Pd Core-shell nanoparticles having anti-cancer/anti-microbial functions," *Life Sciences*, vol. 183, pp. 28–36, 2017.

[18] W. Fang, J. Yang, J. Gong, and N. Zheng, "Photo-and pH-triggered release of anticancer drugs from mesoporous silica-coated Pd@ Ag nanoparticles," *Advanced Functional Materials*, vol. 22, no. 4, pp. 842–848, 2012.

[19] V. Y. Zadorozhnyy, X. Shi, M. V. Gorshenkov et al., "Ti–Ag–Pd alloy with good mechanical properties and high potential for biological applications," *Scientific Reports*, vol. 6, no. 1, pp. 25142–25149, 2016.

[20] K. Mallikarjuna, O. Nasif, S. Ali Alharbi et al., "Phytogenic synthesis of Pd-Ag/rGO nanostructures using stevia leaf

extract for photocatalytic H2 production and antibacterial studies," *Biomolecules*, vol. 11, no. 2, p. 190, 2021.

[21] E. A. Bakr, H. G. El-Attar, and M. A. Salem, "Colloidal Ag@ Pd core–shell nanoparticles showing fast catalytic eradication of dyes from water and excellent antimicrobial behavior," *Research on Chemical Intermediates*, vol. 45, no. 3, pp. 1509–1526, 2019.

[22] L. H. Abdel-Rahman, B. S. Al-Farhan, D. Abou El-ezz, M. A. Abd–El Sayed, M. M. Zikry, and A. M. Abu-Dief, "Green biogenic synthesis of silver nanoparticles using aqueous extract of moringa oleifera: access to a powerful antimicrobial, anticancer, pesticidal and catalytic agents," *Journal of Inorganic and Organometallic Polymers and Materials*, vol. 32, no. 4, pp. 1422–1435, 2022.

[23] Z. Guan, S. Ying, P. C. Ofoegbu et al., "Green Synthesis of Nanoparticles: Current Developments and Limitations," *Environmental Technology & Innovation*, vol. 26, Article ID 102336, 2022.

[24] A. Shang, S.-Y. Cao, X.-Y. Xu et al., "Bioactive compounds and biological functions of garlic (Allium sativum L.)," *Foods*, vol. 8, no. 7, p. 246, 2019.

[25] J. V. Meerloo, G. J. Kaspers, and J. Cloos, "Cell sensitivity assays: the MTT assay," in *Cancer Cell Culture*Springer, Berlin Germany, 2011.

[26] Z. Darzynkiewicz, X. Huang, and H. Zhao, "Analysis of cellular DNA content by flow cytometry," *Current Protocols in Immunology*, vol. 119, no. 1, 2004.

[27] S. M. N. Moustafa, R. H. Taha, H. M. A. Abdelzaher, and H. A. Elgebaly, "Novel biosynthesis of Ag-nanocomplex for controlling Verticillium wilt disease of olive tree," *Archives of Phytopathology and Plant Protection*, vol. 55, no. 2, pp. 198–216, 2022.

[28] C. Ramteke, T. Chakrabarti, B. K. Sarangi, and R.-A. Pandey, "Synthesis of silver nanoparticles from the aqueous extract of leaves of Ocimum sanctum for enhanced antibacterial activity," *Journal of Chemistry*, vol. 2013, Article ID 278925, 7 pages, 2013.

[29] S. M. Moustafa and R. H. Taha, "Mycogenic nano-complex for plant growth promotion and bio-control of Pythium aphanidermatum," *Plants*, vol. 10, no. 9, p. 1858, 2021.

[30] A. M. Elseman, A. E. Shalan, M. M. Rashad, A. M. Hassan, N. M. Ibrahim, and A. M. Nassar, "Easily attainable new approach to mass yield ferrocenyl Schiff base and different metal complexes of ferrocenyl Schiff base through convenient ultrasonication-solvothermal method," *Journal of Physical Organic Chemistry*, vol. 30, no. 6, Article ID e3639, 2017.

[31] T. Gabriel, A. Vestine, K. D. Kim, S. J. Kwon, I. Sivanesan, and S. C. Chun, "Antibacterial activity of nanoparticles of garlic (allium sativum) extract against different bacteria such as Streptococcus mutans and poryphormonas gingivalis," *Applied Sciences*, vol. 12, no. 7, p. 3491, 2022.

[32] A. Magryś, A. Olender, and D. Tchórzewska, "Antibacterial properties of Allium sativum L. against the most emerging multidrug-resistant bacteria and its synergy with antibiotics," *Archives of Microbiology*, vol. 203, no. 5, pp. 2257–2268, 2021.

[33] L. S. Barreto, M. S. Tokumoto, I. C. Guedes, H. G. D. Melo, F. D. R. Amado, and V. R. Capelossi, "Evaluation of the anticorrosion performance of peel garlic extract as corrosion inhibitor for ASTM 1020 carbon steel in acidic solution," *Matèria. Revista Internacional d'Art*, vol. 22, no. 3, 2017.

[34] J. Z. Mbese and P. A. Ajibade, "Preparation and characterization of ZnS, CdS and HgS/poly (methyl methacrylate) nanocomposites," *Polymers*, vol. 6, no. 9, pp. 2332–2344, 2014.

[35] C. E. A. Botteon, L. B. Silva, G. V. Ccana-Ccapatinta et al., "Biosynthesis and characterization of gold nanoparticles using Brazilian red propolis and evaluation of its antimicrobial and anticancer activities," *Scientific Reports*, vol. 11, no. 1, pp. 1974–2016, 2021.

[36] A. M. Nassar, A. M. Elseman, I. H. Alsohaimi, N. F. Alotaibi, and A. Khan, "Diaqua oxalato strontium (II) complex as a precursor for facile fabrication of Ag-NPs@ SrCO3, characterization, optical properties, morphological studies and adsorption efficiency," *Journal of Coordination Chemistry*, vol. 72, no. 5-7, pp. 771–785, 2019.

[37] A. A. Abdelwahab, A. Elseman, N. Alotaibi, and A. Nassar, "Simultaneous voltammetric determination of ascorbic acid, dopamine, acetaminophen and tryptophan based on hybrid trimetallic nanoparticles-capped electropretreated graphene," *Microchemical Journal*, vol. 156, 2020.

[38] A. M. Nassar and N. F. Alotaibi, "Eggshell recycling for fabrication of Pd@ CaO, characterization and high-performance solar photocatalytic activity," *Environmental Science and Pollution Research*, vol. 28, no. 3, pp. 3515–3523, 2021.

[39] S. Berhanu, F. Habtamu, Y. Tadesse, F. Gonfa, and T. Tadesse, "Fluorescence sensor based on polyaniline supported Ag-ZnO nanocomposite for malathion detection," *Journal of Sensors*, vol. 2022, Article ID 9881935, 11 pages, 2022.

[40] Z. Zhang, H. Liu, L. Ni, Z.-L. Zhao, and H. Li, "Scalable synthesis of hcp ruthenium-molybdenum nanoalloy as a robust bifunctional electrocatalyst for hydrogen evolution/oxidation," *Journal of Energy Chemistry*, vol. 72, pp. 176–185, 2022.

[41] E. Ibrahim, L. H. Abdel-Rahman, A. M. Abu-Dief, A. Elshafaie, S. K. Hamdan, and A. Ahmed, "Electric, thermoelectric and magnetic characterization of γ-Fe_2O_3 and Co_3O_4 nanoparticles synthesized by facile thermal decomposition of metal-Schiff base complexes," *Materials Research Bulletin*, vol. 99, pp. 103–108, 2018.

[42] A. Saadat, A. Banaei, P. Mcardle, and R. Jafari, "Spectral, structural, and antibacterial study of copper (II) complex with N_2O_2 donor schiff base ligand and its usage in preparation of CuO nanoparticles," *Journal of Chemistry*, vol. 2022, Article ID 8913874, 13 pages, 2022.

[43] S. Lohrasbi, M. a. J. Kouhbanani, N. Beheshtkhoo, Y. Ghasemi, A. M. Amani, and S. Taghizadeh, "Green synthesis of iron nanoparticles using plantago major leaf extract and their application as a catalyst for the decolorization of azo dye," *BioNanoScience*, vol. 9, no. 2, pp. 317–322, 2019.

[44] Z. Chen, D. Rao, J. Zhang et al., "Highly active and CO-tolerant trimetallic NiPtPd hollow nanocrystals as electrocatalysts for methanol electro-oxidation reaction," *ACS Applied Energy Materials*, vol. 2, no. 7, pp. 4763–4773, 2019.

[45] A. A. El-Refai, G. A. Ghoniem, A. Y. El-Khateeb, and M. M. Hassaan, "Eco-friendly synthesis of metal nanoparticles using ginger and garlic extracts as biocompatible novel antioxidant and antimicrobial agents," *Journal of Nanostructure in Chemistry*, vol. 8, no. 1, pp. 71–81, 2018.

[46] M. Nasrollahzadeh, S. M. Sajadi, and M. Maham, "Green synthesis of palladium nanoparticles using Hippophae rhamnoides Linn leaf extract and their catalytic activity for the Suzuki–Miyaura coupling in water," *Journal of Molecular Catalysis A: Chemical*, vol. 396, pp. 297–303, 2015.

[47] Z. Vaseghi, O. Tavakoli, and A. Nematollahzadeh, "Rapid biosynthesis of novel Cu/Cr/Ni trimetallic oxide nanoparticles with antimicrobial activity," *Journal of Environmental Chemical Engineering*, vol. 6, no. 2, pp. 1898–1911, 2018.

[48] A. Eastman, "Cell cycle checkpoints and their impact on anticancer therapeutic strategies," *Journal of Cellular Biochemistry*, vol. 91, no. 2, pp. 223–231, 2004.
[49] G. I. Shapiro and J. W. Harper, "Anticancer drug targets: cell cycle and checkpoint control," *Journal of Clinical Investigation*, vol. 104, no. 12, pp. 1645–1653, 1999.
[50] A. Gour and N. K. Jain, "Advances in green synthesis of nanoparticles," *Artificial Cells, Nanomedicine, and Biotechnology*, vol. 47, no. 1, pp. 844–851, 2019.
[51] M. Murali, S. Anandan, M. A. Ansari et al., "Genotoxic and cytotoxic properties of zinc oxide nanoparticles phyto-fabricated from the obscure morning glory plant Ipomoea obscura (L.) ker gawl," *Molecules*, vol. 26, no. 4, p. 891, 2021.
[52] A. A. Alshatwi, J. Athinarayanan, and P. Vaiyapuri Subbarayan, "Green synthesis of platinum nanoparticles that induce cell death and G2/M-phase cell cycle arrest in human cervical cancer cells," *Journal of Materials Science: Materials in Medicine*, vol. 26, no. 1, pp. 7–9, 2015.
[53] M. Van Engeland, L. J. Nieland, F. C. Ramaekers, B. Schutte, and C. P. Reutelingsperger, "Annexin V-affinity assay: a review on an apoptosis detection system based on phosphatidylserine exposure," *Cytometry*, vol. 31, no. 1, pp. 1–9, 1998.
[54] M. Reda, A. Ashames, Z. Edis, S. Bloukh, R. Bhandare, and H. Abu Sara, "Green synthesis of potent antimicrobial silver nanoparticles using different plant extracts and their mixtures," *Processes*, vol. 7, no. 8, p. 510, 2019.
[55] K. Gopinath, V. Karthika, S. Gowri, V. Senthilkumar, S. Kumaresan, and A. Arumugam, "Antibacterial activity of ruthenium nanoparticles synthesized using Gloriosa superba L. leaf extract," *Journal of Nanostructure in Chemistry*, vol. 4, no. 1, pp. 83–86, 2014.
[56] P. Andal and Roopakala, "Graphene oxide supported ruthenium, silver and ruthenium-silver nanoparticles as catalyst with antibacterial activity," *Asian Journal of Chemistry*, vol. 30, no. 1, pp. 89–96, 2018.
[57] N. Yadav, A. K. Jaiswal, K. K. Dey et al., "Trimetallic Au/Pt/Ag based nanofluid for enhanced antibacterial response," *Materials Chemistry and Physics*, vol. 218, pp. 10–17, 2018.
[58] R. Algotiml, A. Gab-Alla, R. Seoudi, H. H. Abulreesh, M. Z. El-Readi, and K. Elbanna, "Anticancer and antimicrobial activity of biosynthesized Red Sea marine algal silver nanoparticles," *Scientific Reports*, vol. 12, no. 1, pp. 2421–2518, 2022.
[59] G. B. Fields, "Mechanisms of action of novel drugs targeting angiogenesis-promoting matrix metalloproteinases," *Frontiers in Immunology*, vol. 10, p. 1278, 2019.

Hindawi
Journal of Chemistry
Volume 2022, Article ID 4030999, 31 pages
https://doi.org/10.1155/2022/4030999

Review Article

Green Nanotechnology: Recent Research on Bioresource-Based Nanoparticle Synthesis and Applications

Laila S. Alqarni,[1,2] **Maha D. Alghamdi**,[1] **Aisha A. Alshahrani**,[1] **and Amr M. Nassar**[3]

[1]*Department of Chemistry, Faculty of Science, Albaha University, Albaha, Saudi Arabia*
[2]*Department of Chemistry, Faculty of Science, Imam Mohammad Ibn Saud Islamic University, Riyadh, Saudi Arabia*
[3]*Chemistry Department, College of Science, Jouf University, Sakaka, Saudi Arabia*

Correspondence should be addressed to Amr M. Nassar; amnassar@ju.edu.sa

Received 28 May 2022; Revised 25 June 2022; Accepted 15 July 2022; Published 9 August 2022

Academic Editor: Ajaya Kumar Singh

In the last decades, the idea of green nanotechnology has been expanding, and researchers are developing greener and more sustainable techniques for synthesizing nanoparticles (NPs). The major objectives are to fabricate NPs using simple, sustainable, and cost-effective procedures while avoiding the use of hazardous materials that are usually utilized as reducing or capping agents. Many biosources, including plants, bacteria, fungus, yeasts, and algae, have been used to fabricate NPs of various shapes and sizes. The authors of this study emphasized the most current studies for fabricating NPs from biosources and their applications in a wide range of fields. This review addressed studies that cover green techniques for synthesizing nanoparticles of Ag, Au, ZnO, CuO, Co_3O_4, Fe_3O_4, TiO_2, NiO, Al_2O_3, Cr_2O_3, Sm_2O_3, CeO_2, La_2O_3, and Y_2O_3. Also, their applications were taken under consideration and discussed.

1. Introduction

Green nanotechnology is the biosynthesis of nanomaterials from natural bioactive agents such as plant materials, microbes, and various biowastes such as agricultural residues, eggshells, vegetable waste, fruit peels, and others, accompanied by the use of nanoproducts to achieve sustainability [1, 2]. It is a low-cost, simple, safe, low-risk, nontoxic, and environmentally friendly approach [3, 4]. Green nanotechnology is a vital feature of clean technologies aimed at environmental remediation and the conversion of extra-bioactive products into more lucrative and environmentally friendly green nanomaterials. Human biowaste is increasing in tandem with population growth, posing a significant danger to environmental purity. As a result, finding a safe and economic solution to this problem, which has a high environmental cost, has become critical [5–7]. Many researchers have lately considered strategies to benefit from these bioresources by recycling them into acceptable and environmentally beneficial products from this standpoint [8]. One of these methods is green nanotechnology, which uses recyclable bioresources in the production of nanomaterials [9–11]. High pressure, energy, temperature, or toxic substances are not required. It is a biosafe and low-cost method for fabricating nanomaterials for applications in catalysis, solar cells, medicinal medicines, industrial industries, sensors, water desalination, water purification, and air purification [12, 13] (see Figure 1).

The prevalence of green route techniques is based on the fact that they allow the production of nanomaterials in a regulated and clean environment hence environmentally friendly [14]. There are various available methods or approaches to the green route that include utilizing plant extracts and synthesizing nanoparticles using fungi, bacteria, viruses, and algae [15]. Each of these green methods portrays specific advantages over environmental conservation and disadvantages.

The first green route technique is plant extracts, and it is considered the most reliable approach when it comes to eco-friendly, biocompatible, and safe nanoparticles. The approach has various advantages that include the free availability of plants that are harmless, easy to handle, and cheap

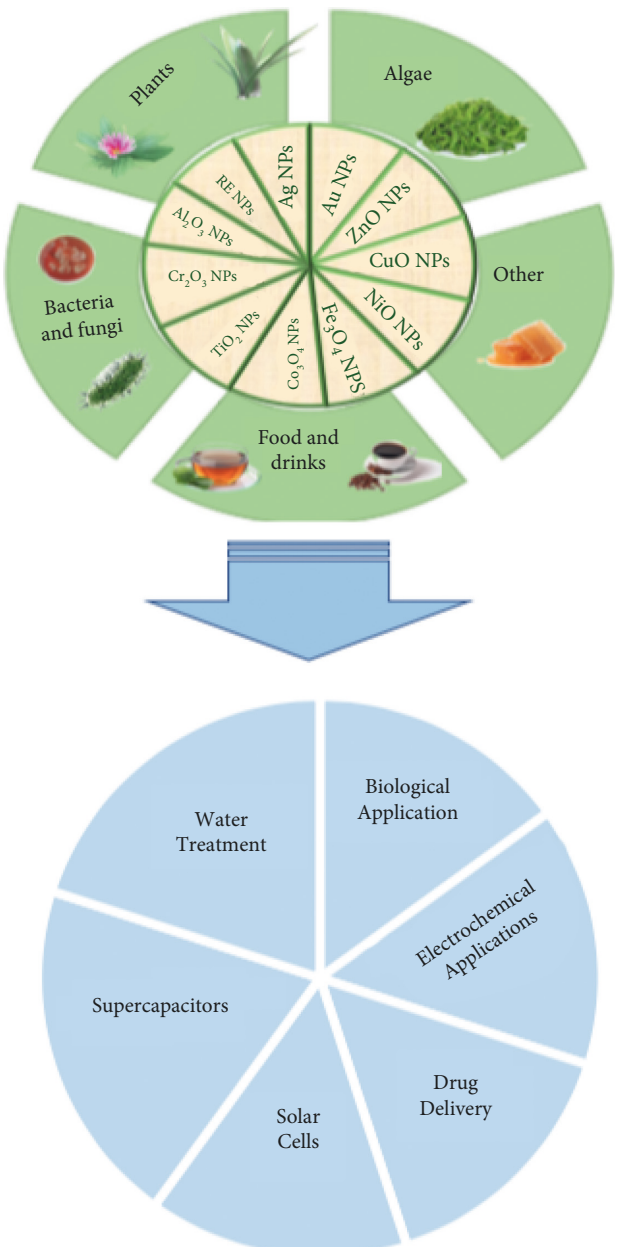

Figure 1: Green methods of nanoparticle synthesis and their applications.

material to allow various nanoparticle syntheses [16]. The approach also entails using distinct parts of the plant such as fruits, flowers, leaves, and roots with various biomolecules such as amino acids and carbohydrates. The approach also depicts some disadvantages that include the potential loss of original color, shape, and size of the plant's part used in the synthesis process [16]. This is because, during plant incubation, the precursor salts change the solution color to reflect the iron salts used in intensifying the nanoparticle production [17]. Another approach involves green route synthesis utilizing bacteria, which also involves various advantages. The advantage is that bacteria can reduce the metal ions, mainly when manipulating bacteria [18]. The easier-to-manipulate bacteria have seen the enhanced adoption of bacterial synthesis of nanoparticles [19]. However, this approach is limited or disadvantaged since it needs the control of multiple factors such as cell wall functional groups and temperature control, making the entire process complex [1]. The third green route approach includes fungi-mediated biosynthesis and is considered an efficient process. The advantage of this method is the high presence of intracellular enzymes in various shapes and the ability of competent fungi to synthesize a larger number of nanoparticles [20]. The demerit of this approach is based on high variability when it comes to starting biosynthetic biomaterial where some involve fungal biomass, while others use fungal cell filtrate [21]. The last method of nanoparticle synthesis includes the use of algae that do not regard leaf or root structure. The merit associated with this method is the ability to synthesize different metallic types using microalgae [22]. The disadvantage is based on the procedure of using algae that involves washing seaweeds and drying them over the sunlight, which may lead to the loss of many materials. Table 1 summarizes the major merits and demerits of the main green routes.

Although green nanotechnology is an interesting and diverse subject of study, it is still considered a new technology. Most of the recent articles that deal with the synthesis of nanometal and metal oxides via green methods have been presented in this review.

2. Recent Studies of Nanoparticles Synthesized via the Green Methods

2.1. Silver Nanoparticles (Ag NPs). Sekatawa et al. used *Camellia sinensis* and *Prunus africana* leaves to evaluate green-synthesized nanomaterials such as silver nanoparticles (Ag NPs) as antibiotic alternatives. Biosynthesized AgNPs had maximal growth inhibitory zones of 21 mm against carbapenem-resistant bacteria, with minimum inhibitory concentration and minimum bactericidal concentration of 125 and 250 g/ml, respectively [24].

Dutta et al. have developed a one-pot green synthesis technique for silver nanoparticles (Ag NPs) utilizing *Citrus limetta* peel extract. *Micrococcus luteus, Streptococcus mutans, Staphylococcus epidermidis, Staphylococcus aureus,* and *Escherichia coli* were all found affected by synthesized Ag NPs. Ag NPs also showed antifungal action against Candida species, as well as anti-biofilm and cell membrane permeabilization properties [25].

The bioreduction of silver nitrate using *Parkia speciosa* leaf aqueous extract resulted in the green production of silver nanoparticles (Ag NPs). Water treatment through photocatalytic methodology (methylene blue under solar irradiation) (Figure 2), antioxidant (DPPH radical scavenging method), and antibacterial capabilities (*Escherichia coli, Staphylococcus aureus, Pseudomonas aeruginosa, and Bacillus subtilis*) were all demonstrated for the biosynthesized Ag NPs [26].

Silver nanoparticles were additionally prepared with silver nitrate as a precursor and an aqueous extract of fresh *Gomphrena globosa* (*Globe amaranth*) leaves as a reducing and stabilizing agent. Silver ions (Ag^+) are rapidly reduced to

Table 1: General merits and demerits of the main green routes for nanoparticle synthesis.

Green method	Merits	Demerits	Reference
Plant extract	Free availability of plants that are harmless, easy to handle, and cheap material to allow various nanoparticle synthesis	The potential loss of original color, shape, and size of the plant part used in the synthesis process	[23]
Bacteria	Ability to reduce the metal ions especially when manipulating bacteria are employed	It needs the control of multiple factors such as cell wall functional groups and temperature control making the entire process complex	[18, 19]
Fungi	High presence of intracellular enzyme in a variety of shapes and the ability of competent fungi to synthesize larger number of nanoparticles	High variability when it comes to starting biosynthetic biomaterial where some involve fungal biomass, while others use fungal cell filtrate	[1, 20, 21]
Alga	Ability to synthesize different metallic types with the use of microalgae	It involves washing seaweeds and drying them over the sunlight that may lead to loss of many materials	[22]

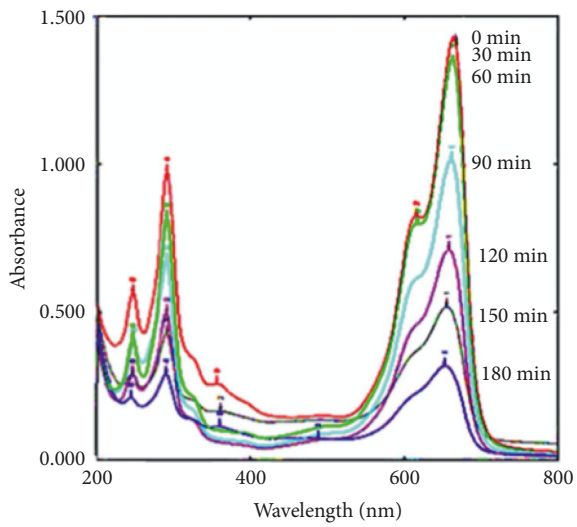

Figure 2: UV-Vis absorption spectra of photocatalytic degradation of methylene blue dye in the presence of green Ag NPs [26].

metallic silver nanoparticles (Ag^0) by active phytochemicals in the leaves. Three Gram-positive bacteria (*Staphylococcus aureus, Bacillus subtilis,* and *Micrococcus luteus*) and three Gram-negative bacteria (*Escherichia coli, Pseudomonas aeruginosa,* and *Klebsiella pneumoniae*) demonstrate good antibacterial activity against the biosynthesized Ag NPs [27].

*Alginate, fucoid*an, and *laminaran* are polysaccharides extracted from marine algae. The activity of *Saccharina cichorioides* and *Fucus evanescens* as reducing and stabilizing agents in the biogenic production of silver nanoparticles was investigated. The antibacterial and cytotoxic characteristics of the nanoparticles were also tested. Furthermore, silver nanoparticles had significant antibacterial activities, which were more prominent in fucoidan-derived samples [28].

For the assessment of effective antibacterial, anticancer, and photocatalyst properties, metallic silver nanoparticles (Ag NPs) were biosynthesized utilizing *Sambucus ebulus* extract [29]. Synthesized Ag NPs@SEE showed improved performance on cancer cell lines and good antibacterial capabilities against Gram-positive microorganisms (MIC value of 1.5 g/ml for *S. aureus*). Silver nanoparticles generated by *Sambucus ebulus* have the potential to be used as low-cost and efficient nanoparticles for environmental and biological applications, according to these studies [29].

Yugay et al. described a green chemistry technique for the biological production of Ag NPs utilizing extracts from *Panax ginseng* non-transformed callus, rolC transgenic callus, and hairy roots, as well as an assessment of their effectiveness against crop-damaging fungal pathogens [30]. *Fusarium graminearum*, *Fusarium avenaceum*, *Fusarium poae*, and *Fusarium sporotrichioides*, which are involved with Fusarium head blight disease in cereals, were extremely affected by the biosynthesized nanoparticles. Furthermore, nanosilver's antifungal activity was effectively applied to the surface sterilization of infected wheat kernels without affecting seed germination [30].

As an antibacterial, flexible strain sensor, silver nanoparticles were prepared by solid-state reduction of hydroxyethyl cellulose and compounded into a chemically cross-linked hydrogel. The composite hydrogels have been used to develop an antibacterial strain sensor with a gauge factor (GF) of 4.07 [31].

Using a bacterial T10 strain isolated from an atypical environment, functionalized silver nanoparticles were synthesized [32]. Within 1 hour of incubation, stable and well-disseminated Ag NPs were produced extracellularly utilizing the bacterial extract. Antimicrobial activity against clinical infections was observed, as well as a synergistic impact with antibiotics. By coating Ag NPs on bandages, the antibacterial activity of the resulting Ag NPs was evaluated against clinical pathogens. These findings show that the bacterial extracts are a good source for green Ag NP production and might be utilized to combat infections [32].

Hamida et al. isolated, purified, cultivated, and molecularly characterized a new cyanobacteria species (*Desertifilum sp*. IPPAS B-1220) and then utilized its aqueous extract to produce silver nanoparticles [33]. These studies demonstrated for the first time the ability of a new cyanobacteria strain, *Desertifilum* IPPAS B-1220, to produce tiny NPs that were effective anticancer and antibacterial materials against cancer cell lines and harmful bacterial strains [33].

From fungal metabolites of Penicillium oxalicum, biogenic production of silver nanoparticles (Ag-NPs) as potential antibiotics has been carried out [34]. The antibacterial activity of biosynthesized silver nanoparticles was tested

using the well diffusion technique and a UV-visible spectrophotometer against *Staphylococcus aureus*, *S. dysenteriae*, and *Salmonella typhi*. For both *S. aureus* and *Shigella dysenteriae*, the maximum zone of inhibition was 17.5 ± 0.5 mm (mm), whereas for *Salmonella typhi* it was 18.3 ± 0.60 mm. *P. oxalicum* that biosynthesized silver nanoparticles have remarkable antibacterial activity. These findings suggest that biosynthesized silver nanoparticles have substantial promise for a variety of biological applications, including bactericidal agents against resistant bacteria, infection prevention, wound healing, and anti-inflammation [34].

A new fungus, *Piriformospora indica*, has been identified as a good source for creating simple and consistent Ag NPs. These biogenic nanoparticles are cytotoxic and were found to have inherent properties that make them appropriate for anticancer action. Human breast adenocarcinoma (MCF-7), human cervical carcinoma (HeLa), human liver hepatocellular carcinoma (HepG2) cell lines, and embryonic kidney cell line (HEK-293) were used to test the in vitro cytotoxicity of biologically generated AgNPs (BSNPs) and chemically synthesized AgNPs (SNPs). In comparison with SNPs, the antiproliferative results demonstrated that BSNPs had high cytotoxic action against MCF-7, HeLa, and HepG2 cell lines [35].

2.2. Gold Nanoparticles (Au NPs). In comparison with gold bulk structure, gold nanoparticles have unique and unexpected capabilities that have been proposed for a variety of applications including therapeutic agent delivery, antifungal, antibacterial, anticancer, colorimetric sensor, photodynamic treatment, and electrochemical sensor [36, 37].

Mentha aquatic extract was used to produce Au nanoparticles utilizing a biosynthetic method [38]. The Au NPs were produced and employed as a conductive mediator to modify the tramadol electrochemical sensor. For the measurement of tramadol in aqueous solution, the modified paste electrode containing Au NPs and 1-butyl-3-methylimidazolium tetrachloroborate demonstrated good catalytic activity.

Fanoro et al. [39] used *Combretum erythrophyllum* plant leaves to describe a simple, green, and cost-effective plant-mediated production of gold nanoparticles (Au NPs). CE leaf extract was used as a reducing and capping agent in the synthesis, which was carried out at room temperature. With a minimum inhibitory concentration of 62.5 g/mL, the Au NPs showed broad-spectrum antibacterial activity against pathogenic Gram-positive (*Staphylococcus epidermidis* (ATCC 14990), *Staphylococcus aureus* (ATCC 25923), and *Mycobacterium smegmatis* (MC 215)) and Gram-negative bacteria (*Proteus mirabilis* (ATCC 7002) and *Escherichia coli* (ATCC 25)). Additionally, the as-prepared Au NPs were extremely stable, with good cell viability in both normal (BHK-21) and malignant cancer cell lines (cervical and lung cancer).

The reduction of hydrogen tetrachloroaurate (III) ($HAuCl_4{\cdot}3H_2O$) solution by the aqueous leaf extract of *Ananas comosus* [40] was used to produce a bio-directed synthesis of gold nanoparticles (Au NPs). The solid-phase breakdown of low-density polyethylene (LDPE) film was used to investigate the photocatalytic capability of Au NPs. Nanocomposite film photoinduced degradation was greater than pure LDPE film. After 240 hours of sun irradiation, an LDPE film containing 1.0% Au NPs had a degradation efficiency of 90.8%. The nanoparticles' durability was demonstrated by their capacity to be reused in the photocatalytic degradation reaction for up to five cycles without significant loss of catalytic efficacy [40].

The green synthesis of Au NPs and co-functionalization with *Curcuma pseudomontana* extracted curcumin (CUR) is studied [41]. The human red blood cell technique revealed a maximal inhibitory efficacy of 94% for CUR-Au NPs. CUR-Au NPs also showed strong antioxidant and radical scavenging properties. To successfully utilize the biological use of the particles, this work establishes a platform for unique synthetic Au NPs created by employing reducing agents in the form of isolated curcumin [41].

The effective characteristics of Au NPs synthesized from an aqueous extract of *Pimenta dioica* leaves were studied by Fadaka et al. [42]. The catalytic activity of produced nanoparticles was tested by degrading a methylene blue dye in the presence of $NaBH_4$ as a reducing agent, which took just two minutes. Au NPs have a strong antioxidant capacity. Furthermore, the produced Au NPs had a substantial inhibitory impact against both Gram-positive and Gram-negative bacteria, with zones of inhibition of 4 and 9 mm for *S. aureus* and *E. coli*, respectively [42].

Perveen et al. [43] synthesized gold nanoparticles from *Trachyspermum ammi* seed extract (TA-Au NPs), tested their efficiency against drug-resistant *Listeria monocytogenes* and *Serratia marcescens* biofilms, and assessed their anticancer potential against HepG2 cancer cell lines. The biofilm inhibitory activity of synthesized TA-Au NPs against *L. monocytogenes* (73%) and *S. marcescens* (81%) was demonstrated. Important factors in biofilm formation and maintenance, including exopolysaccharide (EPS), motility, and CSH, were strongly reduced at the studied subminimum inhibitory doses (sub-MICs). Furthermore, TA-Au NPs successfully annihilated mature biofilms of *S. marcescens* and *L. monocytogenes* by 64% and 58%, respectively. Reduced biofilm formation in test pathogens might be explained by the induction of intracellular ROS generation in TA-Au NPs treated bacterial cells. The administration of TA-Au NPs caused cellular growth to be stopped in a concentration-dependent manner. In HepG2 cancer cell lines, TA-Au NPs reduce intracellular GSH, making the cells more susceptible to ROS production and inducing death [43].

Fresh peel aqueous extract of *Benincasa hispida* was used as a reducing and stabilizing agent, resulting in a rapid and environmentally friendly approach for the synthesis of gold nanoparticles (GNPs). The produced GNPs exhibited significant antibacterial activity against a variety of Gram-positive and Gram-negative microorganisms. In vitro cytotoxicity of the biosynthesized GNPs against a human cervical cancer cell line was also impressive. Peel extracts of

B. hispida may be utilized to easily synthesize GNPs, which can be exploited as a natural source of antibacterial and anticancer agents [44].

The capability of the marine bacteria *Paracoccus haeundaensis* to synthesize gold nanoparticles (Au NPs) outside of the cell has been established [45]. On HaCaT and HEK293 normal cells, the Au NPs do not limit growth, but they do inhibit growth in A549 and AGS cancer cells in a concentration-dependent manner. As a result, Au NP synthesis using *P. haeundaensis* is straightforward and nontoxic to human cells, implying that they could be useful in biomedical applications [45].

Syed et al. [46] focused their study on gold sulfide nanoparticles (Au_2S NPs) and employed the fungus *Humicola sp.* to biosynthesize these NPs. Normal and cancer (Daudi, ZR-75-1) cell lines showed decreased cytotoxicity when exposed to Au_2S NPs. This innovative fungal-based approach offers an inexpensive and environmentally friendly biosynthesis of Au_2S nanoparticles that might be useful in bioimaging and labeling applications [46].

Acay [47] investigated the bioactive characteristics of gold nanoparticles (Au NPs) produced from edible *Morchella esculenta* (ME) using a hot water extract method in room settings (ME-Au NPs). In the A549 and HepG2 cell lines, the ME-Au NPs demonstrated excellent antibacterial and cytotoxic action against a variety of pathogenic microorganisms. This work showed that an inexpensive and harmless fungal extract may be employed as a reducing and stabilizing agent in the synthesis of size-controlled, large-scale, and biocompatible Au NPs for future diagnostic and therapeutic applications.

Gold nanoparticles with anticancer properties were created using green synthesis and an endophytic strain, *Fusarium solani* ATLOY-8, isolated from the plant *Chonemorpha fragrans*. These NPs were found to be cytotoxic to cervical cancer cells (He La) and human breast cancer cells (MCF-7) in a dose-dependent manner [48].

2.3. Zinc Oxide Nanoparticles (ZnO NPs). Metal or metal oxide NPs have emerged as attractive materials in the evolution of nanoscience [49]. Zinc oxide nanoparticles (ZnO NPs) in particular have amazing uses in a wide range of domains, including cosmetics, optical and electrical sectors, biomedicine, and catalysis [49]. Several research studies have shown cost-effective solutions involving diverse chemicals, plants, and microorganisms mediated ZnO NPs, including photocatalytic degradation [41], sensing studies [50], solar cell [51], photocatalytic activity, photocorrosion resistance, and recyclability [52]. Additionally, these nanoparticles are exploited as medication carriers, as well as in the cosmetics and pharmaceutical sectors [53]. ZnO nanoparticles have the potential to be employed as an antibacterial agent in biological applications to kill pathogenic germs [54].

The synthesis of nanoparticles via biological pathways, particularly employing fungal extracts, is gaining popularity in the field of nanotechnology due to its low cost and environmental friendliness, as well as its broad antibacterial performance. ZnO nanoparticles were produced from the white-rot fungus *Phanerochaete chrysosporium* using 0.01 M $ZnSO_47H_2O$ and 0.1 N NaOH as precursors. *P. chrysosporium* is a wood-degrading fungus with two types of extracellular peroxidases: lignin peroxidase (Lip) and manganese peroxidase (Man) (MnP). Under the experimental conditions, ZnO nanoparticles also exhibited efficient antibacterial action against *Staphylococcus aureus* and *Escherichia coli*. As a result, Sharma et al.'s work investigated fungal-mediated production and antibacterial applications of ZnO nanoparticles [55].

Zaka et al. developed a technique for green synthesis of ZnO and Ag NPs via the callus extract (CE) of the medicinally significant *Cannabis sativa*. Four bacterial strains were employed to investigate the applicability of these biosynthesized NPs on biological entities, including *Bacillus subtilis, Klebsiella pneumonia, Staphylococcus aureus,* and *Pseudomonas aeruginosa*. For the antifungal test, five fungal strains were used: Mucor, *Aspergillus flavus, Aspergillus fumigatus, Aspergillus niger, and Fusarium solani*. The HepG2 cell line was also used in the cytotoxicity experiment. The study revealed significant antibacterial and antifungal activity. It also outperformed the control in terms of cytotoxicity [56].

Antifungal properties of ZnO-based nanomaterials, which include reduction in growth and reproduction of pathogenic fungus such as *Fusarium sp.*, *Rhizoctonia solani*, and *Macrophomina phaseolina,* were one property of green ZnO NPs. Zaki et al. demonstrated the extracellular production of ZnO NPs with the assistance of a possible fungal antagonist (*Trichoderma harzianum*). The study's findings demonstrate a unique fungicidal action in an in vitro assay for the total suppression of fungal growth of investigated plant pathogenic fungi, as well as a significant reduction in cotton seedling disease signs under greenhouse conditions. The formulation of a trichogenic ZnO NPs form considerably increased its antifungal activity. Finally, the use of biocontrol agents such as *T. harzianum* might be a safe technique for the medium-scale production of ZnO NPs and their application for fungal disease control for cotton [57].

Ameen et al. reported the synthesis of ZnO NPs with diameters ranging from 13 to 15 nm utilizing *Acremonium potronii*, a novel fungus species found in fruits, soil, and marine environment. ZnO NPs can destroy around 93% of the dye. Their study indicates the potential of fabricated ZnO NPs as dye removal catalysts and provides a platform for *A. potronii* use [49].

Zinc nanoparticles were synthesized utilizing a new simple green chemistry approach that included *Ulva lactuca* seaweed extract as a reducing and capping agent. Overall, they concluded that the synthesis of multifunctional Ul-ZnO NPs using widely accessible seaweed products may be advocated as a viable eco-friendly alternative to chemical techniques currently employed for nanosynthesis of antimicrobials and insecticides based on their findings [58].

The synthesis of zinc oxide nanoparticles utilizing *Aspergillus niger* (A/ZnO NPs) is another green approach of preparation. As an alternative to chemical and/or physical approaches, biosynthesizing zinc oxide NPs using fungal

extracts may be a more efficient and environmentally friendly solution. Furthermore, for process optimization, the results of the biomedical available test may be employed in the synthesis of ZnO NPs, which are used for large-scale fabrication in a variety of medical applications [59].

Zinc oxide nanoparticles (ZnO NPs) were also prepared utilizing the marine sponge extract *Spongia officinalis*, as well as analysis of their antibacterial and possible insecticidal effects. Overall, their work suggests that *S. officinalis*-mediated ZnO NPs might be used for mosquito control and medication development [60].

Photocatalytic degradation activity is a promising practical way for removing dye toxicity. ZnO NPs were generated by biogenic synthesis. In terms of structural, optical, thermal, and photocatalytic characteristics, ZnO NPs have the necessary physicochemical qualities. The leaf extract of *Syzygium cumini* was utilized to synthesize nanoparticles for the elimination of MB dye toxicity with many qualities such as eco-friendliness, low cost, non-toxicity, and low time consumption. Synthesized nanoparticles were successful in degrading the MB dye by about 91.4% at pH 7 and 180 minutes of exposure time in sunshine (Figure 3) [61].

Umavathi et al.'s group have worked to create zinc oxide (ZnO) nanoparticles using a leaf extract of *Parthenium hysterophorus*. ZnO nanoparticles were shown to have significant antibacterial action against bacterial and fungal species. *Sesamum indicum* seed germination and vegetative development have been substantially enhanced [62].

Green synthesis of ZnO NPs was also performed utilizing aqueous leaf extract of *Becium grandiflorum* (AM: "Yedegamentisie"). During the synthesis of ZnO NPs, plant extract biomolecules (such as phenols, flavonoids, saponins, glycosides, steroids, tannins, and alkaloids) were utilized as capping and reducing agents. The synthesized ZnO NPs have been used to eliminate MB dye from an aqueous solution by acting as a photocatalyst and adsorbent. It also demonstrated antimicrobial activity against two Gram-positive (*Staphylococcus epidermidis and Staphylococcus aureus*) and three Gram-negative bacteria (*Escherichia coli, Klebsiella pneumonia, and Pseudomonas aeruginosa*) [63].

The antibacterial properties of zinc oxide nanoparticles (ZnO NPs) against *Staphylococcus aureus, Staphylococcus epidermidis*, *Escherichia coli*, and *Pseudomonas aeruginosa*, as well as bacteria commonly found in human mouths and associated with dental conditions, including *Aggregatibacter actinomycetemcomitans*, *Porphyromonas gingivalis*, *Prevotella intermedia*, *Streptococcus mutans,* and *Streptococcus sanguinis,* have been evaluated. Green synthesis was used to grow ZnO NPs using the Mexican plant *Dysphania ambrosioides*, also known as "epazote," which has been used as a dewormer by native Mexican populations and is now widely used in traditional Mexican cuisine. It is rich in organic compounds such as flavonoids and terpenes, which may aid in the synthesis of nanoparticles (NPs). Most of the bacterial strains employed in this investigation were susceptible to synthetic and commercial NPs, with *Prevotella intermedia* being the most sensitive to ZnO NPs, according to the antibacterial test [64].

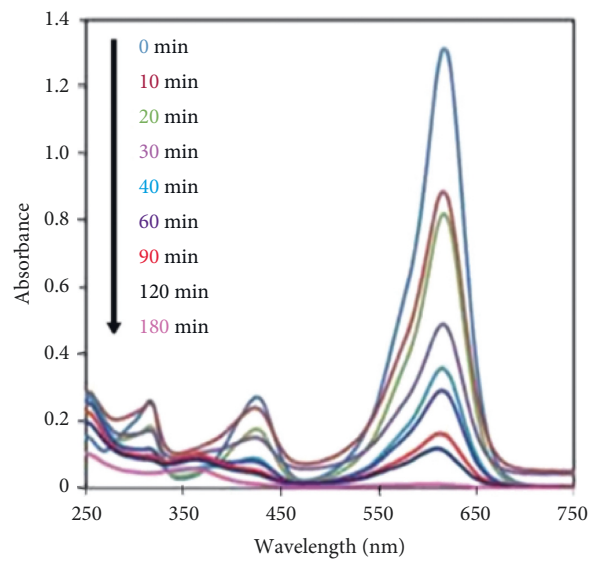

Figure 3: UV-Vis absorption spectra of photocatalytic degradation of methylene blue dye in the presence of green ZnO NPs [61].

Additionally, zinc oxide nanoparticles (ZnO NPs) were prepared by combustion technique using ecologically benign green extract (*Lantana camara* flowers) as a fuel. Surendra group examined at a great photodegradation (98%) performance of methylene blue (MB) dye under UV light, as well as an electrochemical assessment that showed an efficient oxidation-reduction process carried out in 0.1 M KCl with graphite electrode paste. Furthermore, the anti-inflammatory activity of produced ZnO NPs was investigated, and it was discovered that ZnO-2 is a highly effective PLA2 inhibitor with a MIC of 41 g/mL [65].

Developing a sustainable and effective method for dealing with organic contaminants in industrial waste is a never-ending challenge. The extract of *Passiflora foetida* fruit peels, which acts as a reducing (i.e., metal salt reduction) and stabilizing agent, was used to produce ZnO nanoparticles (ZnO NPs) using a controlled ultrasonic cavitation approach. Given their excellent reusability and photocatalytic efficacy, as well as their flexibility to green synthesis, green-manufactured ZnO NPs are a promising candidate for wastewater treatment [66].

Serrà et al. have demonstrated that biomimetic ZnO-modified micro/nanofern *fractal architectures* with highly enhanced sunlight photocatalytic efficiency and photocorrosion resistance can be synthesized using a novel, simple, inexpensive, and green electrochemical deposition approach in high stirring conditions. As a result, the ZnO@ZnS bioinspired micro/nanoferns are very promising photocatalysts for water remediation due to their ease of fabrication and ability to dramatically increase sunlight photocatalytic efficiency, as well as their practically negligible photocorrosion and simple recyclability in terms of non-catalyst poisoning [52].

Soto-Robles et al. described an accessible and simple green strategy for the production of ZnO nanoparticles utilizing *Justicia spicigera* extract. In terms of photocatalytic

activity, the catalysts decomposed about 90% of the dye in just 120 minutes [67].

Zinc oxide nanoparticles (ZnO NPs) were also synthesized using *Nilgirianthus ciliatus* leaf extract. The findings of the experiments demonstrate that the ZnO NP produced in this work has outstanding antibacterial and anticancer action. Furthermore, normal L929 fibroblast cell lines are nontoxic. As a result, the research on green-produced ZnO NP will be useful in advancing its future research in biological areas [68].

Additionally, diverse vegetable extracts (onion, cabbage, carrot, and tomato) make zinc oxide nanoparticles (ZnO NPs), which succeeded over other techniques of synthesis in terms of simplicity, environmental friendliness, and the removal of hazardous substances. The dye-sensitive solar cell based on ZnO NPs has been fabricated, and the device's efficiency has been determined by monitoring current density-voltage behavior under artificial sunlight. The improved dye molecule adsorption onto the surface of ZnO NPs accounts for the higher efficacy of the constructed dye-sensitive solar cell. As a result, using green-produced ZnO NPs to create dye-sensitive solar cells is a simple and practical solution for future well-being [51].

The biosynthesis of zinc oxide nanoparticles with *Cocos nucifera* leaf (CNL) extract has been described, as well as the evaluation of their antibacterial activity before and after calcination using various microorganisms. These ZnO nanoparticles can be used as both an antibacterial agent and a biocompatible carrier molecule in drug delivery [69].

Green procedures for the fabrication of ZnO nanoparticles with *Lactobacillus spp.* extract are cost-effective and eco-friendly, according to studies. Green ZnO nanoparticles have improved antibacterial and biocompatibility testing. MTT test results on cell viability tests revealed high biocompatibility efficacy against the HT29 cancer cell line in this investigation. The remarkable inhibition zones indicated the antibacterial effectiveness of ZnO nanoparticles against several Gram-positive and Gram-negative bacterial and fungal diseases (mm). They have found that bio-mediated ZnO nanostructures are an effective novel antibacterial and anticancer material in this study [70].

Zinc oxide nanocomposites were synthesized using intracellular fabrication by *lactic acid bacteria.* The antibacterial activity of ZnO NPs was further examined via fluorescence microscopy against two clinically relevant drug-resistant pathogens, Gram (+) and Gram (−). Furthermore, the acquired results allow us to characterize the intracellular ZnO NP production pathway for the first time. The carboxyl functional group was shown to be the most important in the production of ZnO NPs [71].

Lactobacilli strains were used to biosynthesize zinc oxide nanoparticles (ZnO NPs). The findings revealed that the minimal amount of biosynthesized ZnO NPs attributed to the formation of integrated yogurt properties. Furthermore, the biosynthesized ZnO NPs added to yogurt might be an excellent supply of zinc for those who are zinc-deficient, such as the elderly or vegetarians who do not consume meat yet are at risk of zinc insufficiency [72].

Hairy-shaped ZnO nanostructures were fabricated using ureolytic bacteria and applied as a photocatalyst for the degradation of dyes such as methylene blue (MB), methyl orange (MO), rhodamine B (Rho-B), and fresh textile effluents. The hairy-shaped ZnO nanostructure has good photocatalytic activity of textile dye in sunlight, which is connected with light intensity, according to this study [73].

The biological uses of zinc oxide nanoparticles (ZnO NPs) are numerous. *Bacillus megaterium* (NCIM 2326) cell-free extract was used as a bioreductant to produce anisotropic ZnO NPs with a predetermined form and size. ZnO NPs were tested in normal human mesenchymal stem cells for their multifaceted effect on *Helicobacter pylori* strains (hMSc). Furthermore, the ZnO NPs were shown to be more biocompatible with human mesenchymal stem cells (hMSCs) and to be possibly safe in mammalian cells. They found that the anti-*H. pylori* dose of ZnO NPs was safe for hMSC and could be used effectively as a nanoantibiotic, which supports this study [74].

2.4. Copper Oxide Nanoparticles (CuO NPs). Many researchers were interested in copper oxide nanoparticles (CuO NPs) because of its electric, catalytic, optical, textile, photonic, monofluid, and pharmacological properties, which are dependent on the shape and size of the nanoparticles [75].

Aerva javanica plant leaf extract was utilized to greenly synthetize CuO NPs. The antibacterial potential of the CuO NPs was investigated against a variety of bacterial and fungal diseases. CuO NPs have the highest antibacterial activity against all of the tested bacterial and fungal pathogens, according to the findings. Copper oxide nanoparticles were compared to the medicines norfloxacin and amphotericin B for antimicrobial activity. Copper oxide nanoparticles had minimum inhibitory concentrations (MICs) and minimum bactericidal concentrations (MBCs) of 128 g/mL against all tested bacterial pathogens. CuO NPs had a MIC of 160 g/mL and a minimum fungicidal concentration (MFC) of 160 g/mL. CuO NPs can therefore be used as broad-spectrum antibacterial. At doses below 60 g/mL, the cytotoxic activity of the produced CuO NPs revealed that toxicity was insignificant [75].

Calotropis procera-mediated production of copper oxide nanoparticles (CuO NPs) utilizing aqueous plant extract and their anti-pathogenic activity against phytopathogens was also applied. The findings demonstrated that greenly generated CuO NPs had high biological potential and powerful antioxidant activity, indicating that they might be employed in phytopathology to attack plant infections [76].

Rubia cordifolia is an important botanical resource in traditional Chinese medicine and Ayurveda in India. The goal is to make biocompatible copper oxide nanoparticles (CuO NPs) from R. cordifolia bark extracts, define the chemical transitions involved, and investigate their biomedical and environmental implications. As a result, this is the first study to account for the many uses of phyto-CuO NPs. Furthermore, the green synthesis of CuO NPS has

potential uses in therapeutic development for life-threatening illnesses and environmental concerns [77].

Thespesia populnea is a Malvaceae tree that grows in tropical climates, particularly in mangrove forests. *Thespesia populnea* aqueous bark extract is combined with copper metals efficiently against skin infection-producing microorganisms, according to this study. CuO NPs have higher antimicrobial activity against skin infection-causing bacteria including *Staphylococcus aureus* (MTCC 102), *Streptococcus pyogenes* (MTCC 102), *Pseudomonas aeruginosa* (MTCC 358), and fungal strains such as *Trichophyton rubrum* (MTCC 296) and *Candida albicans* (MTCC 183). When compared to other microbial strains, *Trichophyton rubrum* (MTCC 296) displayed a large zone of inhibition [78].

Allium sativum extract was used in the green production of CuO nanoparticles. The antimicrobial activity revealed that bacteria and fungi were effectively infected. The antioxidant activity indicated free radical scavenging activity's capability. Anti-inflammatory action against egg albumin has been discovered. The anti-larvicidal action on *Anopheles subpictus* mosquito larvae revealed the significant potential nature of affection. CuO nanoparticles made from environmentally friendly synthesis have unique uses in pharmaceuticals, optics, batteries, gas sensors, catalysts, cosmetics, and semiconductors in the twenty-first century. CuO nanoparticles may also be used in the formulation of drugs for human life-threatening disorders and different harmful cancer therapies in the future [79].

Ghareib et al. have used prefabricated *Aspergillus fumigatus mycelium* to biosynthesize copper oxide nanoparticles (CuO NPs). These NPs have been shown to have antibacterial action against two significant human infections, *Staphylococcus aureus* and *Klebsiella pneumonia*. They also managed to degrade 97% of the methylene blue (MB) dye in direct sunshine after 200 minutes [80].

CuO nanoparticles were effectively biosynthesized for the creation of antibacterial active textiles using active enzymes/proteins released by fungus while taking into account their cytotoxicity. The fungus, *Aspergillus terreus* strain AF-1, was permitted to exude active components such as enzymes and the protein required to cap the CuO NPs after they had been generated. Cotton textiles were treated with CuO NPs at a safe dosage, and their antibacterial activity was assessed by comparing the fabrics before and after treatment. Fabrics were treated with CuO NPs at a tolerable dosage (100 g/mL), resulting in probable antibacterial activity against pathogenic bacteria, according to the cytotoxicity data [81].

El-Batal et al. have studied whether a certain fungus can biosynthesize copper oxide nanoparticles (CuO NPs) with the help of gamma rays and how effective it is as an antibacterial agent in agricultural areas. *Penicillium chrysogenum* filtrate was used to make CuO NPs using copper sulfate at varied gamma radiation dosages. CuO NPs may therefore be used as a substantial antibacterial agent in the agricultural domain to inhibit the multiplication of plant harmful fungus and bacteria due to their exceptional properties [82].

Oc-5 and Acv-11, two endophytic actinomycetes isolates, were isolated from healthy leaves of the medicinal plant *Oxalis corniculata L.* in this investigation. Using the 16S rRNA gene sequence, these isolates were identified as *Streptomyces zaomyceticus* Oc-5 and *Streptomyces pseudogriseolus* Acv-11. These strains' biomass extracts were utilized to make copper oxide nanoparticles in a more environmentally friendly way (CuO NPs). The findings of this study clearly demonstrated that biosynthesized CuO NPs have good bioactivity and thus provide a foundation for the development of various biotechnological applications in the near future [83].

Copper oxide nanoparticles (TA-CuO NPs) were produced utilizing a cell-free extract of *Trichoderma asperellum*, and their photothermal induced anticancer activity was evaluated in this study. The research supported the development of anticancer nanotherapeutics using biogenic TA-CuO NPs for promising in vitro photothermolysis of cancer cells [84].

The ureolytic fungus *Neurospora crassa, Pestalotiopsis sp.*, and *Myrothecium gramineum* were studied for their ability to produce nanoscale copper carbonate and the function of fungal extracellular protein. These findings reveal that fungal extracellular protein plays a key role in the production and size of certain nanometal carbonates and give direct experimental evidence for the synthesis of copper carbonate nanoparticles using fungal ureolytic activity. This method may be used to make particular and/or unique metal carbonate nanoparticles with practical applications, as well as precursors to other biomineral products including oxides [85].

Copper oxide nanoparticles (CuO NPs) are used in a variety of industries, including biomedicine. CuO NPs were produced from the filtrate of *Aspergillus terreus*. Biotechnology and induced radiation were used to create a new composite of P (AA-AN) NPs CuO. The batch approach was used to estimate the distribution coefficient value (Kd) of 47Sc(III) and 47Ca(II) ions for the synthetic novel composite. A chromatographic column filled with the novel composite material was used to investigate the radiochemical separation of 47Sc(III) from an irradiated calcium target. Using 1 M HCl, a recovery yield of 78.2% for 47Sc(III) was achieved. The eluted 47Sc passed quality control tests (chemical, radionuclide, and radiochemical purities) and was found to be suitable for nuclear medicine applications [86].

Metal nanoparticles (NPs) made through mycofabrication serve an important role in cancer therapies and provide a medical strategy. The study employed an endophytic fungus isolated from the *Aegle marmelos* medicinal tree in the Western Ghats of India to make copper oxide nanoparticles (CuO NPs). Among the 16 pigmented endophytic fungal strains recovered from the collected materials, the endophytic fungus FCBY1 had the strongest antagonistic and antioxidant capabilities [87].

The CuO NPs had the best antibacterial and antifungal activity against human clinical infections, and the particles also explained free radical/ROS scavenging at low concentrations. The anticancer actions of CuO NPs were explained

in a concentration-dependent way, and the findings of this study demonstrate the importance of CuO NPs in cancer therapies [87].

Copper oxide nanoparticles (CuO NPs) were generated by a biological approach employing *marine endophytic actinomycetes* as a reducing and stabilizing agent. As a result, they concluded that *actinomycetes-mediated* CuO NPs have great medicinal applications against biofilm-producing bacteria and cancer cells and that they would be employed in future biomedical investigations [88].

Biosynthesis of non-precious metal nanoparticles is of great interest because metallic nanoparticle-based disinfection is a potential strategy for microbial pollution management in drinking water. Lv et al.'s group have presented a unique and effective technique for directly microbiological production of copper nanoparticles (Cu NPs) by *Shewanella loihica* PV-4, as well as their antibacterial activity. Cu NPs with strong antibacterial activity are particularly appealing for drinking water disinfection because of their cost-effective and environmentally sustainable production. Microorganisms are effective mechanisms for making biocompatible metal nanoparticles. Copper, a necessary component of life, offers promising medicinal properties. Copper, on the other hand, lacks a suitable form for efficient in vivo delivery, limiting its use. They used a copper-resistant bacterial strain from a copper mine to make biosynthesized copper nanoparticles (BCuNPs). BCuNPs had a greater antibacterial impact and was proven to be safer than copper sulfate against normal cell lines such HaCat, Vero, and hFOB [89].

Microorganism-based biosynthesis has developed as an environmentally acceptable, clean, and viable alternative to chemical and physical processes. The manufacture of copper oxide nanoparticles (CuO NPs) utilizes cell-free culture supernatant of *marine Streptomyces sp*. The effect of enhancing CuO NPs against paracetamol-induced liver damage was confirmed by histological inspection of the CuO NP groups [10].

Kouhkan et al.'s group have indicated the lethal effects of copper oxide nanoparticles (CuO NPs) produced by probiotic bacteria (*Lactobacillus casei subsp. casei*) against Gram-negative and Gram-positive bacteria, as well as cancer cell lines. CuO NPs may have antibacterial and cytotoxic effects on cancer cells by limiting their development, raising oxidative stress, and causing apoptosis, according to these findings [90].

Nabila and Kannabiran's group have evaluated the antibacterial activity of copper oxide nanoparticles (CuO NPs) produced by *actinomycetes* against a variety of human and fish infections [91]. The antibacterial activity of *actinomycetes*-mediated biosynthesized CuO NPs shows that it can fight bacterial infections in both humans and fish. This is the first study of CuO NP production mediated by actinomycetes [91].

To create well-dispersed Cu nanoparticles (Cu NPs) encapsulated in carbonized bacterial *cellulose*, a simple one-step approach is presented (CBC). The findings reveal that the composites produced have a flawless core-shell structure and exhibit outstanding oxidation resistance and stability [92].

Figure 4 shows TEM images of Ag NPs, Au NPs, ZnO NPs, and CuO NPs synthesized via different green methods.

2.5. Cobalt Oxide Nanoparticles (Co_3O_4 NPs). Nanotechnology is the fabrication, characterization, and application of nanoscale materials. Nanomaterials have drawn researchers from various sectors in recent decades due to their high surface-to-volume ratio and other unique and outstanding features. Cobalt and cobalt oxide nanoparticles (NPs) have a wide range of medicinal applications. Because of its antioxidant, antimicrobial, antifungal, anticancer, larvicidal, antileishmanial, anticholinergic, wound healing, and antidiabetic capabilities, cobalt and cobalt oxide NPs have been widely used in lithium-ion batteries, pigments and dyes, electronic thin film, capacitors, gas sensors, heterogeneous catalysis, and environmental remediation. Cobalt and cobalt oxide NPs have been synthesized using a variety of chemical and physical methods [93].

Green synthesis was used to prepare Co_3O_4 NPs from *Euphorbia heterophylla L.* leaf extract (ELEs). In the preparation of Co_3O_4 nanoparticles, ELE uses secondary metabolite molecules such as alkaloid as a weak base source and saponin as a capping agent. Co_3O_4 NPs were characterized via FTIR, UV-Vis, and XRD TEM images. Photocatalytic activity of Co_3O_4 NPs in the removal of methylene blue was about 63.105% for 3 hours [94].

To produce cobalt oxide as a reducing agent, Mohammadi et al. used *walnut green* skin extract, which contains a high amount of phenolic component. Green synthesis was used to make the nanoparticles, which were then identified and examined using SEM, XRD, FTIR, and VSM. The magnetic characteristics of the cobalt oxide nanoparticles generated by the VSM were measured, and the results showed that the nanoparticles were super-magnetic [95].

GCoO NPs were produced by co-precipitation with the grape *Jumbo Muscadine* (*Vitis rotundifolia*). UV-Vis, FTIR, XRD, and SEM were used to evaluate the produced GCoO NPs. The degradation of Acid Blue 74 (AB-74) dye was used to determine the photocatalytic activity of the GCoO NPs, and a full degradation of 98% was achieved during a reaction period of 150 minutes at pH 10 and a concentration of 60 mg/100 mL. The results of this investigation showed that GCoO NPs have good performance compared with some of the prior findings, making them a promising candidate for use as a catalyst alternative to current wastewater treatment methods [96].

Matinise et al. [97] used *Moringa oleifera* extract to establish a better, less expensive, more dependable, simple, and precise process for fabricating cobalt oxide (Co_3O_4) nanoparticles. Various characterization approaches were used to investigate the electrochemical activity, crystalline structure, shape, isothermal behavior, and optical features of Co_3O_4 nanoparticles. The production of Co_3O_4 nanoparticles was validated using XRD and EDS. In 3 M KOH solution, cyclic voltammetry (CV), galvanostatic charge-

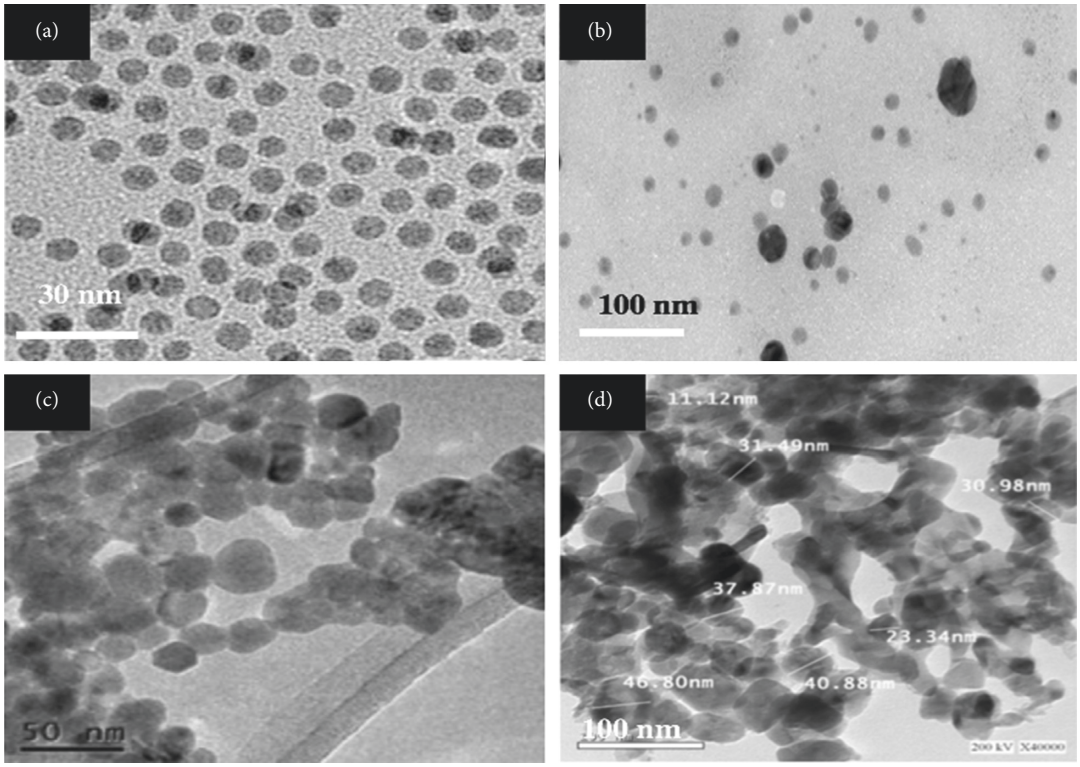

Figure 4: TEM images of several metals. (a) Ag NPs [25], (b) Au NPs [42], (c) ZnO NPs [67], and (d) CuO NPs [81].

discharge (GCD), and electrochemical impedance spectroscopy (EIS) were used to examine the pseudo-capacitor behavior of spinel Co_3O_4 nanoparticles on nickel foam electrode. The CV curve displayed two redox peaks, showing the Ni/Co_3O_4 electrode's pseudo-capacitive properties. The electrochemical process on the surface electrode is kinetically and diffusion controlled, as evidenced by the EIS data, which indicated a tiny semicircle and Warburg impedance. At a discharge current density of 2 A/g, the charge-discharge findings indicate that the specific capacitance of the Ni/Co_3O_4 electrode is approximately 1060 F/g.

Co_3O_4 NPs were synthesized utilizing *Populus ciliata (safeda)* leaf extract and cobalt nitrate hexahydrate as a cobalt source. Different techniques such as FTIR, XRD, TEM, and SEM were used to analyze the synthesized NPs. The antibacterial activity of the produced Co_3O_4 NPs was tested against Gram-negative and Gram-positive bacteria, and it was discovered to be active against *Escherichia coli* (*E. coli*), *Klebsiella pneumoniae* (*K. pneumonia*), *Bacillus subtilis* (*B. subtilis*), and *Bacillus licheniformis* (*B. licheniformis*). One-way ANOVA with "Dunnett's multiple comparison test" was used to examine the activity findings statistically. *B. subtilis* had the highest mean activity (21.8 ± 0.7), and *E. coli* had the lowest mean activity (14.0 ± 0.6) [98].

The cobalt oxide nanoparticles (Co_3O_4 NPs) were synthesized using *Piper nigrum (P. nigrum)* leaf extract as a green technique and calcined at different temperatures. XRD was used to investigate the crystalline nature. The amorphous phase changed to the crystalline phase as calcination increased. The UV-visible light absorbance phenomena were observed using diffuse reflectance spectroscopy (DRS), and the band gap energy was calculated using Tauc's plot, which was found to decrease with calcination. The surface morphology was studied using SEM, and the surface functional groups were classified using FTIR spectroscopy. The antibacterial efficiency of Co_3O_4 NPs was tested against Gram-positive and Gram-negative bacteria and their antioxidant capability using ABTS assay [99].

Korkmaz [100] investigated Co_3O_4 NPs produced using a green synthesis method to avoid the toxicity of chemical production. The reducing agent was *Allium tuncelianum*, an endemic species in Tunceli, and the cobalt source was $Co(NO_3)_2{\cdot}6H_2O$. FTIR, XRD, SEM, and HR-TEM methods were used to characterize the synthesized Co_3O_4 NPs. The XRD pattern revealed that the Co NPs were face-centered cubic (FCC) in nature, with an average crystallite size of about 23 nm and a COD (R^2): 0.982 value. In SEM images collected at 200 nm, the Co_3O_4 NPs showed a typically spherical form. In comparison with RPE normal cells, Co_3O_4 NPs had a low IC50 value against HeLa cells.

2.6. Magnetic Iron Oxide Nanoparticles (Fe_3O_4 NPs). For the manufacture of metal oxide nanoparticles, a green technique has gained a lot of interest. Iron oxide nanoparticles are an example of metal oxide nanoparticles (IONPs). Because of their magnetic character, which allows them to be easily retrieved from the reaction mixture by applying an external magnetic field, IONPs have attracted a lot of attention in recent years. Although there are a range of chemical and physical synthesis processes available, green synthesis is

safer, more sustainable, and physiologically acceptable. The main biological resources used for green synthesis are plants and microorganisms [101].

Sathishkumar et al. [102] developed a sustainable green chemical approach to produce magnetic Fe_3O_4 nanoparticles using the aqueous fruit extract of edible *C. guianensis*. Different high-throughput characterization techniques, including UV-visible, FTIR, XPS, DLS, and zeta potential analysis, were used to confirm the synthesized NPs. XRD, AFM, HRTEM, and SQUID VSM also show that crystalline CG Fe_3O_4 NPs with a mean diameter of 17 ± 10 nm are produced. CG Fe_3O_4 NPs have a remarkable bactericidal activity against a variety of human diseases, demonstrating their antibacterial potential. CGFe_3O_4NPs had a substantial dose-dependent cytotoxic effect on treated human hepatocellular carcinoma cells (HepG2).

An affordable co-precipitation approach was used to make Fe_3O_4 NPs with four different weight percentages of *Punica granatum* fruit peel extract as a green stabilizer. The NPs had spherical forms with an average size of 14.38 nm, as seen in transmission electron microscopy images. UV-Vis spectroscopy and band gap results suggested that the Fe_3O_4 NPs stabilized with the extract were successfully prepared. The particle zeta potential was improved from 29.24 to 35.62 mV after adding the stabilizer concentration. Under hyperthermia, the thermoresponsive performance of Fe_3O_4 nanofluids with green extract may provide a surprising heating capability. The samples had adequate magnetic resonance imaging (MRI) signals, according to the results. 5-fluorouracil, an anticancer medication, was successfully loaded onto Fe_3O_4 NPs with 2 weight percent of the extract, resulting in a maximal release of 79% in a pH 7.4 environment. In cytotoxicity tests, drug-loaded Fe_3O_4 NPs at concentrations of 15.62 and 31.25 $\mu g \cdot ml^{-1}$ killed 29% and 35% of HCT116 colorectal cancer cells, respectively. Fe_3O_4 NPs produced in green-synthesized could be a viable choice for magnetic hyperthermia therapy, MRI nanoagents, and medication administration in colorectal cancer [103].

Aqueous extract of *Graptophyllum pictum* leaf (GPLE) was used to successfully produce nanoscale magnetite particles (MNPs) in an environmentally acceptable manner. GPLE served as a base source and a capping agent in the production of MNPs. Through calcination, alkaloids in GPLE were hydrolyzed in water and hydroxylated Fe^{2+} to generate Fe_3O_4 nanoparticle powder. MNP production was observed by a color change from pale yellow to dark brown after the addition of leaf extract. UV-Vis, XRD, and FTIR were used to characterize the produced nanoparticles. MNP production suggested the surface plasmon resonance at a maximum wavelength of 291 nm, according to the findings. The average size of a crystallite is 23.17 nm. The MNPs created using a green synthesis process show promise in a variety of medical applications, including medication delivery [104].

The ability of *Lagenaria siceraria* leaf extract to green synthesize (Fe_3O_4 NPs) was discovered, and their properties were investigated using UV-Vis, SEM, EDX, XRD, zetasizer, and FTIR. Fe_3O_4 NPs synthesized in this way were naturally stabilized, cubic in shape, and ranged in size from 30 mm to 100 nm. The leaf phytochemicals have an important role as a reducing agent, assisting in the environmentally benign synthesis of Fe_3O_4 NPs with increased antioxidant properties. The antibacterial properties of synthesized Fe_3O_4 NPs were tested against Gram-negative *Escherichia coli* and Gram-positive *Staphylococcus aureus*. The zone of inhibition for *Escherichia coli* was found to be 10 mm, and for *Staphylococcus aureus*, it was found to be 8 mm. Natural Fe_3O_4 NPs with herbal properties can thus be employed in a variety of biological applications [105].

A green approach for producing magnetic iron oxide nanoparticles (Fe_3O_4) was developed, with an aqueous extract of *spent tea* waste as the reducing agent, which was then used to make the magnetic and biodegradable Fe_3O_4/cellulose nanocomposite. Advanced techniques such as UV-Vis, FTIR, XRD, SEM, TGA, and VSM were used to compare the nanostructures. The produced nanocomposite exhibited a spherical form with an average particle size of 15.5 nm, which was less than the mean particle size of pure Fe_3O_4 nanoparticles (28 nm). The produced nanocomposite also had a greater thermal resistance (450–800°C) than pure cellulose, according to these findings. The magnetic property of the nanocomposite (25 emu/g), which was lower than that of pure Fe_3O_4 nanoparticles (45 emu/g), was another notable aspect. Furthermore, the swelling capacity of the nanocomposite was investigated as one of its functional capabilities, and it was found to be 139.3 g/g, which was higher than the swell capacity of pure cellulose (66.8 g/g). According to the findings, the produced Fe_3O_4/cellulose nanocomposite is recommended for use in metronidazole drug delivery systems due to its adequate and acceptable qualities, which include high absorption capacity, regulated magnetic transferability, biodegradability, and nontoxicity [106].

Using aqueous extracts of *Pandanus odoratissimus* leaves, one-step green chemistry was used for the preparation of Fe_3O_4 NPs at room temperature. With an average diameter of ~5.0 nm, Fe_3O_4 NPs have a homogeneous particle size distribution. The nanoparticles' BET surface area and average pore diameter were found to be ~150 m^2/g and ~3.0 nm, respectively. The phase purity of the produced materials was additionally confirmed by FTIR, Raman, EDAX, and XPS. Fe_3O_4 NPs were used as electrocatalysts in 0.1 M KOH electrolyte solution for electrochemical water splitting processes. The dual nature of Fe_3O_4 electrocatalysts in water electrolysis for oxygen reduction reaction and oxygen evolution reaction is confirmed by polarization investigations [107].

Viju Kumar and Prem [108] fabricated iron oxide nanoparticles from *Phyllanthus niruri* leaf extract using a green technique. Additionally, the antibacterial property of the green-produced iron oxide nanoparticles was evaluated. For iron nanoparticles, a comparison with the chemical technique of creation is also made. The IR, UV-Vis, surface morphology, and size determination using TEM, SEM, and XRD are all used to characterize nanoparticles. Analytical tests revealed that the iron oxide nanoparticles generated using these two approaches are almost comparable in size and shape. The antibacterial activity of the produced iron

oxide nanoparticles against *E. coli* and *P. aeruginosa* was substantial. The studies indicated that employing plant extracts to synthesize iron oxide nanoparticles is more helpful because it is a cost-effective, energy-efficient method.

2.7. Titanium Dioxide Nanoparticles (TiO_2 NPs). The green sustainable production of titanium dioxide nanoparticles (TiO_2 NPs) sparked a lot of interest in the preceding quarter. The bioreduction and capping processes are aided by bioactive components found in organisms such as plants and bacteria [109].

Photocatalysis using semiconductor nanoparticles is considered being the most effective method for reducing toxic dyes. Singh et al. [110] have used green-manufactured titanium dioxide nanoparticles (TiO_2NPs) made from *Phyllanthus emblica (amla)* leaf extract to remove Coralline Red dye. Chemical analysis and microscopy methods were used to characterize the synthesized NPs, which indicated the synthesis of crystalline, spherical NPs with a size range of 20–30 nm and tiny aggregates. Furthermore, under solar illumination, synthesized TiO_2 showed significant photocatalytic degradation capacity for Coralline Red dye, with apparent rate constants (KAPP) and degradation efficiencies of 0.005 min1 and 93%, respectively. As a result, this study adds to the growing body of knowledge in green chemistry research for developing a water purification platform that is both successful and cost-effective.

A green and simple synthesis of TiO_2 NPs was achieved utilizing *Carica papaya* leaf extract, which might be used as a photocatalyst. The tetragonal crystal structure of TiO_2 NPs is shown by XRD analysis, which also demonstrates their crystalline character. TEM and FE-SEM images reveal the cage-like morphology and offer diametric measurements of the spherical TiO_2 NPs, which are well accounted to be less than 20 nm. The average particle size is 15.6 nm, according to the calculations. The mesoporous nature of TiO_2 particles is revealed by BET measurements, which show surface area and mean pore size of 81.653 m^2g^{-1} and 8.0615 nm, respectively. The UV-visible spectrum reveals a significant absorption peak at 303 nm, and the matching band gap energy value of 3.85 eV is determined. Within 180 min of incubation under UV exposure at the optimum dosage of 25 mg, TiO_2 NPs show remarkable photocatalytic effectiveness (91.19%) toward photodegradation of RO-4 dye [111].

Maurya et al. [112] used *Bixa orellana* seed extract to prepare mesoporousTiO_2 nanoparticles from titanium (IV) butoxide solution, which they then used to make a DSSC photoanode. The technology provides DSSC that is environmentally friendly, less expensive, and more efficient. XRD, SEM, TEM, and N_2 sorption measurements were used to describe the structure, morphology, size, and porosity of TiO_2 nanoparticles. The desorption technique was used to determine the amount of dye loading by TiO_2, which demonstrated substantially higher dye loading for plant seed-generated nanoparticles (G-TNP). The photovoltaic conversion efficiencies of TNP and G-TNP were 1.03% and 2.97%, respectively. As a result, the produced mesoporous TiO_2 nanoparticles can be used as potential photoanode materials in DSSC applications.

Sethy et al. [113] used an aqueous solution of *Syzygium cumini* leaf extract as a capping agent to fabricate TiO_2 NPs. The photocatalytic removal of lead ions from industrial effluent was tested using these green-generated TiO_2 NPs. HRTEM, EDS, FTIR, XRD, DLS, and BET were used to characterize the nanoparticles obtained. The results showed that produced TiO_2 NPs have a spherical morphology with a large surface area of 105 m^2/g. In a self-designed reactor, photocatalytic investigations of TiO_2 NPs for lead removal from explosive wastewater were conducted. The lead content was determined using inductively coupled plasma spectroscopy (ICP). Chemical oxygen demand (COD) was reduced by 75.5%, and lead (Pb^{2+}) was reduced by 82.53%, according to the findings. This is the first time that green TiO_2 NPs have been used in this way.

For the first time, TiO_2 nanoparticles were synthesized from *lemon peel* extract using a green synthesis approach. Hesperidin flavanol, found in a hydrolyzed extract of lemon peel, releases aglycone, which acts as a capping and reducing agent. XRD, EDX, TEM, SEM, and UV-Vis techniques are used to characterize the synthesized materials. According to the SEM results, the produced specimen is entirely made up of agglomerated structures. A thorough examination using TEM reveals that the particles are spherical in shape, with particle sizes ranging from 80 to 140 nm. The band gap of 3.08 eV is visible in the Tauc plot created from the UV-Vis spectra. The produced TiO_2 photocatalytic activity to the breakdown of rhodamine B (RhB) is also investigated. The results showed that synthesized particles have a photocatalytic activity of more than 70%, which is significantly higher than commercial TiO_2 particles [114].

Green synthesis of titanium dioxide nanoparticles (TiO_2 NPs) and generation of a nanocomposite were achieved using *pristine pomegranate peel* extract (PPP) (PPP-TiO_2). SEM, dynamic light scattering (DLS), X-ray powder diffraction (XRD), and zeta potential (ζ-potential) were used to analyze the produced nanocomposite. The DLS data clearly reveal that TiO_2 NPs have a peak intensity of 100%, a *Z*-average value of 620 nm, and a PDI of 0.178, indicating that they are monodisperse and homogeneous. Bimodal distribution peaks in the PPP-TiO2 DLS result indicate the existence of both TiO2 and PPP in the composite. The mean hydrodynamic diameter (*Z*-average) of PPP-TiO_2 was found to be 1230 nm, with 87.5% peak intensity. The ζ-potential measurements indicate that PPP-TiO_2 NPs (−11.4 mV) are more stable than TiO_2 NPs (−6.96 mV). The biological activity was tested against Gram-positive and Gram-negative microorganisms using the well diffusion method, the microbial inhibition concentration (MIC), the minimum bactericidal concentration (MBC), and the live/dead cell assay. For the same harmful bacteria, the antibacterial activity of PPP-TiO_2 was 1.5 times higher than that of PPP plus TiO_2 NPs. Furthermore, the results revealed that the diameter inhibition zone (DIZ) inhibited *S. aureus* better than *E. coli* and *P. aeruginosa*. Furthermore, the microbial populations and organic matter in real water samples were

determined using biological oxygen demand (BOD5). The results showed that samples containing PPP-TiO_2 had lower BOD5 values than TiO_2 NPs [115].

Thakur et al. [116] used *Azadirachta indica* leaf extract to synthesize titanium dioxide nanoparticles. The presence of terpenoids, flavonoids, and proteins, which are thought to be responsible for the production and stabilization of titanium dioxide nanoparticles, is indicated by FTIR research, while the crystalline character of titanium dioxide nanoparticles is revealed by XRD studies. The spherical form and size ranged from 15 to 50 nm, according to transmission electron microscopy photographs. TiO_2 nanoparticles were spherical in shape and ranged in size from 25 to 87 nm, according to SEM analysis. *Escherichia coli*, *Bacillus subtilis*, *Salmonella typhi*, and *Klebsiella pneumoniae* were used to test the antibacterial efficacy of produced TiO_2 nanoparticles and TiO_2 compound. The results showed that TiO_2 nanoparticles inhibited all of the bacteria from growing. When comparing TiO_2 nanoparticles to TiO_2 compound, the antibacterial activity is more prominent. *Salmonella typhi* and *Escherichia coli* had the lowest MIC (minimum inhibitory concentration) values of 10.42 g/mL of nanoparticles, but *Klebsiella pneumoniae* had the lowest MBC value of 83.3 g/mL.

2.8. Nickel and Nickel Oxide Nanoparticles (Ni and NiO NPs). Ni NPs and NiO NPs are attracting increasing interest in the research field. These nanoparticles have applications in many fields including energy, electronics, catalysis, environment, biological sensing, biomedicine, and corrosion inhibition [117].

Plant-based synthesis of Ni and NiO is used widely with a production rate that is very high compared with using microorganism. Infrared spectroscopy showed that the reduction in metal salts into their corresponding NPs was caused by secondary metabolites such as terpenoids, flavones, pyrones, aldehydes, amides, and carboxylic acids that were made from plant extracts [117].

Nickel (Ni) nanoparticles (NPs) were effectively prepared using metal salt and an extract of the leaves of the wild plant *Calotropis gigantea*, which acts as a reducing and stabilizing agent. After analyzing catalytic efficiency, the maximum methylene blue dye degradation efficiency was determined to be 98.8%. Synthesized NPs had shelf life of 3 months. Biological tests revealed that the prepared Ni NPs exhibited antibacterial properties against *E. coli* and *Bacillus subtilis* [118].

Additionally, Nio/NiO nanoparticles were prepared using the extract of the seeds of *Lactuca serriola*. The prepared Ni NPs were tested for their antibacterial activity and photocatalytic behavior. The prepared composite demonstrated antibacterial activity and promising photocatalytic feature [119].

There is increasing interest in preparing NiO NPs using different parts of plants including leaves, seeds, bark, and gum. The prepared green particles were applied in many fields due to their low toxicity. One of the major fields in application is using these nanoparticles as catalysis. NiO NPs were found to be photocatalysis for many pollutants [120–123]. They were also found to be electrocatalysis for oxygen evolution reactions [124].

Olajire and Mohammed prepared NiO NPs from leaf extract of *Ananas comosus* and utilized the synthesized NPs to promote polymer photodegradation. Using the solid-phase degradation of low-density polyethylene (LDPE) film, NiO NPs showed promising photocatalytic behavior. They accordingly suggested to include NiO NPs into the polymer matrix to promote its photodegradation [120].

The seeds extract of *Hordeum vulgare* plant, which is high in phenolic content and antioxidants, was used to reduce the precursor metal salt into nickel (Ni) and nickel oxide (NiO) nanoparticles (NPs). Ni and NiO were used as photocatalysts for the degradation of methylene blue dye [121].

Another utilization of seed extract was using the extract of *Salvia hispanica* L. (chia) seeds as the capping agent to prepare Ni NPs. The prepared nanoparticles displayed superparamagnetic behavior identified by VSM analysis and photocatalytic capacity and low cytotoxicity that is concentration-dependent. These interesting properties made greenly synthesized NiO NPs a strong candidate for a variety of applications, including disease prevention and the elimination of residual toxins [122].

Olive tree leaves were also used as a reducing agent for the production of NiO NPs using $Ni(NO_3)_2$ as a precursor and D-sorbitol as the capping agent. The NPs were used for adsorption application where they were tested against two dyes, methylene blue and methyl orange. The results showed adsorption capabilities of 96% for methylene blue and 88% for methyl orange [123].

Green synthesis of nickel oxide nanoparticles using phytochemicals from peels was also investigated. Selvanathan et al. used three different sources to prepare NiO NPs. Using nickel (II) acetate tetrahydrate as a precursor, three different green methods were used. Two of the used green methods are peels, which are the peel extract of papaya and dragon fruit, in addition to the leaf extract of aloe vera. The resulting NPs were then employed as electrocatalysts in the oxygen evolution reaction with aloe vera extract-mediated NiO_x NPs showing the highest electrocatalytic activity [124].

C. gigantea leaf extract was also used to prepare NiO NPs using a solution combustion technique. The nanoparticles were used as a sensor for nitrite pollutant in water and showed excellent photocatalysis behavior toward methylene blue with antibacterial activity [125].

NiO NPs have many applications in the energy field. The green-synthesized NPs were employed in energy storage devices, photodiodes, and supercapacitor.

NiO NPs were also synthesized using maize (*Zea mays* L.) dry silk extract. NiO NPs were used as the negative electrode in an asymmetric supercabattery device, and the activated carbon was the positive electrode. Due to the excellent electrochemical energy storage properties, this device can be considered strong candidate for future energy storage applications [126].

Cactus plant extract was used for the synthesis of NiO NPs. The synthesized NPs exhibited capabilities to be used for pseudo-capacitance [127]. *Allium cepa* bulb extract was

also used to produce nickel oxide nanoparticles with greater dielectric constants [128]. Guava leaves aqueous extract was also utilized as a green source to prepare NiO NPs that has potential application as electrodes in supercapacitor devices [129].

The biological application of NiO NPs synthesized using plant includes numerous researches. Applications include antibacterial and anticancer activity, acaricidal efficacy, biosensing, cellular metabolism, and pest management.

Nickel oxide nanoparticles (NiO NPs) were created using *E. heterophylla* (L.) leaf extract as a reducing/capping agent. On human erythrocytes, NiO NPs reveal important nontoxic qualities and interference in the activity of the coagulation cascade on PRP and PPP in human blood. NiO NPs have been shown to have strong bactericidal action against pathogenic bacterial strains. The nanoparticles also exhibit considerable cytotoxicity against human lung cancer (A549) and human hepatocarcinoma (HepG2) cell lines [130].

Suresh and Balamurugan prepared NiO NPs utilizing Moringa leaf extract using a sonication-assisted green synthesis approach. The prepared NPs showed antibacterial activity against Staphylococcus aureus and Escherichia coli [131].

Additionally, *Eichhornia crassipes* (Ec) extract was used to make nickel oxide nanoparticles (NiO NP), and the NP's influence on fermentative hydrogen generation was studied. Supplementing with ecosynthesized Eco-NO_2 NP was found to increase fermentation hydrogen generation and controls changes in critical node metabolites and gene expression that are necessary for cellular function and efficiency [132].

A new pesticide for arthropod pests based on greenly synthesized NiO NPs was studied by Abdel-Ghany et al. NiO was prepared using the aqueous extract of *Melia azedarach* ripened fruits. The synthesized NiO NPs were evaluated for their in vitro acaricidal efficacy against the camel tick *Hyalomma dromedarii*. NiO NPs showed a significant effect against various developmental stages of the tick [133].

The aqueous leaf extract of *Rauwolfia serpentina* was used to prepare NiO NPs. The prepared NPs were investigated against pulse beetle, Callosobruchus maculatus. Insects treated with NiO nanoparticles exhibited dose-dependent reductions in fecundity and lengthened developmental periods. In addition, no significant influence on seed germination was seen across treatments except at 40 ppm. So, making NiO NPs in an environmentally friendly way could be a big part of getting rid of bruchids in black gram and other pulses [134].

Sarkar et al. used an extract of the plant *Coriandrum sativum* to make nickel oxide nanoparticles (NiO NPs). UV-visible spectroscopy, UV-thermal melting, circular dichroism, and fluorescence spectroscopy were used to investigate the interaction of produced NiO NPs with calf thymus DNA (CT DNA). CT DNA was used in place of nucleic acid biosensors. The NiO NPs bonded electrostatically with CT DNA in all experimental investigations. It was concluded that NiO NP-nucleic acid coupled materials can be utilized as nanobiosensors for a variety of applications in pharmacy, environment, and detection [135]. Additionally, NiO NPs were used to enhance glucose sensing. The nanoparticles were manufactured using *Nigella sativa* extract were incorporated on glassy carbon electrode and used as sensor for glucose determination. The proposed sensor had a quick response time and high sensitivity to glucose with the detection limit of 3 μM [136].

Another important application of greenly synthesized NiO NPs was in the field of enhancing mechanical and chemical properties. The prepared nanoparticles when incorporated or coated on different matrices exhibited properties such as wettability, biocompatibility, improved thermal behavior, and anticorrosion behavior leading to different applications.

Ramalingam et al. used *Gymnema sylvestre* extracts to prepare nickel oxide nanoparticles. Electrospun polycaprolactone/gelatin hybrid nanofibrous mats were infiltrated with the produced nanoparticles creating nanofibrous mats with superior wettability, improved mechanical characteristics, biocompatibility, and robust antibacterial activity. These properties make these mats an efficient anti-infective wound dressing candidate [137].

Using *Delonix elata* leaf extract as a reducing and capping agent, nickel oxide nanoparticles (NiO NPs) were created utilizing an ultrasonic wave-assisted green synthesis method. The electrochemical corrosion behavior of NiO NPs was studied in the presence of different aqueous electrolyte media with different pH values. The synthesized NiO NPs were applied as coating on Zn and Mg leading to effectively reduced corrosion of the plates in all the media with a stronger effect in the acidic media (1 M H_2SO_4) [138]. In addition, Suresh and Balamurugan prepared NiO NPs utilizing Moringa leaf extract using a sonication-assisted green synthesis approach. The prepared NPs increased the corrosion resistance of Zn, [131].

In contrast to plants, there is very little literature on the synthesis of NiO nanoparticles utilizing fungus. Nonetheless, nickel oxide nanoparticles were produced by some types of fungi and algae. Fungi, both living and dead, were employed to create NiO NPs. Fungi may generate nanoparticles within their cells in a process known as intracellular synthesis or outside their cells in a process known as extracellular synthesis. Because of the restricted space within the cells, nanoparticles in the intercellular process are often smaller than those in the extracellular process [139].

Marine macroalgae extract was also employed as a reducing and coating agent to produce nickel oxide nanoparticles. The nanoparticles had a crystalline form and a spherical shape with a mean particle size of 32.64 nm. TGA measurements revealed the presence of organic elements originating from the sea on the surface of NiO NPs. The prepared nanoparticles were found to be very effective catalyst for the production of pyridopyrimidine derivatives in aqueous conditions. The green catalysis led to faster reactions, higher yields (up to 96%), recyclability (7 runs), and environment-friendly process [140].

Figure 5 exhibits TEM images of NiO NPs, Co_3O_4 NPs, Fe_2O_3 NPs, and TiO_2 NPs synthesized via different green techniques.

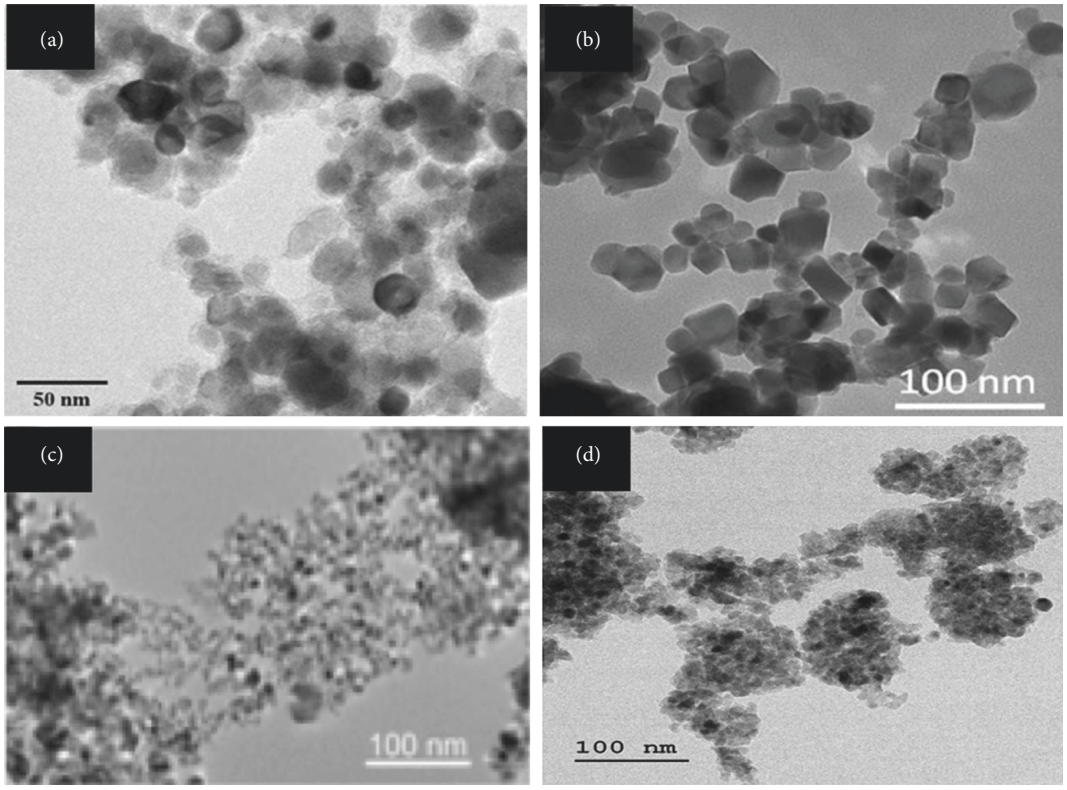

Figure 5: TEM images of (a) NiO NPs [136], (b) Co_3O_4 NPs [98], (c) Fe_2O_3 NPs [103], and (d) TiO_2 [110].

2.9. Aluminum Oxide Nanoparticles (Al_2O_3 NPs). Biological methods are employed to create Al_2O_3 NPs in diverse morphologies and sizes from plant components such as leaves, seed fruits, and flowers. The hydrophilic heterocyclic components are primarily responsible for nanoparticle production and stability [141]. Al_2O_3 NPs were also synthesized using food such as tea and caffeine [142] and using algae [143] and fungi [144].

Sumesh et al. used the aqueous leaf extract of "*Muntingia Calabura*" to prepare aluminum oxide nanopowder. The prepared particles were employed as a filler powder for the sisal/coir, sisal/banana, and banana/coir-based hybrid composites. Adding only 3% of weight of Al_2O_3 NPs had a significant effect on their mechanical properties and degradation temperature [145, 146]. The nanopowder made the flexural properties of hybrid fibers better by reducing the empty space and making sure that the fibers and matrix were well attached [147].

Al_2O_3 NPs prepared using the extract of neem leaves were also applied to enhance the mechanical properties of the cutting tools made of cement carbide. The nanoparticles were self-adherent to the cutting texture gaps. The presence of the nanoparticles was found to improve the properties and hence the performance of the cutting tools [148].

Additionally, the extract of *Aerva lanata* leaves and terminalia chebula seeds was used to produce Al_2O_3 NPs. The size and shape of the nanoparticles formed were different, having a shape of spherical agglomeration and a size in the range of 50–70 nm in the case of Aerva lanata leaves while having a sphere and a size range of 50–100 nm in the case of *Terminalia chebula* seeds [149].

Five different plants were also used to prepare Al_2O_3 NPs. *Syzygium aromaticum*, *Origanum vulgare*, *Origanum majorana*, *Theobroma cacao*, and *Cichorium intybus* extracted were utilized in the microwave-assisted synthesis using aluminum nitrate as a precursor. The average size of clusters of nanoparticles varied with different routes from 60 nm to 300 nm [150].

Using *Lyngbya Majuscula* algae extract, high-efficiency, cost-effective, and green aluminum nanoparticles (Al_2O_3 NPs) were synthesized. Al_2O_3 NPs showed antibacterial efficacy toward several bacterial strains, *Streptococcus aureus*, Bacillus subtilis, *Klebsiella pneumoniae*, *Salmonella Paratyphi*, *Candida albicans*, and *Aspergillus flavus* [143].

Using an extract from the algae *Sargassum ilicifolium* as bioreducing and a stabilizing agent, ceramic alpha aluminum oxide nanoparticles were prepared. The synthesized Al_2O_3 nanoparticles exhibited high purity, were a rhombohedral shape, and were alpha crystalline in nature with an average size of 20 ± 2.1 nm [151].

Al_2O_3 NPs were prepared using the fungus *Colletotrichum sp*. The in vitro studies of the nanoparticles' antibacterial properties against several foodborne pathogens showed that Al_2O_3 NPs were especially effective against *F. oxysporum* and can be considered as an effective antimicrobial agent to prevent food deterioration caused by food pathogens [144].

2.10. Chromium and Chromium Oxide (Cr and Cr_2O_3). Cr_2O_3 stands out among metal oxides due to its unique thermodynamic stability, hardness, chemical resistance, and

antiferromagnetic characteristics. Cr_2O_3 also exhibits *n*-type and *p*-type semiconductor properties. For making Cr_2O_3 NPs, researchers have looked into reducing and stabilizing agents made from different biological sources [152].

Satgurunathan et al. prepared chromium nanoparticles (Cr NPs) using the *Allium sativum* aqueous extract and potassium dichromate as a precursor. The synthesized nanoparticles were found to be effective in boosting the growth of prawn *Macrobrachium rosenbergii* (Cr NP) by using them as dietary supplements [153].

Chromium oxide (Cr_2O_3) nanoparticles were also synthesized using *Abutilon indicum* (L.) sweet leaf extract as a reducing and capping agent. The prepared nanoparticles had antioxidant and anticancer efficacy toward cancerous cells MCF-7 compared with the chemically prepared nanoparticles. Additionally, the biosynthesized nanoparticles were found to be more biocompatible with Vero cell lines than nanoparticles prepared by chemical methods (Figure 6). This increased efficiency for the greenly synthesized nanoparticles could be attributed to the synergetic effect of the plant phytochemicals and the nanoparticles [154].

Ahmed Mohamed et al. used *Hyphaene thebaica* as a bioreductant to produce chromium oxide nanoparticles (Cr_2O_3 NPs) for nanomedicinal uses. The nanoparticles had a size of around 25–38 nm. In vitro experiments were used to assess the biological characteristics of Cr_2O_3 NPs that showed biocompatibility and antibacterial and antioxidant activity. Additionally, the greenly synthesized nanoparticles showed inhibition of poliovirus at moderate levels [155].

Hassan et al. used *Callistemon viminalis* (bottle brush) flower extracts as a reducing and capping agent to make Cr_2O_3 nanoparticles (NPs). The prepared nanoparticles had high crystallinity and different sizes based on the annealing temperature with diameters of 15 and 17 nm by annealing them at 400 and 500°C, respectively. The prepared nanoparticles showed strong antibacterial activity. An MTT cytotoxic test was performed on *Leishmania tropica* amastigotes and promastigotes to test anticancer activity, yielding IC50 values of 44 g/ml and 10.56 g/ml, respectively. The anticancer activity test was also performed against HepG2 cancer cells, showing IC50 of 46.32 g/ml. Furthermore, Cr_2O_3 NPs showed strong DPPH radical scavenging, moderate reducing power, and overall antioxidant potential [156].

A simple, straightforward green synthesis technique was used by Sackey et al. to biosynthesize selective single-phase black-Cr_2O_3 nanoparticles. The procedure includes utilizing the extract of sweet potato skins and chromic nitrate salt as a precursor. A linear increase in the magnetism of Cr_2O_3 nanoparticles with the field strength was found, which was suggested to be due to the presence of uncompensated spins at the nanoparticles' surface, leading to a nonmagnetic or antiferromagnetic state. The structural, electronic, and magnetic characteristics of Cr_2O_3 were further confirmed using density functional theory (DFT) [157].

Sharma and Sharma prepared Cr_2O_3 NPs from *Cannabis sativa* leaf extract. The nanoparticles demonstrated anticancer activity against HepG2 cell line. They also showed anticorrosion behavior showing a maximal corrosion inhibition efficacy at 303 K [158].

Pomegranate extract was also used to produce chromium oxide nanoparticles from $K_2Cr_2O_7$ salt solutions. The prepared nanoparticles were utilized in a nanocomposite with polyamide. The produced nanocomposite was applied to adsorb U(VI) from polluted water [159].

Chromium oxide nanoparticles were produced by reducing potassium dichromate solution with natural honey as a reducing agent. Natural honey contains carbohydrates that are constituted a major component in the synthesis process. The prepared nanoparticles expressed both antioxidant and antibacterial activities [160].

Bacteria strains were also used as a reducing and capping agent to prepare chromium oxide nanoparticles. *Erwinia amylovora* bacteria were used to biosynthesize Cr_2O_3 NPs. The size of NPs was observed to be 32.35 nm nanometers. The prepared nanoparticles were tested for antibacterial activity, and they showed inhibition for bacterial growth [161].

Using effluent from electroplating bacteria strain *Bacillus subtilis*, Kanakalakshmi et al. prepared Cr(III) nanoparticles. The nanoparticles ranged in size from 4 to 50 nm. Several bacterial strains were inhibited by the prepared nanoparticles suggesting their antibacterial efficacy [162]. Fungi were also employed to make Cr_2O_3 nanoparticles. Using a biological method, Chromium oxide nanoparticles were created using a fungal extract of Aspergillus Niger. According to the XRD analysis and EDX, the size of biologically generated Cr_2O_3 NPs is 36 nm with a hexagonal shape. The EDX demonstrated further that the produced nanoparticles were pure with small amount of impurities in the sample [163].

Figure 7 depicts some of TEM images of Al_2O_3 NPs and Cr_2O_3 NPs synthesized via different green methods.

2.11. Rare Earth Metal and Their Oxides Nanoparticles (RE NPs). Rare earth oxides are attracting increasing interest due to various properties including luminescence efficiency, catalysis, biological activity, photocatalysis, electronics, and sensors. Green synthesis techniques involving diverse plants such as algae, bacteria, and fungus are replacing the usage of physical and chemical resources in the creation of nanostructures.

2.11.1. Samarium and Samarium Oxide Nanoparticles (Sm and Sm_2O_3 NPs). The inherent characteristics of samarium oxide (Sm_2O_3) piqued the interest of researchers. Sm_2O_3 is used for IR radiation absorption in glass, as catalytic oxides for organic reactions, and as neutron absorption control rods in nuclear power reactors. Sm_2O_3 is a high k-dielectric substance that has been intensively researched for its prospective use in several electronic devices.

Samarium nanoparticles were produced from ginger extract utilizing a green chemistry synthesis technique. The synthesized metal nanoparticles showed anticancer efficacy against human colorectal cancer cells. The cytotoxicity results showed that IC50 values for samarium nanoparticles on

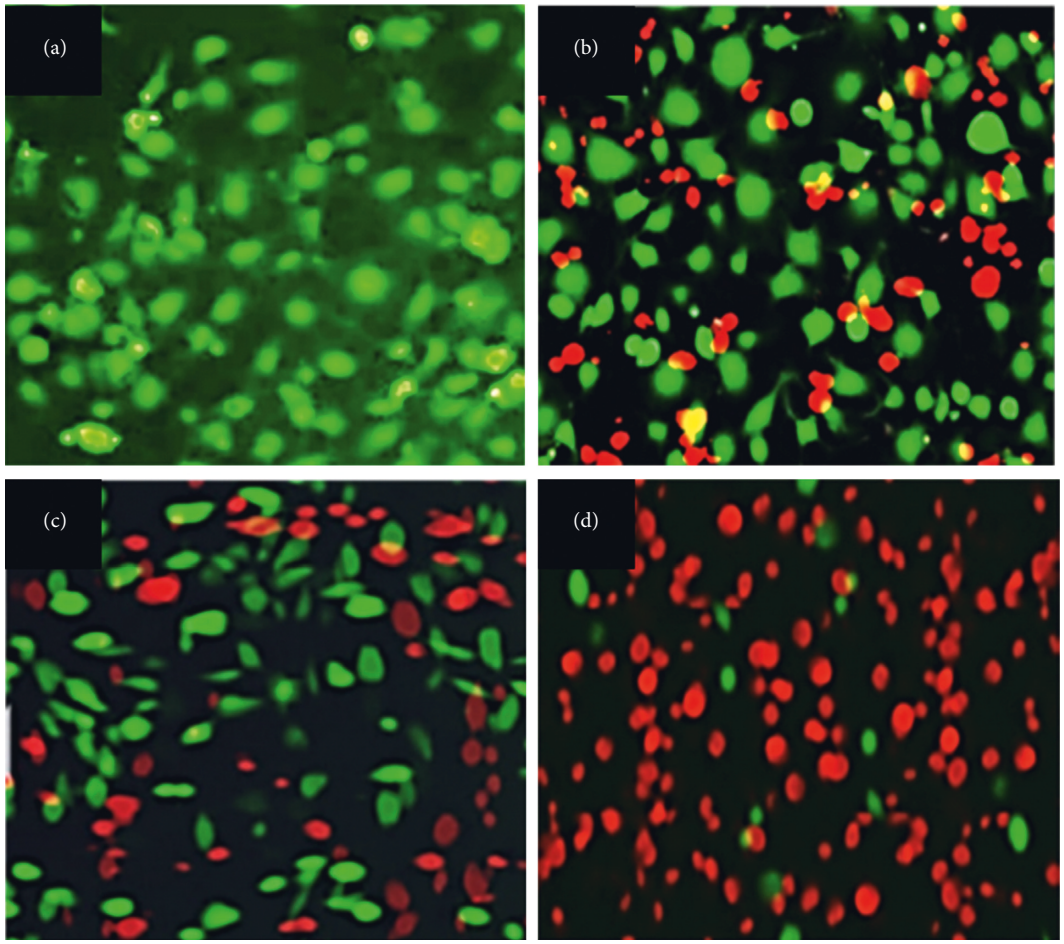

Figure 6: Anticancer activity against MCF-7 cancer cells. The green dyed cells are the live cells, while red dyed cells are the dead cells. (a) Control, (b) treated with plant extract, (c) treated with chemically synthesized Cr_2O_3 NPs, and (d) treated with green-synthesized Cr_2O_3 NPs [154].

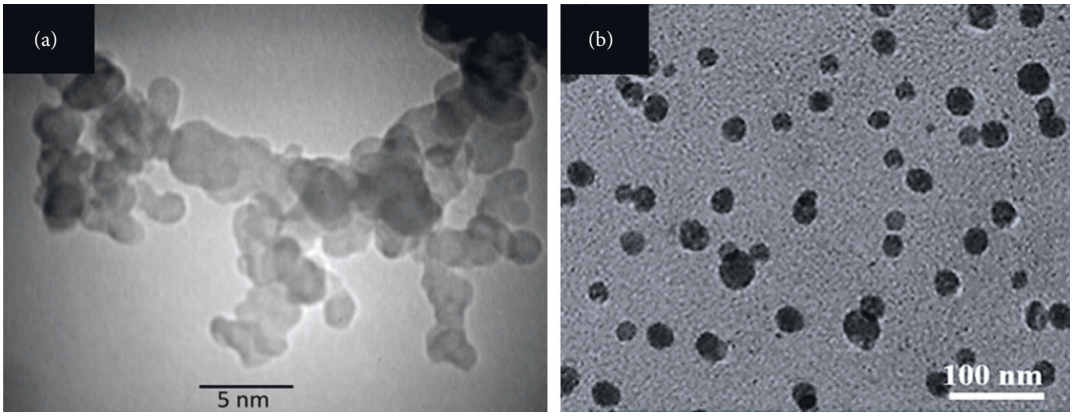

Figure 7: TEM images of (a) Al_2O_3 NPs [150] and (b) Cr_2O_3 NPs [154].

the HCT116 cell line had a value of 90 (equivalent to 23.1 mg/ml) and 81 M (equivalent to 20.7 mg/ml) after 24 and 48 hours of incubation durations, respectively [164].

Muthulakshmi et al. prepared samarium oxide nanoparticles using the hydrothermal method and utilized the leaf extract of *Andrographis paniculata*. The prepared nanoparticles had body-centered cubic structure and average size of 30–50 nm. The metal oxide nanoparticles showed antibacterial, anti-inflammatory, and antioxidant efficacy. The antibacterial behavior was observed against *E. coli* and *S. aureus,* and the antioxidant activity was found to be stronger than vitamin C [165].

Samarium oxide nanoparticles were also prepared using the flower extract of *Hibiscus syriacus* Ardens. The greenly

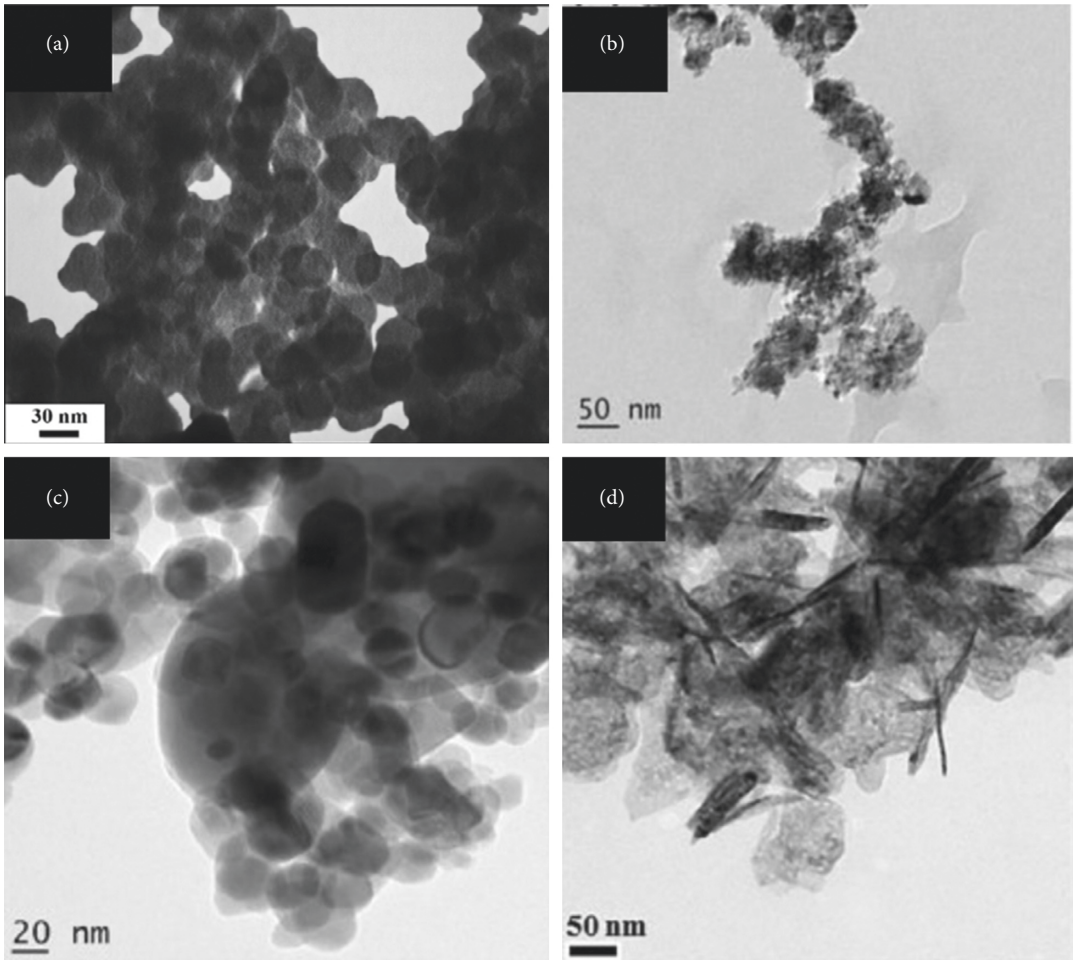

Figure 8: TEM images of (a) Sm_2O_3 NPs [166], (b) CeO_2 NPs [175], (c) La_2O_3 NPs [187], and (d) Y_2O_3 NPs [190].

synthesized nanometal oxide was used as a catalyst for benzimidazole derivative synthesis. Many advantages were attributed to the use of Sm_2O_3 NPs including high yield, faster reactions, simpler synthesis process, and greener approach. The catalysis was recovered and reused 4 times while maintaining its activity [166].

Sm_2O_3 nanoparticles (NPs) were synthesized using *Caesalpinia pulcherrima* leaf extract (CPE), as a reducing and capping agent. Sm_2O_3 NPs had a cubic shape and an average size of 73.27 nm. The photocatalytic activity of Sm_2O_3 NPs is operated at an E_g of 4.76 eV, which is in the UV region. Sm_2O_3 NPs were found to obtain photocatalysis behavior toward malachite green under UV lighting. 80.14% of malachite green degraded in two hours when utilizing Sm_2O_3 nanoparticles as a photocatalyst [167].

Microwave-assisted synthesis of samarium oxide (Sm_2O_3) nanoparticles with a narrow size distribution without the need of a surfactant or template was effective, and the approach was dubbed "green synthesis" since strong bases and acids were replaced with environmentally benign urea. The particle size changed with changing the concentration of urea. The lowest size of nano-Sm_2O_3 nanoparticles (13–16 nm) was discovered at a urea concentration of 1.2 mol/L by adjusting the urea content. The prepared nanoparticles showed outstanding UV-responsive characteristics and distinguished deep UV and NIR regions, which proposed their possible application in photoelectric devices [168].

Another method employed the bacterium *Anabaena cylindrica*, which bioaccumulates Sm^{3+} and then generates nanosized intracellular Sm particles exclusively in its less numerous heterocysts (HCs). *A. cylindrica* was discovered to be an appropriate representative microorganism for green Sm recovery and the production of easily identifiable Sm NPs. *A. cylindrica* was only effective in its HCs and not in its vegetative cells (VCs), which had an average size of 9–12 nm [169, 170].

2.11.2. Cerium Oxide Nanoparticles (CeO_2 NPs). Due to its various uses in catalysis, cancer treatment, photocatalytic degradation of pollutants, sensors, and polishing agents, cerium oxide nanoparticles (CeO_2 NPs) are gaining increasing demands in a variety of sectors. Various green approaches have been used to prepare cerium oxide NPs; however, plant extract is most commonly used [171–173]. Food-based items such as starch, sugar, a mixture of seashell, *Aloe vera* (*A. vera*), grapes, pomegranates, and diluted egg whites have also been utilized as

Table 2: Most important characteristics of nanoparticles synthesized using plant extracts.

NPs	Green synthesis agent	NP precursor	NP size	NP application	Year	Reference
Ag	*Camellia sinensis* and *Prunus africana*	$AgNO_3$	17–21	Antibacterial	2019	[24]
Ag	*Citrus limetta* peel	$AgNO_3$	18	Antimicrobial	2020	[25]
Ag	*Parkia speciosa* leaves	$AgNO_3$	31–35	Photocatalyst	2019	[26]
Ag	*Gomphrena globosa* (globe amaranth) leaf	$AgNO_3$	15.64–22.61	Antibacterial	2020	[27]
Ag	*Sambucus ebulus*	$AgNO_3$	30–35	Photocatalyst, antibacterial, and anticancer	2022	[29]
Ag	*Panax ginseng*	$AgNO_3$	50–90	Antifungal	2021	[30]
Ag	Hydroxyethyl cellulose	$AgNO_3$	3–8	Antibacterial strain sensor	2021	[31]
Au	Licorice root	$HAuCl_4$	53.7	Antimicrobial, anticancer	2021	[36]
Au	Mentha	$HAuCl_4$	Not detected	Electrochemical sensor	2019	[38]
Au	*Combretum erythrophyllum*	$HAuCl_4$	4–38	Antimicrobial, anticancer	2021	[39]
Au	*Ananas comosus*	$HAuCl_4$	18.85	Photocatalyst	2021	[40]
Au	*Curcuma pseudomontana*	$HAuCl_4$	39	Antimicrobial, antioxidant, anti-inflammatory	2021	[41]
Au	*Pimenta dioica* leaves	$HAuCl_4$	Not detected	Photocatalyst, antioxidant, antibacterial agents	2021	[42]
Au	Seed extract of *Trachyspermum ammi*	$HAuCl_4$	16.63	Anticancer	2021	[43]
Au	*Benincasa hispida*	$HAuCl_4$	22.18	Cytotoxicity antimicrobial	2021	[44]
ZnO	The callus extract	$Zn(CH_3COO)_2$	16.43	Antibacterial and antifungal application	2021	[56]
ZnO	*Syzygium cumini*	$Zn(CH_3COO)_2$	10–12.55	Photocatalytic degradation	2021	[61]
ZnO	Leaf extract of *Parthenium hysterophorus*	$Zn(NO_3)_2$	10	Antimicrobial and vegetative growth applications	2021	[62]
ZnO	*Becium grandiflorum* leaf	$Zn(CH_3COO)_2$	1.35	Antimicrobial activity and adsorption of methylene blue	2021	[63]
ZnO	*Dysphania ambrosioides* extract	$Zn(NO_3)_2$	5–30	Antibacterial properties	2021	[64]
ZnO	*Lantana camara* flowers	$Zn(NO_3)_2$	21.4–27.2	Photocatalytic, electrochemical, anti-inflammatory	2021	[65]
ZnO	*Passiflora foetida* fruit peels	$Zn(NO_3)_2$	58	Degradation of hazardous organic dye	2021	[66]
ZnO	Fern-like microleaves	$ZnCl_2$	Not detect	Photocatalytic, photocorrosion, resistance, recyclability	2019	[52]
ZnO	*Justicia spicigera*	$Zn(NO_3)_2$	10–100	Photocatalytic activity	2021	[67]
ZnO	*Nilgirianthus ciliatus* leaf	$ZnSO_4$	20	Its antibacterial activity, anticancer	2021	[68]
ZnO	Vegetable extracts (onion, cabbage, carrot, and tomato)	$Zn(CH_3COO)_2$	17–24	Dye sensitivity solar cells	2021	[51]
ZnO	*Cocos nucifera* leaf	$Zn(CH_3COO)_2$	109–215	Antibacterial biocompatible carrier in drug delivery	2022	[69]
CuO	*Aerva javanica* plant leaf	$CuCl_2$	18 to 23	Antibacterial application	2021	[75]
CuO	*Calotropis procera*	$CuSO_4$	20 to 80	Antibacterial application, antifungal application	2022	[76]
CuO	*Rubia cordifolia* bark extract	$CuSO_4$	50.72	Antibacterial, antioxidant, larvicidal photocatalytic	2022	[77]
CuO	*Thespesia populnea*	$Cu(CH_3COO)_2$	60 to 80	Antimicrobial application	2022	[78]
CuO	*Allium sativum* extract	$Cu(NO_3)_2$	20–50	Antimicrobial, antioxidant, antilarvicidal	2020	[79]
Co_3O_4	*Euphorbia heterophylla L.* leaf extract	$Co(NO_3)_2$	69.75	Photocatalytic activity	2019	[94]
Co_3O_4	Walnut green skin extract	$Co(NO_3)_2$	60–80	Magnetic applications	2021	[95]
Co_3O_4	*Jumbo Muscadine* (*Vitis rotundifolia*)	$CoCl_2$	650	Photocatalytic activity	2020	[96]
Co_3O_4	*Moringa oleifera* natural extract	$CoCl_2$	20–50	High-performance hybrid supercapacitors	2018	[97]
Co_3O_4	Leaf extract of *Populus ciliata* (Safeda)	$Co(NO_3)_2$	25–35	Potential biological	2020	[98]
Co_3O_4	*Piper nigrum* (*P. nigrum*) leaf extract	$CoSO_4$	21.68–77.48	Biological properties	2021	[99]
Co_3O_4	An endemic species *Allium tuncelianum*	$Co(NO_3)_2$	23	Anticancer activity	2021	[100]
Fe_3O_4	Aqueous fruit extract of edible *C. guianensis*	$FeCl_3$	17 ± 10	Antibacterial and cytotoxicity activities	2018	[102]

Table 2: Continued.

NPs	Green synthesis agent	NP precursor	NP size	NP application	Year	Reference
Fe_3O_4	*Punica granatum* fruit peel extract	$FeCl_3FeCl_2$	14.38	Magnetic hyperthermia therapy, MRI nanoagent drug delivery in colorectal cancer	2021	[103]
Fe_3O_4	Aqueous extract of *Graptophyllum pictum* leaf	$FeSO_4$	23.17	Medical applications such as drug carrier and targeted therapy	2017	[104]
Fe_3O_4	*Lagenaria siceraria* leaf extract	$FeCl_3$	30–100	Biological applications	2017	[105]
Fe_3O_4	Aqueous extract of spent tea waste	$Fe_2(SO_4)_3$	15.5	Drug delivery system	2020	[106]
Fe_3O_4	Aqueous extracts of *Pandanus odoratissimus* leaves	$FeCl_3FeSO_4$	~5.0	Efficient bifunctional electrocatalytic activity	2018	[107]
Fe_3O_4	*Phyllanthus niruri* extract	$(NH_4)_2Fe(SO_4)_2$	15	Antimicrobial activity	2018	[108]
Fe_3O_4	*Phyllanthus emblica* (amla) leaf extract	$Ti(OCH(CH_3)_2)_4$	20–30	Optical and photocatalytic water purification	2020	[110]
TiO_2	*Carica papaya* leaf extract	$Ti(OC_3H_7)_4$	15.6	A photocatalyst	2019	[111]
TiO_2	*Bixa orellana* seed extract	$Ti(C_4H_9O)_4$	306	Solar cells	2019	[112]
TiO_2	*Syzygium cumini* leaf extract	$Ti(OC_3H_7)_4$	10	Photocatalytic removal of lead (Pb) in explosive industrial wastewater	2020	[113]
TiO_2	Lemon peel extract	TiO_2	80–140	Photocatalytic activity	2022	[114]
TiO_2	Pristine pomegranate peel extract	$Ti(OCH(CH_3)_2)_4$	620	Antimicrobial activity for water disinfection	2019	[115]
TiO_2	*Azadirachta indica* leaf extract	TiO_2	25–87	Antibacterial activity	2019	[116]
Ni	*Calotropis gigantea* leaves	$Ni(NO_3)_2$	20–40	Photocatalyst antibacterial agent	2018	[118]
Ni^o/ NiO	*Lactuca serriola* seeds	$NiCl_2$	<100	Photocatalyst antibacterial agent	2022	[119]
NiO	*Ananas comosus* leaves	$NiCl_2$	1.42 ± 1.76	Photocatalyst	2020	[120]
NiO	*Hordeum vulgare* seeds	$Ni(NO_3)_2$	Not detected	Photocatalyst	2020	[121]
NiO	*Salvia hispanica L.* (chia) seeds	$Ni(NO_3)_2$	30	Photocatalyst	2021	[122]
NiO	Olive tree leaf	$Ni(NO_3)_2$	42	Adsorption	2022	[123]
NiO	Peel of papaya peel of dragon fruit, leaf of *Aloe vera*	$Ni(CH_3COO)_2$	8.1–11.5	Electrocatalysts	2021	[124]
NiO	*C. gigantea* leaves	$Ni(NO_3)_2$	31	Sensor for nitrite photocatalyst antibacterial agent	2020	[125]
NiO	Maize (*Zea mays L.*) dry silk	$Ni(CH_3COO)_2$	10–20	Electrochemical	2020	[126]
NiO	*Opuntia ficus* (cactus)	$Ni(NO_3)_2$	16	Pseudo-capacitance	2020	[127]
NiO	*Allium cepa* bulb	$Ni(NO_3)_2$	30–90	Capacitor applications	2022	[128]
NiO	Guava leaves	$NiSO_4$	70–100	Electrodes in supercapacitor devices	2021	[129]
NiO	*E. heterophylla (L.)* leaves	$Ni(NO_3)_2$	12–15	Anticancer and antibacterial agent	2020	[130]
NiO	Moringa leaf	$Ni(NO_3)_2$	12	Antibacterial agent anticorrosion	2021	[131]
NiO	*Eichhornia crassipes*	$NiCl_2$	9.1 ± 2.6	Cellular function and efficiency	2021	[132]
NiO	*Melia azedarach* ripened fruits	$Ni(NO_3)_2$	21–35	Acaricidal activity	2021	[133]
NiO	*Rauwolfia Serpentina*	$Ni(NO_3)_2$	4–20	Pest management	2021	[134]
NiO	*Coriandrum sativum*	$Ni(CH_3COO)_2$	95	Nanobiosensors	2020	[135]
NiO	*Nigella sativa*	$Ni(NO_3)_2$	20	Sensor for glucose determination	2022	[136]
NiO	*Gymnema sylvestre*	$Ni(NO_3)_2$	17 ± 2	Wound dressing	2019	[137]
NiO	*Delonix elata* leaf	$Ni(NO_3)_2$	17–18	Anticorrosion	2021	[138]
Al_2O_3	*Muntingia calabura* leaf	$Al(NO_3)_3$	50.16	Filler to enhance mechanical properties	2019	[145, 146]
Al_2O_3	Neem leaves	$AlCl_3$	525.25	Enhance mechanical properties	2019	[148]
Al_2O_3	*Aerva lanta* leaves and *Terminalia chebula* seeds	$Al(NO_3)_3$	50–100	Not detected	2018	[149]
Al_2O_3	*Syzygium aromaticum*, *Origanum vulgare*, *Origanum majorana*, *Theobroma cacao*, and *Cichorium intybus*	$Al(NO_3)_3$	10	Not detected	2017	[150]
Cr	*Allium sativum*	$K_2Cr_2O_7$	31–64	Dietary supplements for prawns	2019	[153]
Cr_2O_3	*Abutilon indicum (L.)* sweet leaf	$Cr_2(SO_4)_3$	17–42	Anticancer and antioxidant agent	2021	[154]
Cr_2O_3	*Hyphaene thebaica* plant	$Cr(NO_3)_3$	25–38	Anticancer antioxidant agent poliovirus inhibition	2020	[155]
Cr_2O_3	*Callistemon viminalis* (bottle brush) flower	$K_2Cr_2O_7$	15–17	Antibacterial agent anticancer agent antioxidant activity	2019	[156]

Table 2: Continued.

NPs	Green synthesis agent	NP precursor	NP size	NP application	Year	Reference
Cr_2O_3	Sweet potato skins	$Cr(NO_3)_3$	17–50	Magnetic applications	2021	[157]
Cr_2O_3	*Cannabis sativa* leaf	$Cr(NO_3)_3$	85–90	Anticorrosion	2021	[158]
Cr_2O_3	Pomegranate extract	$K_2Cr_2O_7$	12	Adsorption	2021	[159]
Sm_2O_3	Ginger	$SmCl_3$	69.2	Anticancer activity	2019	[164]
Sm_2O_3	*Andrographis paniculata* leaf	$SmCl_3$	30–50	Antibacterial, anti-inflammatory, and antioxidant activity	2020	[165]
Sm_2O_3	*Hibiscus syriacus* Ardens	$Sm(NO_3)_3$	30–70	Catalyst	2021	[166]
Sm_2O_3	*Caesalpinia pulcherrima* leaf	$Sm(NO_3)_3$	73.27	Photocatalysis	2020	[167]
Sm_2O_3	Bacterium *Anabaena cylindrica*	$Sm(NO_3)_3$	9–12	Not detected	2019 2022	[169, 170]
CeO_2	*Brahma kamal* leaf	$Ce(NO_3)_3$	3–5	Catalysis	2022	[175]
CeO_2	*Hoodia gordonii*	$Ce(NO_3)_3$	4.68–71.3	Nanocosmetics	2022	[176]
CeO_2	*Rubia cordifolia L.* leaf	$Ce(NO_3)_3$	22	Anticancer	2018	[177]
CeO_2	*Azadirachta indica*	$Ce(NO_3)_3$	10–50	Improve diesel engine efficiency	2022	[178]
La	*Muntingia calabura* leaf	$La(NO_3)_2$	>100	Antibacterial antioxidant photocatalytic	2020	[185]
La_2O_3	*Datura metel* leaf	$La(NO_3)_2$	200–500	Not detected	2019	[186]
La_2O_3	*Centella asiatica* leaf Tridax leaf	$La(NO_3)_2$	20	Photocatalysis antimicrobial	2022	[187]
Y_2O_3	*Liriope platyphylla* rhizome	$Y(NO_3)_3$	10–15	Catalysis	2017	[189]
Y_2O_3	Forsythiae Fructus fruit	$Y(NO_3)_3$	11	Anticancer	2018	[190]

extracts to generate CeO_2 NPs [171]. Natural macromolecule polymers may also be employed as templates for bio-directed synthesis of CeO_2 NPs [174].

Cerium oxide nanoparticles were prepared using the leaf extract of Brahma Kamal in aqueous solution. The resulting nano-oxide was employed as an efficient catalysis in the reaction of amino acyl chloride derivatives with NaHSe followed by adding α-bromoesters to synthesize selenoesters of amino acids [175].

Ditlopo et al. used *Hoodia gordonii* natural extract as a chelating agent in the biosynthesis of CeO_2 nanocrystals. In the solar spectrum, the diffuse reflectivity profile of such CeO_2 revealed a unique UV selectivity. While UV reflectance is modest, it reaches 63% in the visible and near infrared. Their relative generation of reactive oxygen species (ROS) was found to be less than 1 throughout a broad concentration range (0.5–1000 g/ml). This high photostability combined with good UV selectivity suggested employing green CeO_2 nanocrystals in nanocosmetics [176].

Cerium oxide (CeO_2) nanoparticles (NPs) were produced using *Rubia cordifolia* L. leaf extract as a reducing agent. CeO_2 NPs underwent partial agglomeration that took a net structure. The greenly synthesized nanoparticles showed anticancer activity using MTT and reactive oxygen species (ROS) quantification tests against MG-63 human osteosarcoma cells. The treated cells were found to have loss of cell membrane integrity, oxidative stress, and apoptosis as a result of treating them with cerium oxide (CeO_2) nanoparticles [177].

CeO_2 nanoparticles were also synthesized using *Azadirachta indica* plant extract. Adding biosynthesis-derived cerium oxide nano-additions to the LGO25 fuel mix was found to be an excellent way to improve diesel engine performance while lowering emissions [178].

Cerium oxide nanoparticles (CeO_2 NPs) were synthesized in an ecologically friendly and cost-effective manner using bioactive natural ingredients such as flower honey, pine honey, chestnut honey, and turmeric extracts. The synthesized nanoparticles' sizes, surface charges, morphologies, band gap energies, antioxidants, and photocatalytic activity were compared. The synthesized CeO_2 NPs were of spherical forms. Honey-derived NPs had particle sizes of 1.23, 2.61, and 3.02 nm for blossom, chestnut, and pine honey, respectively. Turmeric extract yielded NPs with a particle size of 6.08 nm. According to the DPPH technique, all green-synthesized nanoparticles had strong antioxidant activity, with IC50 values ranging from 32.4 to 64.5 μg/ml. Under UV light irradiation, high degradation efficiencies (between 83.9 and 93.4%) for methylene blue dye were achieved due to the CeO_2 NPs' strong redox property [179].

Interestingly, an innovative method using marine oyster extract has also been employed to prepare CeO_2 NPs. Marine oyster extract is an effective source of bioreducing and capping/stabilizing agents that was used in a one-pot method to prepare CeO_2 NPs. The nanoparticles had face-centered cubic shape with an average size of 15 nm according to SEM and TEM. The prepared nanoparticles exhibited biocompatibility. Furthermore, the nano-oxide showed photocatalytic activity toward methylene blue with degradation of 99% [180].

Khaligh and Asoodeh prepared cerium oxide nanoparticles (CeO2 NPs) utilizing *Spirulina platensis* microalgae. After preparation was done, CeO_2 NPs were nanoencapsulated using an ultrasonic emulsification process to produce create cerium oxide nanoemulsion (CeO_2-NE). CeO_2-NE had a stronger impact on cancerous colon cell HT29, bacterial growth, antioxidant capability, and ferric ion reduction [181].

Table 3: Most important characteristics of nanoparticles synthesized using microorganisms.

NPs	Green synthesis agent	NP precursor	NP size	NP application	Year	Reference
Algae						
Ag	Brown algae	$AgNO_3$	18–29	Antibacterial	2020	[28]
ZnO	*Ulva lactuca* seaweed extract	$Zn(CH_3COO)_2$	10–50	Antimicrobials and insecticides	2018	[58]
NiO	Marine macroalgae	$NiCl_2$	32.64	Catalyst	2021	[140]
Al_2O_3	*Lyngbya majuscula* algae	$KAl(SO_4)_2$	36.42	Antibacterial agent	2022	[143]
Al_2O_3	*Sargassum ilicifolium* algae	$Al_2(SO_4)_3$	20 ± 2.1	Not detected	2018	[151]
CeO_2	*Spirulina platensis* microalgae	Not detected	Not detected	Anticancer antibacterial antioxidant	2022	[181]
CeO_2	Carrageenan hydrogel	$Ce(NO_3)_3$	18–60	Medicinal application	2018	[182]
Bacteria						
Ag	Bacterial T10 strain	$AgNO_3$	46–52.7	Antimicrobial	2018	[32]
Ag	*Desertifilum* IPPAS B-1220	$AgNO_3$	4.5–26	Antibacterial cytotoxicity	2020	[33]
Au	*Paracoccus haeundaensis*	$HAuCl_4$	20.93	Antioxidant activity antiproliferative of cancer cell lines	2019	[45]
ZnO	*Lactobacillus spp.*	$Zn(CH_3COO)_2$	32	Antimicrobial and anticancer application	2021	[70]
ZnO	Lactic acid bacteria	$Zn(NO_3)_2$	20	Antibacterial activity-biosensors in medical diagnostics or food control	2018	[71]
ZnO	*Lactobacillus gasseri*	$ZnSO_4$	22	Antimicrobial activity on food pathogens	2021	[72]
ZnO	Ureolytic bacteria	$Zn(CH_3COO)_2$	10–15	Photocatalytic activity of textile dye	2020	[73]
ZnO	*Bacillus megaterium* (NCIM 2326) cell-free extract	$ZnNO_3$	45 to 150	Antibacterial application	2018	[74]
CuO	Endophytic actinomycetes *Streptomyces spp.*	$CuSO_4$	78–80	Biotechnological application	2019	[83]
CuO	Marine entophytic actinomycetes	$CuSO_4$	20	Medicinal applications against biofilm-producing bacteria and cancer cells	2022	[88]
CuO	*Shewanella loihica* PV-4	$CuCl_2$	10–16	Microbial pollution management in drinking water	2018	[89]
CuO	Marine Streptomyces sp.	$CuSO_4$	1.72–13.49	Biological applications	2021	[10]
CuO	Probiotic bacteria (*Lactobacillus casei subsp. Casei*)	$CuSO_4$	40–110	Anticancer and antibacterial activities	2020	[90]
CuO	Actinomycetes	$CuSO_4$	61.7	Antibacterial activity against selected human and fish pathogen	2018	[91]
Cu	Bacterial cellulose	$Cu(NO_3)_2$	33.8, 22.8 and 21.7	Excellent oxidation resistance and stability	2020	[92]
Cr_2O_3	*Erwinia amylovora*	$K_2Cr_2O_7$	32.35	Antibacterial activity	2020	[161]
Cr	*Bacillus subtilis*	Electroplating industry wastewaters	4 to 50	Antibacterial and anticancer	2017	[162]
Fungi						
Ag	*Penicillium oxalicum*	$AgNO_3$	67	Bactericidal agent anti-inflammation	2019	[34]
Ag	*Piriformospora indica*	$AgNO_3$	16–30	Anticancer	2019	[35]
Au	*Humicola sp.*	$HAuCl_4$	22	Anti-promastigote	2022	[46]
Au	*Morchella esculenta*	$HAuCl_4$	16.51	Cytotoxicity and antimicrobial	2021	[47]
Au	*Fusarium solani* ATLOY-8	$HAuCl_4$	40–45	Cytotoxicity	2021	[48]
ZnO	White-rot fungus *Phanerochaete chrysosporium*	$ZnSO_4$	15–24	Antibacterial applications	2021	[55]
ZnO	*Trichoderma harzianum*	$Zn(CH_3COO)_2$	8–23	Antifungal activity	2021	[57]
ZnO	*Acremonium potronii*	$Zn(CH_3COO)_2$	13–15	The degradation of MB dye	2021	[49]
ZnO	*Aspergillus niger*	$Zn(CH_3COO)_2$	35	Medical applications	2021	[59]
CuO	Performed biomass of *Aspergillus fumigatus*	$Cu(NO_3)_2$	6	Antibacterial photocatalytic activities	2019	[80]
CuO	*Aspergillus terreus* strain AF-1	$CuSO_4$	11–47	Bactericidal activity	2021	[81]
CuO	*Penicillium chrysogenum*-mediated mycogenic	$CuSO_4$	9.70	Antimicrobial activity against some plant pathogens	2020	[82]
CuO	Indigenous	$Cu(NO_3)_2$	10–190	In vitro photothermolysis of cancer cells, anticancer nanotherapeutics	2019	[84]

Table 3: Continued.

NPs	Green synthesis agent	NP precursor	NP size	NP application	Year	Reference
$Cu(CO_3)_2$	Ureolytic	$CuCl_2$	10–20	The influence of extracellular protein on the formation and morphology of such nanominerals	2017	[85]
CuO	*Aspergillus terreus*	$CuSO_4$	15.75 ± 3.95	Nuclear medicine applications	2020	[86]
CuO	Endophytic fungus *Aspergillus terreus*	$CuSO_4$	Below 100	Antibacterial and antifungal activity-anticancer therapies	2021	[87]
Al_2O_3	*Fungus colletotrichum sp.*	$AlCl_3$	30	Antimicrobial agent	2017	[144]
Cr_2O_3	*Aspergillus niger* fungus	$Cr_2(SO_4)_3$	36	Not detected	2018	[163]

Table 4: Most important characteristics of nanoparticles synthesized using other green sources.

NPs	Green synthesis agent	NP precursor	NP size	NP application	Year	Reference
ZnO	Marine sponge extract *Spongia officinalis*	$Zn(CH_3COO)_2)$	3.22–11.5	Mosquito control and drug development	2022	[60]
Cr_2O_3	Natural honey	$K_2Cr_2O_7$	24.7205	Antioxidant and antibacterial activities	2020	[160]
Sm_2O_3	Urea	$Sm(NO_3)_3$	13–33	Potential application in photoelectric materials and devices	2017	[168]
CeO_2	Flower honey, chestnut honey, pine honey, turmeric extracts	$Ce(NO_3)_3$	1.23–6.08	Antioxidant anticancer photocatalysis	2022	[179]
CeO_2	Marine oyster	$Ce(NO_3)_3$	15	Photocatalysis	2021	[180]

Using the sol-gel process, carrageenan hydrogel was used to produce cerium oxide nanoparticles (CeO_2 NPs) using cerium nitrate as a precursor. CeO_2 NPs had an estimated band gap of 2.69 eV and a diameter varied between 18 and 60 nm, with an average size of 34 nm. In vitro cytotoxicity testing on the WEHI 164 cell line revealed low toxicity, which proposed CeO_2 NPs as strong candidate for medicinal applications [182].

2.11.3. Lanthanum and Lanthanum Oxide Nanoparticles (La and La_2O_3 NPs). Because of its many uses in electronics, sensors, insulators, antimicrobial agents, biomedicines, and biocatalysts, lanthanum oxide nanoparticles (La_2O_3 NPs) have been gaining increasing interest [183]. Several plant extracts have been utilized for the green synthesis of La_2O_3 [184].

Biogenic lanthanum (La) nanoparticles were manufactured using the leaf extract of *Muntingia calabura*. SEM revealed that the size of La nanoparticles was less than 100 nm. The prepared metal nanoparticles possessed antioxidant activity that was studied using DPPH test and revealed an inhibition of 70.06%. The prepared nanometal also showed antibacterial efficacy toward several bacterial strains. A blood compatibility investigation revealed that La nanoparticles have a role in blood coagulation and thrombolytic action. The prepared La NPs were also tested for their photocatalytic behavior showing an efficiency in degrading Coomassie brilliant blue dye in visible light [185].

Lanthanum oxide nanoparticles were prepared using *Datura metel* leaf extract. With the increase in time and incubation, the precursor of $La(OH)_3$ changed to LaOOH and finally to pure hexagonal La_2O_3 nanocrystals [186].

Utilizing the leaf powders of *Centella asiatica* and Tridax plants, lanthanum oxide (La_2O_3) nanoparticles (NPs) were produced using a simple green combustion process. The efficiency of both oxides NPs was investigated using electrochemical and photocatalytic methods. La_2O_3 NPs prepared using Tridax plants showed better photocatalytic behavior with a degradation of 60%. Both La_2O_3 NPs showed promising antibacterial properties [187].

2.11.4. Yttrium Oxide Nanoparticles (Y_2O_3 NPs). Yttrium oxide (Y_2O_3) nanoparticle is well-known oxide due to its technological applications. It has also been employed in imaging, polarizer, cancer treatments, and antibacterial and antioxidant applications. Using green methods, it has been prepared using plant leaf and fruit extracts. The greenly synthesized particles were specifically tested as catalysts, antibacterial agents, and anticancer agents [188].

Liriope platyphylla rhizome extract was used to make green Y_2O_3 NPs using yttrium nitrate hexahydrate as a precursor. The leaf extract works as a reducing agent. The greenly synthesized oxide nanoparticles were used as a heterogeneous green catalyst for the synthesis of 1,3-thiazolidin-4-ones, which has special importance in medicine. Unlike many used catalysts, the prepared green Y_2O_3 NPs had a good-to-excellent yield [189].

Nagajyothi et al. prepared yttrium oxide nanoparticles (Y_2O_3 NPs) utilizing the aqueous fruit extract of Forsythiae Fructus and an average size of 11 nm. The green Y_2O_3 NPs showed substantial anticancer action against renal carcinoma cells but has no toxicity on the normal cells [190].

Figure 8 illustrates TEM images of rare earth metal NPs synthesized via different green methods.

The major criteria of metallic nanoparticles, which are recently synthesized via plants, microorganisms, and other green sources and covered in this review, are summarized in Tables 2–4, respectively.

3. Conclusion

Finally, the goal of this review was to present the most recent research on nanoparticle synthesis using green technologies, their characterization, and their use as materials in large-scale fields. The various biosources, such as aqueous plant extracts, bacteria, and fungus, were covered in this study. All of the elements are present: Ag, Au, ZnO, CuO, Co_3O_4, Fe_3O_4, TiO_2, NiO, Al_2O_3, Cr_2O_3, Sm_2O_3, CeO_2, La_2O_3, and Y_2O_3. In addition, the size of green nanoparticles was reviewed in each of the research papers.

Conflicts of Interest

The authors declare that there are no conflicts of interest.

References

[1] D. Zhang, X.-l. Ma, Y. Gu, H. Huang, and G.-w. Zhang, "Green synthesis of metallic nanoparticles and their potential applications to treat cancer," *Frontiers of Chemistry*, vol. 8, p. 799, 2020.

[2] F. Moradi, S. Sedaghat, O. Moradi, and S. Arab Salmanabadi, "Review on green nano-biosynthesis of silver nanoparticles and their biological activities: with an emphasis on medicinal plants," *Inorganic and Nano-Metal Chemistry*, vol. 51, no. 1, pp. 133–142, 2021.

[3] V. Kalpana and V. Devi Rajeswari, "A review on green synthesis, biomedical applications, and toxicity studies of ZnO NPs," *Bioinorganic Chemistry and Applications*, vol. 2018, Article ID 3569758, 12 pages, 2018.

[4] S. Khodadadi, N. Mahdinezhad, B. Fazeli-Nasab, M. J. Heidari, B. Fakheri, and A. Miri, "Investigating the possibility of green synthesis of silver nanoparticles using *Vaccinium arctostaphlyos* extract and evaluating its antibacterial properties," *BioMed Research International*, vol. 2021, Article ID 5572252, 13 pages, 2021.

[5] H. C. A. Murthy, T. Desalegn, M. Kassa, B. Abebe, and T. Assefa, "Synthesis of green copper nanoparticles using medicinal plant *Hagenia abyssinica* (Brace) JF. Gmel. leaf extract: antimicrobial properties," *Journal of Nanomaterials*, vol. 2020, Article ID 3924081, 12 pages, 2020.

[6] A. R. Geetha, E. George, A. Srinivasan, and J. Shaik, "Optimization of green synthesis of silver nanoparticles from leaf extracts of *Pimenta dioica* (Allspice)," *The Scientific World Journal*, vol. 2013, Article ID 362890, 5 pages, 2013.

[7] S. Iravani, "Bacteria in nanoparticle synthesis: current status and future prospects," *International Scholarly Research Notices*, vol. 2014, Article ID 359316, 18 pages, 2014.

[8] J. Aravind Kumar, D. Joshua Amarnath, S. Anuradha Jabasingh et al., "One pot green synthesis of nano magnesium oxide-carbon composite: preparation, characterization and application towards anthracene adsorption," *Journal of Cleaner Production*, vol. 237, Article ID 117691, 2019.

[9] M. Hassanisaadi, G. H. S. Bonjar, A. Rahdar, S. Pandey, A. Hosseinipour, and R. Abdolshahi, "Environmentally safe biosynthesis of gold nanoparticles using plant water extracts," *Nanomaterials*, vol. 11, no. 8, p. 2033, 2021.

[10] S. I. Bukhari, M. M. Hamed, M. H. Al-Agamy, H. S. S. Gazwi, H. H. Radwan, and A. M. Youssif, "Biosynthesis of copper oxide nanoparticles using Streptomyces MHM38 and its biological applications," *Journal of Nanomaterials*, vol. 2021, Article ID 6693302, 16 pages, 2021.

[11] J. Singh, T. Dutta, K.-H. Kim, M. Rawat, P. Samddar, and P. Kumar, ""Green" synthesis of metals and their oxide nanoparticles: applications for environmental remediation," *Journal of Nanobiotechnology*, vol. 16, no. 1, pp. 84–24, 2018.

[12] J. Aravind Kumar, T. Krithiga, K. Vijai Anand et al., "Kinetics and regression analysis of phenanthrene adsorption on the nanocomposite of CaO and activated carbon: characterization, regeneration, and mechanistic approach," *Journal of Molecular Liquids*, vol. 334, Article ID 116080, 2021.

[13] J. A. Kumar, D. J. Amarnath, S. Sathish et al., "Enhanced PAHs removal using pyrolysis-assisted potassium hydroxide induced palm shell activated carbon: batch and column investigation," *Journal of Molecular Liquids*, vol. 279, pp. 77–87, 2019.

[14] P. K. Dikshit, J. Kumar, A. K. Das et al., "Green synthesis of metallic nanoparticles: applications and limitations," *Catalysts*, vol. 11, no. 8, p. 902, 2021.

[15] J. Jeevanandam, S. F. Kiew, S. Boakye-Ansah et al., "Green approaches for the synthesis of metal and metal oxide nanoparticles using microbial and plant extracts," *Nanoscale*, vol. 14, no. 7, pp. 2534–2571, 2022.

[16] Y. T. Gebreslassie and H. G. Gebretnsae, "Green and cost-effective synthesis of tin oxide nanoparticles: a review on the synthesis methodologies, mechanism of formation, and their potential applications," *Nanoscale Research Letters*, vol. 16, no. 1, pp. 97–16, 2021.

[17] H. A. Salam, P. Rajiv, M. Kamaraj, P. Jagadeeswaran, S. Gunalan, and R. Sivaraj, "Plants: green route for nanoparticle synthesis," *International Research Journal of Biological Sciences*, vol. 1, no. 5, pp. 85–90, 2012.

[18] M. Shammout and A. Awwad, "A novel route for the synthesis of copper oxide nanoparticles using Bougainvillea plant flowers extract and antifungal activity evaluation, MW Shammout and AM Awwad. A novel route for the synthesis of copper oxide nanoparticles using Bougainvillea plant flowers extract and antifungal activity evaluation," *Chemistry International*, vol. 7, no. 1, pp. 71–78, 2021.

[19] S. Panhwar, J. A. Buledi, D. Mal, A. R. Solangi, A. Balouch, and A. Hyder, "Importance and analytical perspective of green synthetic strategies of copper, zinc, and titanium oxide nanoparticles and their applications in pathogens and environmental remediation," *Current Analytical Chemistry*, vol. 17, no. 8, pp. 1169–1181, 2021.

[20] S. A. Fahmy, E. Preis, U. Bakowsky, and H. M. E.-S. Azzazy, "Platinum nanoparticles: green synthesis and biomedical applications," *Molecules*, vol. 25, no. 21, p. 4981, 2020.

[21] S. Kaabipour and S. Hemmati, "A review on the green and sustainable synthesis of silver nanoparticles and one-dimensional silver nanostructures," *Beilstein Journal of Nanotechnology*, vol. 12, no. 1, pp. 102–136, 2021.

[22] J. A. Kumar, T. Krithiga, S. Manigandan et al., "A focus to green synthesis of metal/metal based oxide nanoparticles:

various mechanisms and applications towards ecological approach," *Journal of Cleaner Production*, vol. 324, Article ID 129198, 2021.

[23] V. Soni, P. Raizada, P. Singh et al., "Sustainable and green trends in using plant extracts for the synthesis of biogenic metal nanoparticles toward environmental and pharmaceutical advances: a review," *Environmental Research*, vol. 202, Article ID 111622, 2021.

[24] M. M. I. Masum, M. M. Siddiqa, K. A. Ali et al., "Biogenic synthesis of silver nanoparticles using *Phyllanthus emblica* fruit extract and its inhibitory action against the pathogen *Acidovorax oryzae* strain RS-2 of rice bacterial brown stripe," *Frontiers in Microbiology*, vol. 10, p. 820, 2019.

[25] T. Dutta, N. N. Ghosh, M. Das, R. Adhikary, V. Mandal, and A. P. Chattopadhyay, "Green synthesis of antibacterial and antifungal silver nanoparticles using *Citrus limetta* peel extract: experimental and theoretical studies," *Journal of Environmental Chemical Engineering*, vol. 8, no. 4, Article ID 104019, 2020.

[26] V. Ravichandran, S. Vasanthi, S. Shalini, S. A. A. Shah, M. Tripathy, and N. Paliwal, "Green synthesis, characterization, antibacterial, antioxidant and photocatalytic activity of *Parkia speciosa* leaves extract mediated silver nanoparticles," *Results in Physics*, vol. 15, Article ID 102565, 2019.

[27] P. Tamilarasi and P. Meena, "Green synthesis of silver nanoparticles (Ag NPs) using *Gomphrena globosa* (Globe amaranth) leaf extract and their characterization," *Materials Today Proceedings*, vol. 33, pp. 2209–2216, 2020.

[28] Y. Yugay, R. Usoltseva, V. Silant'ev et al., "Synthesis of bioactive silver nanoparticles using alginate, fucoidan and laminaran from brown algae as a reducing and stabilizing agent," *Carbohydrate Polymers*, vol. 245, Article ID 116547, 2020.

[29] Z. Hashemi, Z. M. Mizwari, S. Mohammadi-Aghdam, S. Mortazavi-Derazkola, and M. Ali Ebrahimzadeh, "Sustainable green synthesis of silver nanoparticles using *Sambucus ebulus* phenolic extract (AgNPs@ SEE): optimization and assessment of photocatalytic degradation of methyl orange and their in vitro antibacterial and anticancer activity," *Arabian Journal of Chemistry*, vol. 15, no. 1, Article ID 103525, 2022.

[30] Y. Yugay, T. Rusapetova, D. Mashtalyar et al., "Biomimetic synthesis of functional silver nanoparticles using hairy roots of Panax ginseng for wheat pathogenic fungi treatment," *Colloids and Surfaces B: Biointerfaces*, vol. 207, Article ID 112031, 2021.

[31] X. Wang, Z. Wang, X. Wang, L. Shi, and R. Ran, "Preparation of silver nanoparticles by solid-state redox route from hydroxyethyl cellulose for antibacterial strain sensor hydrogel," *Carbohydrate Polymers*, vol. 257, Article ID 117665, 2021.

[32] I. Ali, T. Y. Qiang, N. Ilahi, M. Adnan, and W. Sajjad, "Green synthesis of silver nanoparticles by using bacterial extract and its antimicrobial activity against pathogens," *International Journal of Biosciences*, vol. 13, no. 5, pp. 1–5, 2018.

[33] R. S. Hamida, N. E. Abdelmeguid, M. A. Ali, M. M. Bin-Meferij, and M. I. Khalil, "Synthesis of silver nanoparticles using a novel cyanobacteria Desertifilum sp. extract: their antibacterial and cytotoxicity effects," *International Journal of Nanomedicine*, vol. 15, pp. 49–63, 2020.

[34] N. Feroze, B. Arshad, M. Younas, M. I. Afridi, S. Saqib, and A. Ayaz, "Fungal mediated synthesis of silver nanoparticles and evaluation of antibacterial activity," *Microscopy Research and Technique*, vol. 83, no. 1, pp. 72–80, 2020.

[35] N. Aziz, M. Faraz, M. A. Sherwani, T. Fatma, and R. Prasad, "Illuminating the anticancerous efficacy of a new fungal chassis for silver nanoparticle synthesis," *Frontiers of Chemistry*, vol. 7, p. 65, 2019.

[36] N. S. Al-Radadi, "Facile one-step green synthesis of gold nanoparticles (AuNp) using licorice root extract: antimicrobial and anticancer study against HepG2 cell line," *Arabian Journal of Chemistry*, vol. 14, no. 2, Article ID 102956, 2021.

[37] F. Masse, M. Ouellette, G. Lamoureux, and E. Boisselier, "Gold nanoparticles in ophthalmology," *Medicinal Research Reviews*, vol. 39, no. 1, pp. 302–327, 2019.

[38] A. Hojjati-Najafabadi, S. Salmanpour, F. Sen, P. N. Asrami, M. Mahdavian, and M. A. Khalilzadeh, "A tramadol drug electrochemical sensor amplified by biosynthesized Au nanoparticle using mentha aquatic extract and ionic liquid," *Topics in Catalysis*, vol. 65, no. 5-6, pp. 587–594, 2021.

[39] O. T. Fanoro, S. Parani, R. Maluleke et al., "Facile green, room-temperature synthesis of gold nanoparticles using *Combretum erythrophyllum* leaf extract: antibacterial and cell viability studies against normal and cancerous cells," *Antibiotics*, vol. 10, no. 8, p. 893, 2021.

[40] A. Olajire and A. Mohammed, "Bio-directed synthesis of gold nanoparticles using *Ananas comosus* aqueous leaf extract and their photocatalytic activity for LDPE degradation," *Advanced Powder Technology*, vol. 32, no. 2, pp. 600–610, 2021.

[41] N. Muniyappan, M. Pandeeswaran, and A. Amalraj, "Green synthesis of gold nanoparticles using *Curcuma pseudomontana* isolated curcumin: its characterization, antimicrobial, antioxidant and anti-inflammatory activities," *Environmental Chemistry and Ecotoxicology*, vol. 3, pp. 117–124, 2021.

[42] A. Fadaka, O. Aluko, S. Awawu, and K. Theledi, "Green synthesis of gold nanoparticles using *Pimenta dioica* leaves aqueous extract and their application as photocatalyst, antioxidant, and antibacterial agents," *Journal of Multidisciplinary Applied Natural Science*, vol. 1, no. 2, pp. 78–88, 2021.

[43] K. Perveen, F. M. Husain, F. A. Qais et al., "Microwave-assisted rapid green Synthesis of gold nanoparticles using seed extract of *Trachyspermum ammi*: ROS mediated biofilm inhibition and anticancer activity," *Biomolecules*, vol. 11, no. 2, p. 197, 2021.

[44] A. Al Saqr, E.-S. Khafagy, A. Alalaiwe et al., "Synthesis of gold nanoparticles by using green machinery: characterization and in vitro toxicity," *Nanomaterials*, vol. 11, no. 3, p. 808, 2021.

[45] M. P. Patil, M.-j. Kang, I. Niyonizigiye et al., "Extracellular synthesis of gold nanoparticles using the marine bacterium *Paracoccus haeundaensis* BC74171T and evaluation of their antioxidant activity and antiproliferative effect on normal and cancer cell lines," *Colloids and Surfaces B: Biointerfaces*, vol. 183, Article ID 110455, 2019.

[46] A. Syed, M. H. Al Saedi, A. H. Bahkali et al., "αAu2S nanoparticles: fungal-mediated synthesis, structural characterization and bioassay," *Green Chemistry Letters and Reviews*, vol. 15, no. 1, pp. 61–70, 2022.

[47] H. Acay, "Utilization of *Morchella esculenta*-mediated green synthesis golden nanoparticles in biomedicine applications," *Preparative Biochemistry & Biotechnology*, vol. 51, no. 2, pp. 127–136, 2021.

[48] P. Clarance, B. Luvankar, J. Sales et al., "Green synthesis and characterization of gold nanoparticles using endophytic fungi *Fusarium solani* and its in-vitro anticancer and

biomedical applications," *Saudi Journal of Biological Sciences*, vol. 27, no. 2, pp. 706–712, 2020.

[49] F. Ameen, T. Dawoud, and S. AlNadhari, "Ecofriendly and low-cost synthesis of ZnO nanoparticles from *Acremonium potronii* for the photocatalytic degradation of azo dyes," *Environmental Research*, vol. 202, Article ID 111700, 2021.

[50] V. Gerbreders, M. Krasovska, I. Mihailova et al., "ZnO nanostructure-based electrochemical biosensor for Trichinella DNA detection," *Sensing and Bio-Sensing Research*, vol. 23, Article ID 100276, 2019.

[51] A. Degefa, B. Bekele, L. T. Jule et al., "Green synthesis, characterization of zinc oxide nanoparticles, and examination of properties for dye-sensitive solar cells using various vegetable extracts," *Journal of Nanomaterials*, vol. 2021, Article ID 3941923, 9 pages, 2021.

[52] A. Serrà, Y. Zhang, B. Sepúlveda et al., "Highly active ZnO-based biomimetic fern-like microleaves for photocatalytic water decontamination using sunlight," *Applied Catalysis B: Environmental*, vol. 248, pp. 129–146, 2019.

[53] A. R. Prasad, L. Williams, J. Garvasis et al., "Applications of phytogenic ZnO nanoparticles: a review on recent advancements," *Journal of Molecular Liquids*, vol. 331, Article ID 115805, 2021.

[54] I. Chauhan, S. Aggrawal, and P. Mohanty, "ZnO nanowire-immobilized paper matrices for visible light-induced antibacterial activity against *Escherichia coli*," *Environmental Science: Nano*, vol. 2, no. 3, pp. 273–279, 2015.

[55] J. L. Sharma, V. Dhayal, and R. K. Sharma, "White-rot fungus mediated green synthesis of zinc oxide nanoparticles and their impregnation on cellulose to develop environmental friendly antimicrobial fibers," *3 Biotech*, vol. 11, no. 6, p. 269, 2021.

[56] M. Zaka, S. S. Hashmi, M. A. Siddiqui et al., "Callus-mediated biosynthesis of Ag and ZnO nanoparticles using aqueous callus extract of *Cannabis sativa*: their cytotoxic potential and clinical potential against human pathogenic bacteria and fungi," *Green Processing and Synthesis*, vol. 10, no. 1, pp. 569–584, 2021.

[57] S. A. Zaki, S. A. Ouf, F. M. Albarakaty, M. M. Habeb, A. A. Aly, and K. A. Abd-Elsalam, "*Trichoderma harzianum*-mediated ZnO nanoparticles: a green tool for controlling soil-borne pathogens in cotton," *Journal of Fungi*, vol. 7, no. 11, p. 952, 2021.

[58] R. Ishwarya, B. Vaseeharan, S. Kalyani et al., "Facile green synthesis of zinc oxide nanoparticles using *Ulva lactuca* seaweed extract and evaluation of their photocatalytic, antibiofilm and insecticidal activity," *Journal of Photochemistry and Photobiology B: Biology*, vol. 178, pp. 249–258, 2018.

[59] A. Es-Haghi, M. E. Taghavizadeh Yazdi, M. Sharifalhoseini et al., "Application of response surface methodology for optimizing the therapeutic activity of ZnO nanoparticles biosynthesized from *Aspergillus niger*," *Biomimetics*, vol. 6, no. 2, p. 34, 2021.

[60] A. I. Hasaballah, H. A. El-Naggar, S. Abdelbary, M. A. E. Bashar, and T. A. Selim, "Eco-friendly synthesis of zinc oxide nanoparticles by marine sponge, *Spongia officinalis*: antimicrobial and insecticidal activities against the mosquito vectors, *Culex pipiens* and *Anopheles pharoensis*," *BioNanoScience*, vol. 12, no. 1, pp. 89–104, 2022.

[61] H. Sadiq, F. Sher, S. Sehar et al., "Green synthesis of ZnO nanoparticles from *Syzygium cumini* leaves extract with robust photocatalysis applications," *Journal of Molecular Liquids*, vol. 335, Article ID 116567, 2021.

[62] S. Umavathi, S. Mahboob, M. Govindarajan et al., "Green synthesis of ZnO nanoparticles for antimicrobial and vegetative growth applications: a novel approach for advancing efficient high quality health care to human wellbeing," *Saudi Journal of Biological Sciences*, vol. 28, no. 3, pp. 1808–1815, 2021.

[63] M. H. Kahsay, "Synthesis and characterization of ZnO nanoparticles using aqueous extract of *Becium grandiflorum* for antimicrobial activity and adsorption of methylene blue," *Applied Water Science*, vol. 11, no. 2, pp. 45–12, 2021.

[64] R. Álvarez-Chimal, V. I. García-Pérez, M. A. Álvarez-Pérez, and J. Á. Arenas-Alatorre, "Green synthesis of ZnO nanoparticles using a *Dysphania ambrosioides* extract. Structural characterization and antibacterial properties," *Materials Science and Engineering: C*, vol. 118, Article ID 111540, 2021.

[65] M. Swamy, B. Surendra, C. Mallikarjunaswamy, S. Pramila, and N. Rekha, "Bio-mediated synthesis of ZnO nanoparticles using *Lantana camara* flower extract: its characterizations, photocatalytic, electrochemical and anti-inflammatory applications," *Environmental Nanotechnology, Monitoring & Management*, vol. 15, Article ID 100442, 2021.

[66] M. Khan, P. Ware, and N. Shimpi, "Synthesis of ZnO nanoparticles using peels of *Passiflora foetida* and study of its activity as an efficient catalyst for the degradation of hazardous organic dye," *SN Applied Sciences*, vol. 3, no. 5, p. 528, 2021.

[67] C. Soto-Robles, O. Nava, L. Cornejo et al., "Biosynthesis, characterization and photocatalytic activity of ZnO nanoparticles using extracts of *Justicia spicigera* for the degradation of methylene blue," *Journal of Molecular Structure*, vol. 1225, Article ID 129101, 2021.

[68] R. Resmi, J. Yoonus, and B. Beena, "A novel greener synthesis of ZnO nanoparticles from Nilgiriantusciliantus leaf extract and evaluation of its biomedical applications," *Materials Today Proceedings*, vol. 46, pp. 3062–3068, 2021.

[69] S. Gharpure, R. Yadwade, B. Chakraborty et al., "Bioactive properties of ZnO nanoparticles synthesized using *Cocos nucifera* leaves," *3 Biotech*, vol. 12, no. 2, pp. 45–17, 2022.

[70] S. Suba, S. Vijayakumar, E. Vidhya, V. Punitha, and M. Nilavukkarasi, "Microbial mediated synthesis of ZnO nanoparticles derived from Lactobacillus spp: characterizations, antimicrobial and biocompatibility efficiencies," *Sensors International*, vol. 2, Article ID 100104, 2021.

[71] A. Król, V. Railean-Plugaru, P. Pomastowski, M. Złoch, and B. Buszewski, "Mechanism study of intracellular zinc oxide nanocomposites formation," *Colloids and Surfaces A: Physicochemical and Engineering Aspects*, vol. 553, pp. 349–358, 2018.

[72] H. S. El-Sayed, S. M. El-Sayed, and A. M. Youssef, "Novel approach for biosynthesizing of zinc oxide nanoparticles using Lactobacillus gasseri and their influence on microbiological, chemical, sensory properties of integrated yogurt," *Food Chemistry*, vol. 365, Article ID 130513, 2021.

[73] P. Dhandapani, A. A. Prakash, M. S. AlSalhi, S. Maruthamuthu, S. Devanesan, and A. Rajasekar, "Ureolytic bacteria mediated synthesis of hairy ZnO nanostructure as photocatalyst for decolorization of dyes," *Materials Chemistry and Physics*, vol. 243, Article ID 122619, 2020.

[74] M. Saravanan, V. Gopinath, M. K. Chaurasia, A. Syed, F. Ameen, and N. Purushothaman, "Green synthesis of anisotropic zinc oxide nanoparticles with antibacterial and cytofriendly properties," *Microbial Pathogenesis*, vol. 115, pp. 57–63, 2018.

[75] F. Amin, B. Khattak, B. Khattak et al., "Green synthesis of copper oxide nanoparticles using *Aerva javanica* leaf extract and their characterization and investigation of in vitro antimicrobial potential and cytotoxic activities," *Evidence-Based Complementary and Alternative Medicine*, vol. 2021, Article ID 5589703, 12 pages, 2021.

[76] I. H. Shah, M. Ashraf, I. A. Sabir et al., "Green synthesis and characterization of copper oxide nanoparticles using *Calotropis procera* leaf extract and their different biological potentials," *Journal of Molecular Structure*, vol. 1259, Article ID 132696, 2022.

[77] A. Vinothkanna, K. Mathivanan, S. Ananth, Y. Ma, and S. Sekar, "Biosynthesis of copper oxide nanoparticles using *Rubia cordifolia* bark extract: characterization, antibacterial, antioxidant, larvicidal and photocatalytic activities," *Environmental Science and Pollution Research*, pp. 1–12, 2022.

[78] M. Narayanan, F. a. J. Hussain, B. Srinivasan, M. T. Sambantham, L. A. Al-Keridis, and F. A. Al-mekhlafi, "Green synthesizes and characterization of copper-oxide nanoparticles by *Thespesia populnea* against skin-infection causing microbes," *Journal of King Saud University Science*, vol. 34, no. 3, Article ID 101885, 2022.

[79] K. Velsankar, R. M. Aswin Kumar, R. Preethi, V. Muthulakshmi, and S. Sudhahar, "Green synthesis of CuO nanoparticles via *Allium sativum* extract and its characterizations on antimicrobial, antioxidant, antilarvicidal activities," *Journal of Environmental Chemical Engineering*, vol. 8, no. 5, Article ID 104123, 2020.

[80] M. Ghareib, W. Abdallah, M. Tahon, and A. Tallima, "Biosynthesis of copper oxide nanoparticles using the preformed biomass of aspergillus fumigatus and their antibacterial and photocatalytic activities," *Digest Journal of Nanomaterials & Biostructures (DJNB)*, vol. 14, no. 2, 2019.

[81] T. I. Shaheen, A. Fouda, and S. S. Salem, "Integration of cotton fabrics with biosynthesized CuO nanoparticles for bactericidal activity in the terms of their cytotoxicity assessment," *Industrial & Engineering Chemistry Research*, vol. 60, no. 4, pp. 1553–1563, 2021.

[82] A. I. El-Batal, G. S. El-Sayyad, F. M. Mosallam, and R. M. Fathy, "Penicillium chrysogenum-mediated mycogenic synthesis of copper oxide nanoparticles using gamma rays for in vitro antimicrobial activity against some plant pathogens," *Journal of Cluster Science*, vol. 31, no. 1, pp. 79–90, 2020.

[83] S. E.-D. Hassan, A. Fouda, A. A. Radwan et al., "Endophytic actinomycetes Streptomyces spp mediated biosynthesis of copper oxide nanoparticles as a promising tool for biotechnological applications," *Journal of Biological Inorganic Chemistry*, vol. 24, no. 3, pp. 377–393, 2019.

[84] K. Saravanakumar, S. Shanmugam, N. B. Varukattu, D. MubarakAli, K. Kathiresan, and M.-H. Wang, "Biosynthesis and characterization of copper oxide nanoparticles from indigenous fungi and its effect of photothermolysis on human lung carcinoma," *Journal of Photochemistry and Photobiology B: Biology*, vol. 190, pp. 103–109, 2019.

[85] Q. Li and G. M. Gadd, "Biosynthesis of copper carbonate nanoparticles by ureolytic fungi," *Applied Microbiology and Biotechnology*, vol. 101, no. 19, pp. 7397–7407, 2017.

[86] A. M. Mousa, O. A. Abdel Aziz, O. E. Al-Hagar, M. A. Gizawy, K. F. Allan, and M. F. Attallah, "Biosynthetic new composite material containing CuO nanoparticles produced by *Aspergillus terreus* for 47Sc separation of cancer theranostics application from irradiated Ca target," *Applied Radiation and Isotopes*, vol. 166, Article ID 109389, 2020.

[87] V. M. Mani, S. Kalaivani, S. Sabarathinam et al., "Copper oxide nanoparticles synthesized from an endophytic fungus *Aspergillus terreus*: bioactivity and anti-cancer evaluations," *Environmental Research*, vol. 201, Article ID 111502, 2021.

[88] H. Zhao, M. Maruthupandy, F. A. Al-mekhlafi, G. Chackaravarthi, G. Ramachandran, and C. K. Chelliah, "Biological synthesis of copper oxide nanoparticles using marine endophytic actinomycetes and evaluation of biofilm producing bacteria and A549 lung cancer cells," *Journal of King Saud University Science*, vol. 34, no. 3, Article ID 101866, 2022.

[89] Q. Lv, B. Zhang, X. Xing et al., "Biosynthesis of copper nanoparticles using *Shewanella loihica* PV-4 with antibacterial activity: novel approach and mechanisms investigation," *Journal of Hazardous Materials*, vol. 347, pp. 141–149, 2018.

[90] M. Kouhkan, P. Ahangar, L. A. Babaganjeh, and M. Allahyari-Devin, "Biosynthesis of copper oxide nanoparticles using *Lactobacillus casei* subsp. casei and its anticancer and antibacterial activities," *Current Nanoscience*, vol. 16, no. 1, pp. 101–111, 2020.

[91] M. I. Nabila and K. Kannabiran, "Biosynthesis, characterization and antibacterial activity of copper oxide nanoparticles (CuO NPs) from actinomycetes," *Biocatalysis and Agricultural Biotechnology*, vol. 15, pp. 56–62, 2018.

[92] B. Ma, B. Sun, Y. Huang, C. Chen, and D. Sun, "Facile synthesis of Cu nanoparticles encapsulated into carbonized bacterial cellulose with excellent oxidation resistance and stability," *Colloids and Surfaces A: Physicochemical and Engineering Aspects*, vol. 590, Article ID 124462, 2020.

[93] A. Waris, M. Din, A. Ali et al., "Green fabrication of Co and CO_3O_4 nanoparticles and their biomedical applications: a review," *Open Life Sciences*, vol. 16, no. 1, pp. 14–30, 2021.

[94] N. O. M. Dewi, Y. Yulizar, and D. O. B. Apriandanu, "Green synthesis of CO_3O_4 nanoparticles using *Euphorbia heterophylla* L. leaves extract: characterization and photocatalytic activity," *IOP Conference Series: Materials Science and Engineering*, vol. 509, Article ID 012105, 2019.

[95] S. Z. Mohammadi, B. Lashkari, and A. Khosravan, "Green synthesis of CO_3O_4 nanoparticles by using walnut green skin extract as a reducing agent by using response surface methodology," *Surfaces and Interfaces*, vol. 23, Article ID 100970, 2021.

[96] M. S. Samuel, E. Selvarajan, T. Mathimani et al., "Green synthesis of cobalt-oxide nanoparticle using jumbo Muscadine (*Vitis rotundifolia*): characterization and photo-catalytic activity of acid blue-74," *Journal of Photochemistry and Photobiology B: Biology*, vol. 211, Article ID 112011, 2020.

[97] N. Matinise, N. Mayedwa, X. Fuku, N. Mongwaketsi, and M. Maaza, "Green synthesis of cobalt (II, III) oxide nanoparticles using *Moringa oleifera* natural extract as high electrochemical electrode for supercapacitors," *AIP Conference Proceedings*, vol. 1962, Article ID 040005, 2018.

[98] M. Hafeez, R. Shaheen, B. Akram et al., "Green synthesis of cobalt oxide nanoparticles for potential biological applications," *Materials Research Express*, vol. 7, no. 2, Article ID 025019, 2020.

[99] S. Haq, F. Abbasi, M. Ben Ali et al., "Green synthesis of cobalt oxide nanoparticles and the effect of annealing temperature on their physiochemical and biological properties," *Materials Research Express*, vol. 8, no. 7, Article ID 075009, 2021.

[100] Ş. A. Korkmaz, "Green synthesis of cobalt-oxide nanoparticles with an endemic species *Allium tuncelianum* and anticancer activity," *Inorganic and Nano-Metal Chemistry*, pp. 1–7, 2021.

[101] K. Kaur, A. K. Sidhu, and K. Kaur, "Green synthesis: an eco-friendly route for the synthesis of iron oxide nanoparticles," *Frontiers in Nanotechnology*, vol. 3, p. 47, 2021.

[102] G. Sathishkumar, V. Logeshwaran, S. Sarathbabu et al., "Green synthesis of magnetic Fe_3O_4 nanoparticles using *Couroupita guianensis* Aubl. fruit extract for their antibacterial and cytotoxicity activities," *Artificial Cells, Nanomedicine, and Biotechnology*, vol. 46, no. 3, pp. 589–598, 2018.

[103] M. Yusefi, K. Shameli, Z. Hedayatnasab et al., "Green synthesis of Fe_3O_4 nanoparticles for hyperthermia, magnetic resonance imaging and 5-fluorouracil carrier in potential colorectal cancer treatment," *Research on Chemical Intermediates*, vol. 47, no. 5, pp. 1789–1808, 2021.

[104] I. Sari and Y. Yulizar, "Green synthesis of magnetite (Fe_3O_4) nanoparticles using Graptophyllum pictum leaf aqueous extract," *IOP Conference Series: Materials Science and Engineering*, vol. 191, Article ID 012014, 2017.

[105] S. Kanagasubbulakshmi and K. Kadirvelu, "Green synthesis of iron oxide nanoparticles using *Lagenaria siceraria* and evaluation of its antimicrobial activity," *Defence Life Science Journal*, vol. 2, no. 4, pp. 422–427, 2017.

[106] A. Azizi, "Green synthesis of Fe_3O_4 nanoparticles and its application in preparation of Fe_3O_4/cellulose magnetic nanocomposite: a suitable proposal for drug delivery systems," *Journal of Inorganic and Organometallic Polymers and Materials*, vol. 30, no. 9, pp. 3552–3561, 2020.

[107] M. F. Alajmi, J. Ahmed, A. Hussain et al., "Green synthesis of Fe_3O_4 nanoparticles using aqueous extracts of *Pandanus odoratissimus* leaves for efficient bifunctional electro-catalytic activity," *Applied Nanoscience*, vol. 8, no. 6, pp. 1427–1435, 2018.

[108] V. G. Viju Kumar and A. Prem, "Green synthesis and characterization of iron oxide nanoparticles using *Phyllanthus niruri* extract," *Oriental Journal of Chemistry*, vol. 34, no. 5, pp. 2583–2589, 2018.

[109] V. Verma, M. Al-Dossari, J. Singh, M. Rawat, M. G. M. Kordy, and M. Shaban, "A review on green synthesis of TiO_2 NPs: photocatalysis and antimicrobial applications," *Polymers*, vol. 14, no. 7, p. 1444, 2022.

[110] A. Singh, V. Goyal, J. Singh, and M. Rawat, "Structural, morphological, optical and photocatalytic properties of green synthesized TiO_2 NPs," *Current Research in Green and Sustainable Chemistry*, vol. 3, Article ID 100033, 2020.

[111] H. Kaur, S. Kaur, J. Singh, M. Rawat, and S. Kumar, "Expanding horizon: green synthesis of TiO_2 nanoparticles using *Carica papaya* leaves for photocatalysis application," *Materials Research Express*, vol. 6, no. 9, Article ID 095034, 2019.

[112] I. C. Maurya, S. Singh, S. Senapati, P. Srivastava, and L. Bahadur, "Green synthesis of TiO_2 nanoparticles using *Bixa orellana* seed extract and its application for solar cells," *Solar Energy*, vol. 194, pp. 952–958, 2019.

[113] N. K. Sethy, Z. Arif, P. K. Mishra, and P. Kumar, "Green synthesis of TiO_2 nanoparticles from *Syzygium cumini* extract for photo-catalytic removal of lead (Pb) in explosive industrial wastewater," *Green Processing and Synthesis*, vol. 9, no. 1, pp. 171–181, 2020.

[114] G. Nabi, Q.-U.-. Ain, M. B. Tahir et al., "Green synthesis of TiO_2 nanoparticles using lemon peel extract: their optical and photocatalytic properties," *International Journal of Environmental Analytical Chemistry*, vol. 102, no. 2, pp. 434–442, 2022.

[115] M. Abu-Dalo, A. Jaradat, B. A. Albiss, and N. A. Al-Rawashdeh, "Green synthesis of TiO_2 NPs/pristine pomegranate peel extract nanocomposite and its antimicrobial activity for water disinfection," *Journal of Environmental Chemical Engineering*, vol. 7, no. 5, Article ID 103370, 2019.

[116] B. Thakur, A. Kumar, and D. Kumar, "Green synthesis of titanium dioxide nanoparticles using *Azadirachta indica* leaf extract and evaluation of their antibacterial activity," *South African Journal of Botany*, vol. 124, pp. 223–227, 2019.

[117] M. Imran Din and A. Rani, "Recent advances in the synthesis and stabilization of nickel and nickel oxide nanoparticles: a green adeptness," *International journal of analytical chemistry*, vol. 2016, Article ID 3512145, 14 pages, 2016.

[118] M. I. Din, A. G. Nabi, A. Rani, A. Aihetasham, and M. Mukhtar, "Single step green synthesis of stable nickel and nickel oxide nanoparticles from *Calotropis gigantea*: catalytic and antimicrobial potentials," *Environmental Nanotechnology, Monitoring & Management*, vol. 9, pp. 29–36, 2018.

[119] T. Ali, M. F. Warsi, S. Zulfiqar et al., "Green nickel/nickel oxide nanoparticles for prospective antibacterial and environmental remediation applications," *Ceramics International*, vol. 48, no. 6, pp. 8331–8340, 2022.

[120] A. Olajire and A. Mohammed, "Green synthesis of nickel oxide nanoparticles and studies of their photocatalytic activity in degradation of polyethylene films," *Advanced Powder Technology*, vol. 31, no. 1, pp. 211–218, 2020.

[121] M. I. Din, M. Tariq, Z. Hussain, and R. Khalid, "Single step green synthesis of nickel and nickel oxide nanoparticles from *Hordeum vulgare* for photocatalytic degradation of methylene blue dye," *Inorganic and Nano-Metal Chemistry*, vol. 50, no. 4, pp. 292–297, 2020.

[122] Z. Sabouri, A. Rangrazi, M. S. Amiri, M. Khatami, and M. Darroudi, "Green synthesis of nickel oxide nanoparticles using *Salvia hispanica* L. (chia) seeds extract and studies of their photocatalytic activity and cytotoxicity effects," *Bioprocess and Biosystems Engineering*, vol. 44, no. 11, pp. 2407–2415, 2021.

[123] I. M. Rashid, S. D. Salman, A. K. Mohammed, and Y. S. Mahdi, "Green synthesis of nickle oxide nanoparticles for adsorption of dyes," *Sains Malaysiana*, vol. 51, no. 2, pp. 533–546, 2022.

[124] V. Selvanathan, M. Shahinuzzaman, S. Selvanathan et al., "Phytochemical-assisted green synthesis of nickel oxide nanoparticles for application as electrocatalysts in oxygen evolution reaction," *Catalysts*, vol. 11, no. 12, 2021.

[125] C. Rajith Kumar, V. S. Betageri, G. Nagaraju, G. Pujar, B. Suma, and M. Latha, "Photocatalytic, nitrite sensing and antibacterial studies of facile bio-synthesized nickel oxide nanoparticles," *Journal of Science: Advanced Materials and Devices*, vol. 5, no. 1, pp. 48–55, 2020.

[126] A. C. Nwanya, M. M. Ndipingwi, C. O. Ikpo et al., "Zea mays lea silk extract mediated synthesis of nickel oxide nanoparticles as positive electrode material for asymmetric supercabattery," *Journal of Alloys and Compounds*, vol. 822, Article ID 153581, 2020.

[127] H. Gebretinsae, G. Welegergs, N. Matinise, M. Maaza, and Z. Y. Nuru, "Electrochemical study of nickel oxide (NiO) nanoparticles from cactus plant extract," *MRS Advances*, vol. 5, no. 21-22, pp. 1095–1102, 2020.

[128] S. Sahila, N. Prabhu, G. G. Simiyon, and L. Jayakumari, "A novel green and eco-friendly synthesis of nickel oxide nanoparticles by auto combustion technique using *Allium cepa* bulb extract and their dielectric behaviour," *Chemical Data Collections*, vol. 38, Article ID 100837, 2022.

[129] P. Lamba, P. Singh, P. Singh et al., "Bioinspired synthesis of nickel oxide nanoparticles as electrode material for supercapacitor applications," *Ionics*, vol. 27, no. 12, pp. 5263–5276, 2021.

[130] K. Lingaraju, H. Raja Naika, H. Nagabhushana, K. Jayanna, S. Devaraja, and G. Nagaraju, "Biosynthesis of nickel oxide nanoparticles from *Euphorbia heterophylla* (L.) and their biological application," *Arabian Journal of Chemistry*, vol. 13, no. 3, pp. 4712–4719, 2020.

[131] K. C. Suresh and A. Balamurugan, "Evaluation of structural, optical, and morphological properties of nickel oxide nanoparticles for multi-functional applications," *Inorganic and Nano-Metal Chemistry*, vol. 51, no. 2, pp. 296–301, 2021.

[132] Q. Zhang, S. Xu, Y. Li, P. Ding, Y. Zhang, and P. Zhao, "Green-synthesized nickel oxide nanoparticles enhances biohydrogen production of Klebsiella sp. WL1316 using lignocellulosic hydrolysate and its regulatory mechanism," *Fuel*, vol. 305, Article ID 121585, 2021.

[133] H. S. M. Abdel-Ghany, S. Abdel-Shafy, M. M. Abuowarda et al., "In vitro acaricidal activity of green synthesized nickel oxide nanoparticles against the camel tick, *Hyalomma dromedarii* (ixodidae), and its toxicity on Swiss albino mice," *Experimental & Applied Acarology*, vol. 83, no. 4, pp. 611–633, 2021.

[134] M. A. Rahman, A. Parvin, M. S. H. Khan et al., "Efficacy of the green synthesized nickel-oxide nanoparticles against pulse beetle, *Callosobruchus maculatus* (F.) in black gram (*Vigna mungo* L.)," *International Journal of Pest Management*, vol. 67, no. 4, pp. 306–314, 2021.

[135] N. Sarkar, R. S. Sharma, and M. Kaushik, "Green synthesis and physiochemical characterization of nickel oxide nanoparticles: interaction studies with calf thymus DNA," *Luminescence*, vol. 35, no. 2, pp. 178–186, 2020.

[136] M. Youcef, B. Hamza, H. Nora et al., "A novel green synthesized NiO nanoparticles modified glassy carbon electrode for non-enzymatic glucose sensing," *Microchemical Journal*, vol. 178, Article ID 107332, 2022.

[137] R. Ramalingam, M. H. U. T. Fazil, N. K. Verma, and K. D. Arunachalam, "Green synthesis, characterization and antibacterial evaluation of electrospun nickel oxide nanofibers," *Materials Letters*, vol. 256, Article ID 126616, 2019.

[138] M. Sudha, S. Surendhiran, V. Gowthambabu et al., "Enhancement of corrosive-resistant behavior of Zn and Mg metal plates using biosynthesized nickel oxide nanoparticles," *Journal of Bio-and Tribo-Corrosion*, vol. 7, no. 2, pp. 60–16, 2021.

[139] L. P. Silva, C. C. Bonatto, and V. L. P. Polez, "Green synthesis of metal nanoparticles by fungi: current trends and challenges," in *Advances and Applications through Fungal Nanobiotechnology*, pp. 71–89, Springer, Berlin, Germany, 2016.

[140] J. Moavi, F. Buazar, and M. H. Sayahi, "Algal magnetic nickel oxide nanocatalyst in accelerated synthesis of pyridopyrimidine derivatives," *Scientific Reports*, vol. 11, no. 1, pp. 6296–14, 2021.

[141] S. Ghotekar, "Plant extract mediated biosynthesis of Al2O3 nanoparticles-a review on plant parts involved, characterization and applications," *Nanochemistry Research*, vol. 4, no. 2, pp. 163–169, 2019.

[142] P. Sutradhar, N. Debnath, and M. Saha, "Microwave-assisted rapid synthesis of alumina nanoparticles using tea, coffee and triphala extracts," *Advances in Manufacturing*, vol. 1, no. 4, pp. 357–361, 2013.

[143] P. Manogar, J. Esther Morvinyabesh, P. Ramesh et al., "Biosynthesis and antimicrobial activity of aluminium oxide nanoparticles using Lyngbya majuscula extract," *Materials Letters*, vol. 311, Article ID 131569, 2022.

[144] P. Suryavanshi, R. Pandit, A. Gade, M. Derita, S. Zachino, and M. Rai, "Colletotrichum sp.-mediated synthesis of sulphur and aluminium oxide nanoparticles and its in vitro activity against selected food-borne pathogens," *LWT-Food Science and Technology*, vol. 81, pp. 188–194, 2017.

[145] K. R. Sumesh and K. Kanthavel, "Green synthesis of aluminium oxide nanoparticles and its applications in mechanical and thermal stability of hybrid natural composites," *Journal of Polymers and the Environment*, vol. 27, no. 10, pp. 2189–2200, 2019.

[146] K. R. Sumesh, K. Kanthavel, and S. Vivek, "Mechanical/thermal/vibrational properties of sisal, banana and coir hybrid natural composites by the addition of bio synthesized aluminium oxide nano powder," *Materials Research Express*, vol. 6, no. 4, Article ID 045318, 2019.

[147] K. R. Sumesh, K. Kanthavel, A. Ajithram, and P. Nandhini, "Bioalumina nano powder extraction and its applications for sisal, coir and banana hybrid fiber composites: mechanical and thermal properties," *Journal of Polymers and the Environment*, vol. 27, no. 9, pp. 2068–2077, 2019.

[148] N. S. Narayanan, N. Baskar, B. N. Vedha Hari, R. Sankaran, and D. Ramya Devi, "Performance of cutting tool with cross-chevron surface texture filled with green synthesized aluminium oxide nanoparticles," *Scientific Reports*, vol. 9, no. 1, Article ID 17803, 2019.

[149] P. Duraisamy, "Green synthesis of aluminium oxide nanoparticles by using *Aerva lanta* and *Terminalia chebula* extracts," *IJRASET*, vol. 6, no. 1, pp. 428–433, 2018.

[150] M. Hasanpoor, H. Fakhr Nabavi, and M. Aliofkhazraei, "Microwave-assisted synthesis of alumina nanoparticles using some plants extracts," *Journal of Nanostructures*, vol. 7, no. 1, pp. 40–46, 2017.

[151] H. Koopi and F. Buazar, "A novel one-pot biosynthesis of pure alpha aluminum oxide nanoparticles using the macroalgae *Sargassum ilicifolium*: a green marine approach," *Ceramics International*, vol. 44, no. 8, pp. 8940–8945, 2018.

[152] S. Ghotekar, S. Pansambal, M. Bilal, S. S. Pingale, and R. Oza, "Environmentally friendly synthesis of Cr_2O_3 nanoparticles: characterization, applications and future perspective—a review," *Case Studies in Chemical and Environmental Engineering*, vol. 3, Article ID 100089, 2021.

[153] T. Satgurunathan, P. S. Bhavan, and R. D. S. Joy, "Green synthesis of chromium nanoparticles and their effects on the growth of the prawn *Macrobrachium rosenbergii* post-larvae," *Biological Trace Element Research*, vol. 187, no. 2, pp. 543–552, 2019.

[154] S. A. Khan, S. Shahid, S. Hanif, H. S. Almoallim, S. A. Alharbi, and H. Sellami, "Green synthesis of chromium oxide nanoparticles for antibacterial, antioxidant anticancer, and biocompatibility activities," *International Journal of Molecular Sciences*, vol. 22, no. 2, 2021.

[155] H. E. Ahmed Mohamed, S. Afridi, A. T. Khalil et al., "Phytofabricated Cr_2O_3 nanoparticle for multifunctional biomedical applications," *Nanomedicine*, vol. 15, no. 17, pp. 1653–1669, 2020.

[156] D. Hassan, A. T. Khalil, A. R. Solangi, A. El-Mallul, Z. K. Shinwari, and M. Maaza, "Physiochemical properties and novel biological applications of *Callistemon viminalis* -mediated α-Cr_2O_3 nanoparticles," *Applied Organometallic Chemistry*, vol. 33, no. 8, Article ID e5041, 2019.

[157] J. Sackey, R. Morad, A. Bashir, L. Kotsedi, C. Kaonga, and M. Maaza, "Bio-synthesised black α-Cr_2O_3 nanoparticles; experimental analysis and density function theory calculations," *Journal of Alloys and Compounds*, vol. 850, Article ID 156671, 2021.

[158] U. R. Sharma and N. Sharma, "Green synthesis, anti-cancer and corrosion inhibition activity of Cr_2O_3 nanoparticles," *Biointerface Research in Applied Chemistry*, vol. 11, pp. 8402–8412, 2021.

[159] A. A. Elzoghby, A. Bakry, A. M. Masoud, W. S. Mohamed, M. H. Taha, and T. F. Hassanein, "Synthesis of polyamide-based nanocomposites using green-synthesized chromium and copper oxides nanoparticles for the sorption of uranium from aqueous solution," *Journal of Environmental Chemical Engineering*, vol. 9, no. 6, Article ID 106755, 2021.

[160] P. Rayani Nivethitha and D. Carolin Jeniba Rachel, "A study of antioxidant and antibacterial activity using honey mediated chromium oxide nanoparticles and its characterization," *Materials Today Proceedings*, vol. 48, pp. 276–281, 2022.

[161] O. M. Kotb, F. M. A. El-Latif, A. R. Atawia, S. S. Saleh, and S. F. El-Gioushy, "Green synthesis of chromium nanoparticles by aqueous extract of *Melia azedarach*, *Artemisia herba-alba* and bacteria fragments against *Erwinia amylovora*," *Asian Journal of Biotechnology and Bioresource Technology*, vol. 6, pp. 22–30, 2020.

[162] A. Kanakalakshmi, V. Janaki, K. Shanthi, and S. Kamala-Kannan, "Biosynthesis of Cr (III) nanoparticles from electroplating wastewater using chromium-resistant *Bacillus subtilis* and its cytotoxicity and antibacterial activity," *Artificial Cells, Nanomedicine, and Biotechnology*, vol. 45, no. 7, pp. 1304–1309, 2017.

[163] Z. Ahmad, A. Shamim, S. Mahmood, T. Mahmood, and F. U. Khan, "Biological synthesis and characterization of chromium (III) oxide nanoparticles," *Engineering and Applied Science Letters*, vol. 1, no. 2, pp. 23–29, 2018.

[164] I. Ghodrat, A. Divsalar, S. Ayrian, and M. Saeidifar, "Evaluation of the anticancer effects of samarium nanoparticles synthesized by extract of ginger on HCT116 colorectal cancer cells," *Journal of Cell & Tissue*, vol. 10, no. 4, pp. 202–213, 2019.

[165] V. Muthulakshmi, M. Balaji, and M. Sundrarajan, "Biomedical applications of ionic liquid mediated samarium oxide nanoparticles by Andrographis paniculata leaves extract," *Materials Chemistry and Physics*, vol. 242, Article ID 122483, 2020.

[166] S. M. Kazemi, N. Nami, and A. Yahyazadeh, "Bio-directed synthesis of Sm_2O_3 NPs by *Hibiscus syriacus* Ardens flower extract as an effective catalyst in the preparation of benzimidazole derivatives," *Nanochemistry Research*, vol. 6, no. 2, pp. 149–163, 2021.

[167] N. Putri, Y. Yulizar, A. Umar, and D. Apriandanu, "Sm_2O_3 nanoparticles preparation using *Caesalpinia pulcherrima* leaf extract, characterization and photocatalytic activity," *IOP Conference Series: Materials Science and Engineering*, vol. 902, Article ID 012012, 2020.

[168] H. Xue, W. Zhang, X. Li, X. You, J. Rao, and F. Pan, "A facile green synthesis of Sm_2O_3 nanoparticles via microwave-assisted urea precipitation route and their optical properties," *Electronic Materials Letters*, vol. 13, no. 3, pp. 255–259, 2017.

[169] M. Fritz, S. Körsten, X. Chen et al., "High-resolution particle size and shape analysis of the first samarium nanoparticles biosynthesized from aqueous solutions via cyanobacteria *Anabaena cylindrica*," vol. 26, NanoImpact, Article ID 100398, 2022.

[170] C. B. Fischer, S. Körsten, L. M. Rösken et al., "Cyanobacterial promoted enrichment of rare earth elements europium, samarium and neodymium and intracellular europium particle formation," *RSC Advances*, vol. 9, no. 56, pp. 32581–32593, 2019.

[171] S. N. Naidi, M. H. Harunsani, A. L. Tan, and M. M. Khan, "Green-synthesized CeO_2 nanoparticles for photocatalytic, antimicrobial, antioxidant and cytotoxicity activities," *Journal of Materials Chemistry B*, vol. 9, no. 28, pp. 5599–5620, 2021.

[172] M. M. Khan, S. N. Matussin, and A. Rahman, "Recent progress of phytogenic synthesis of ZnO, SnO_2, and CeO_2 nanomaterials," *Bioprocess and Biosystems Engineering*, vol. 45, pp. 619–645, 2022.

[173] S. Kontham, K. Mandava, S. Dosa, F. U. Mohd, O. A. Mohammed, and A. U. Mohammad, "Review on facile synthesis of cerium oxide nanoparticles and their biomedical applications," *Inorganic and Nano-Metal Chemistry*, vol. 52, no. 8, pp. 1183–1195, 2021.

[174] F. Charbgoo, M. B. Ahmad, and M. Darroudi, "Cerium oxide nanoparticles: green synthesis and biological applications," *International Journal of Nanomedicine*, vol. 12, pp. 1401–1413, 2017.

[175] H. S. Lalithamba, M. Raghavendra, and K. V. Yatish, "Efficient application of green synthesized CeO_2 nanoparticles for the preparation of selenoester derivatives of protected amino acids and production of biodiesel from annona squamosa oil," *Journal of Electronic Materials*, vol. 51, no. 7, pp. 3650–3659, 2022.

[176] N. Ditlopo, N. Sintwa, S. Khamlich et al., "From Khoi-San indigenous knowledge to bioengineered CeO_2 nanocrystals to exceptional UV-blocking green nanocosmetics," *Scientific Reports*, vol. 12, no. 1, p. 3468, 2022.

[177] N. Sisubalan, V. S. Ramkumar, A. Pugazhendhi et al., "ROS-mediated cytotoxic activity of ZnO and CeO_2 nanoparticles synthesized using the *Rubia cordifolia* L. leaf extract on MG-63 human osteosarcoma cell lines," *Environmental Science and Pollution Research*, vol. 25, no. 11, pp. 10482–10492, 2018.

[178] S. Ramalingam, G. Sankaranarayanan, S. Senthil, R. Rohith, and R. Santosh Kumar, "Effect of cerium oxide nanoparticles derived from biosynthesis of *Azadirachta indica* on stability and performance of a research CI engine powered by diesel-lemongrass oil blends," *Energy & Environment*, 2022.

[179] Z. Kalaycıoğlu, B. Geçim, and F. B. Erim, "Green synthesis of cerium oxide nanoparticles from turmeric and kinds of honey: characterisations, antioxidant and photocatalytic dye degradation activities," *Advances in Natural Sciences: Nanoscience and Nanotechnology*, vol. 13, no. 1, Article ID 015016, 2022.

[180] S. Safat, F. Buazar, S. Albukhaty, and S. Matroodi, "Enhanced sunlight photocatalytic activity and biosafety of marine-driven synthesized cerium oxide nanoparticles," *Scientific Reports*, vol. 11, no. 1, pp. 14734–11, 2021.

[181] S. F. Khaligh and A. Asoodeh, "Green synthesis and biological characterization of cerium oxide nanoemulsion against human HT-29 colon cancer cell line," *Materials Technology*, pp. 1–21, 2022.

[182] E. Nourmohammadi, R. Kazemi Oskuee, L. Hasanzadeh et al., "Cytotoxic activity of greener synthesis of cerium oxide nanoparticles using carrageenan towards a WEHI 164 cancer cell line," *Ceramics International*, vol. 44, no. 16, pp. 19570–19575, 2018.

[183] H. Dabhane, S. Ghotekar, P. Tambade, and V. Medhane, "Plant mediated green synthesis of lanthanum oxide (La_2O_3) nanoparticles: a review," *Asian Journal of Nanosciences and Materials*, vol. 3, no. 4, pp. 291–299, 2020.

[184] R. F. Madani, I. Sofianty, A. G. P. Sari, R. Maryanti, and A. B. D. Nandiyanto, "Synthesis methods and green synthesis of lanthanum oxide nanoparticles: a review," *Arabian Journal of Chemical and Environmental Research*, vol. 8, no. 2, pp. 287–314, 2021.

[185] K. A. Manoj Kumar, E. Hemananthan, P. Renuka Devi, S. Vignesh Kumar, and R. Hariharan, "Biogenic synthesis, characterization and biological activity of lanthanum nanoparticles," *Materials Today Proceedings*, vol. 21, pp. 887–895, 2020.

[186] R. U. Maheswari, R. Yuvakkumar, G. Ravi, and S. I. Hong, "Organic *Datura metal* leaf extract mediated inorganic rare earth La_2O_3 nanocrystals formation," *Journal of Nanoscience and Nanotechnology*, vol. 19, no. 7, pp. 4033–4038, 2019.

[187] B. Rashmi, S. F. Harlapur, K. Gurushantha et al., "Facile green synthesis of lanthanum oxide nanoparticles using *Centella asiatica* and Tridax plants: photocatalytic, electrochemical sensor and antimicrobial studies," *Applied Surface Science Advances*, vol. 7, Article ID 100210, 2022.

[188] G. Rajakumar, L. Mao, T. Bao et al., "Yttrium oxide nanoparticle synthesis: an overview of methods of preparation and biomedical applications," *Applied Sciences*, vol. 11, no. 5, p. 2172, 2021.

[189] N. Basavegowda, K. Mishra, R. S. Thombal, K. Kaliraj, and Y. R. Lee, "Sonochemical green synthesis of yttrium oxide (Y_2O_3) nanoparticles as a novel heterogeneous catalyst for the construction of biologically interesting 1,3-thiazolidin-4-ones," *Catalysis Letters*, vol. 147, no. 10, pp. 2630–2639, 2017.

[190] P. Nagajyothi, M. Pandurangan, M. Veerappan, D. H. Kim, T. Sreekanth, and J. Shim, "Green synthesis, characterization and anticancer activity of yttrium oxide nanoparticles," *Materials Letters*, vol. 216, pp. 58–62, 2018.

Hindawi
Journal of Chemistry
Volume 2022, Article ID 5375815, 14 pages
https://doi.org/10.1155/2022/5375815

Research Article

Aspartic Acid- and Glycine-Functionalized Mesoporous Silica as an Effective Adsorbent to Remove Methylene Blue from Contaminated Water

Abdullah M. Alswieleh

Department of Chemistry, College of Science, King Saud University, Riyadh, Saudi Arabia

Correspondence should be addressed to Abdullah M. Alswieleh; aswieleh@ksu.edu.sa

Received 26 February 2022; Revised 6 April 2022; Accepted 12 April 2022; Published 26 April 2022

Academic Editor: Ahmed Mourtada Elseman

In this work, aspartic acid- and glycine-functionalized mesoporous silica nanoparticles (Asp-MSNs and Gly-MSNs) were successfully prepared and applied as adsorbents for removal of methylene blue (MB) from contaminated water. The mesoporous structure of the fabricated nanomaterials was confirmed by nitrogen adsorption/desorption with specific surface area of ca. 700 m^2/g and pore volume of 0.9 cm^3/g for both Asp-MSNs and Gly-MSNs. The average size of the nanoadsorbents was estimated to be ca. 290 nm as characterized by scanning electron microscopy (SEM) and transmission electron microscope (TEM). The physical and chemical properties of the Asp-MSNs and Gly-MSNs were also characterized by Fourier transform infrared (FTIR) spectroscopy, zeta potential, and elemental analysis. Asp-MSNs and Gly-MSNs exhibited good adsorption performance for removal of cationic organic dyes (MB). The equilibrium adsorption capacity of Asp-MSNs and Gly-MSNs was found to be 55 $mg{\cdot}g^{-1}$ and 43 $mg{\cdot}g^{-1}$, respectively, under the optimal conditions. The Langmuir model and pseudo-second-order equation exhibited good correlation with the isotherm and adsorption kinetic data for MB, respectively.

1. Introduction

Water pollution with organic dyes from industries, such as leather, plastic, cosmetics, paper, food, and textile, has been a serious environmental issue. Wastewater contaminated with such compounds may create an eco-toxic hazard and cause bioaccumulation. Thus, the decontamination of wastewater has received a great deal of attention worldwide. [1] Most of the organic dyes are very stable and difficult to be biodegraded. [2] Exposure to such hazardous dyes may cause neurological injury, nausea, and vomiting. Due to the strong toxicity in plants, animals, and humans, hazardous dyes should be removed from wastewater before discharging to the environment. [3, 4]

Several physical, chemical, and biological treatment techniques have been developed to decontaminate wastewater. [3–6] Among these techniques, adsorption method has proven to be simple, effective, and economically feasible method for treating of dye-containing wastewater. [6–8] Therefore, different types of adsorbents have been developed to meet different needs, such as activated carbon [9], clay [10], and zeolite. [11] However, such adsorbents have some limitations such as low adsorption capacities and regeneration problems. [4, 6] Therefore, new adsorbents with high adsorption performance are needed to develop.

In recent years, nanostructured materials have been widely explored as high-efficiency sorbents due to their high surface area and high activities. [12–14] Mesoporous silica nanoparticles (MSNs) have been widely researched in biological and environmental fields, because of the excellent structural features, thermal stability, facile modification, and high surface area. [15–17] MSNs have been modified with different functional groups to increase the extraction efficiency, such as amine [18–22] or carboxylic acid [23, 24]. Amine-functionalized MSNs have been fabricated as an adsorbent to remove alizarin yellow and phenol red from wastewater with maximum adsorption capacity of 370.70 $mg\,g^{-1}$ and 400 $mg\,g^{-1}$, respectively. [21] Moreover,

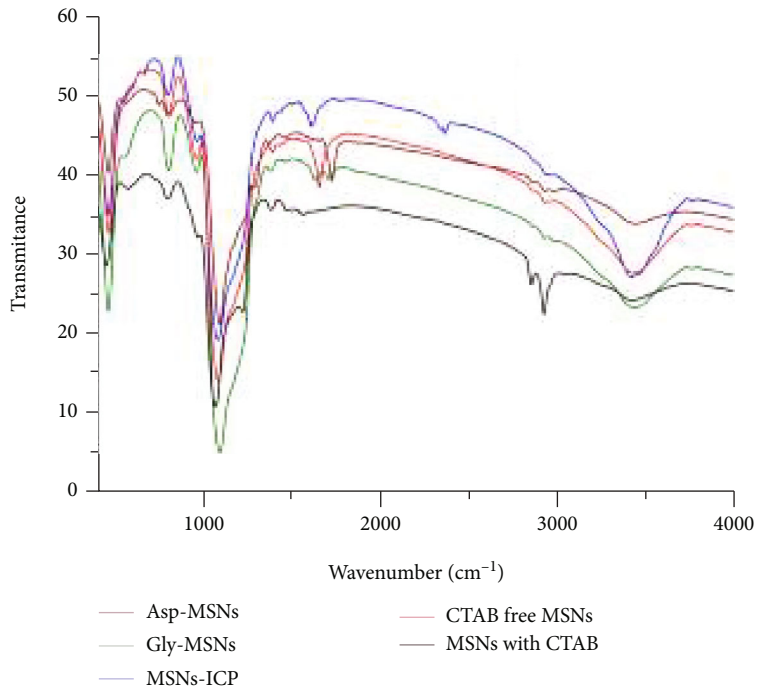

Figure 1: FTIR spectra of (black) MSNs (with CTAB), (red) CTAB free MSNs, (blue) MSNs-ICP, (brown) Asp-MSNs, and (green) Gly-MSNs.

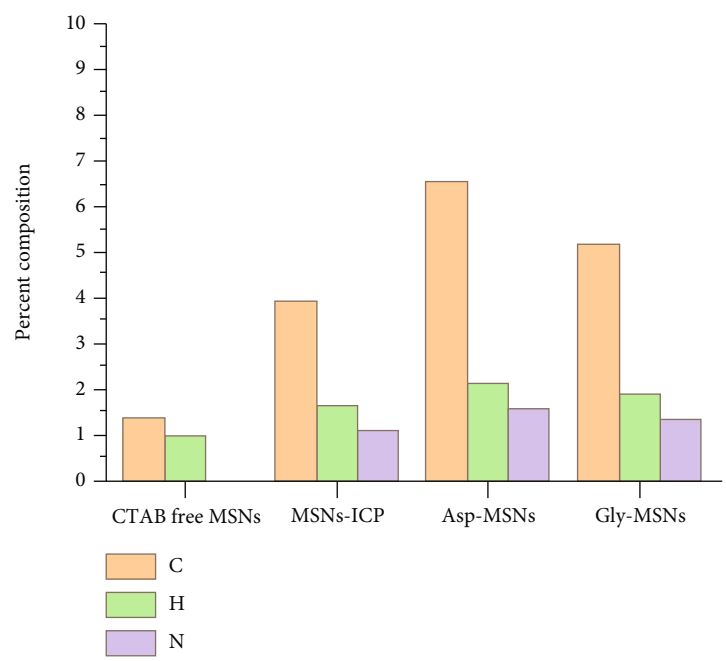

Figure 2: Elemental analysis for CTAB free MSNs, MSNs-ICP, Asp-MSNs, and Gly-MSNs.

amine-modified porous silica was used to remove Ponceau 4R, Rhodamine B, Sunset Yellow, and Brilliant Blue from aqueous solutions with more than 92% extraction efficiency. [22] MSNs modified with carboxylic acid have also been used as adsorbent for removal phenosafranine (PF), methylene blue (MB), rhodamine B (RhB), and orange II (OII), with high extraction capacities for cationic dyes. [23]

Amine and carboxylic groups on the surface may improve the adsorption of ionic organic molecules. The attachment of amino acids on the surface of the adsorbents improved the adsorption efficiency of organic molecules. [25–29] Beagan reported the synthesis of MSNs via Stober method and functionalized with cysteine for removal MB from contaminated water using the batch method. [27]

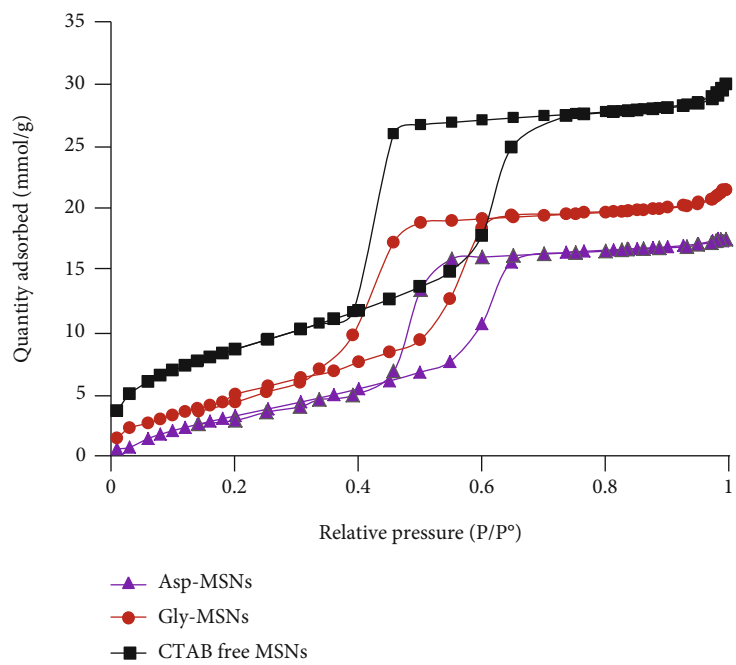

Figure 3: The isotherm obtained for CTAB free MSNs, Gly-MSNs, and Asp-MSNs.

The adsorption capacity was about 70 mg/g in acidic media, and about 140 mg/g in basic media. Histidine attached to MSNs surface was synthesized to remove MB from an aqueous solution. [28] The maximum adsorption efficiency of the fabricated nanoparticles was reported to be 60 mg/g in basic media.

As far as I am aware, very little work has been reported on MSNs modification with amino acids for environmental applications. Hence, in this study, mesoporous silica nanoparticles (MSNs) were combined with amino acids to prepare novel nanosorbents (Asp-MSNs and Gly-MSNs) for the removal of cationic dye (methylene blue (MB)). Therefore, anchoring of aspartic acid and glycine onto the MSNs surface is beneficial for improving the adsorption capacities of MB. The fabricated Asp-MSNs and Gly-MSNs were characterized by FTIR, zeta potential, SEM, and TEM analyses. Batch adsorption tests of MB by Asp-MSNs and Gly-MSNs were carried out at different pH values, initial concentration, and contact time, to study the adsorption kinetics and isotherms.

2. Experimental

2.1. Materials. N-Cetyltrimethylammonium bromide (CTAB, 98%), n-hexane (99%), ammonium hydroxide (NH_4OH, 32 wt%), tetraethyl orthosilicate (TEOS, 98%), dichloromethane (DCM, HPLC grade), 3-isocyanatopropyl triethoxysilane (ICPTES, >95%), L-aspartic acid (Asp, ≥98%), and glycine (Gly, ≥98.5%) were obtained from Sigma-Aldrich. Toluene (98%), hydrochloric acid (HCl, 36%), sodium hydroxide, dimethylformamide (DMF, HPLC grade), pyridine (analytical grade), methanol (HPLC grade), and ethanol (HPLC grade) were brought from Fisher Scientific. Methylene blue (MB) was brought from WINLAB. All chemicals were used as received.

Table 1: Comparison of the surface area, pore volume, and pore size of CTAB free MSNs, Gly-MSNs, and Asp-MSNs.

	Surface area (m^2/g)	Pore volume (cm^3/g)	Pore size (nm)
CTAB free MSNs	1019	1.37	5.5
Gly-MSNs	739	0.92	4.9
Asp-MSNs	684	0.87	4.7

2.2. Fabrication of the Nanoadsorbents

2.2.1. Synthesis of Mesoporous Silica Nanoparticles (MSNs). 160 mL of distilled water (DW), CTAB (1 g), and NH_4OH (4 mL) were added and stirred at 40°C. A mixture of TEOS and n-hexane (25 mL) with 4 : 1 ratio was added slowly to the aqueous solution. The solid was separated and washed with DW and methanol several times. Then, the particles were suspended in 25 mL of acetic acid (12.5 mL) and hydrogen peroxide (12.5 mL) at 120°C. Finally, the solid was separated and washed with DW and methanol several times [30–32].

2.2.2. Aspartic Acid- and Glycine-Functionalized MSNs. The synthesis of aspartic acid-functionalized MSNs (Asp-MSNs) and glycine-functionalized MSNs (Gly-MSNs) was achieved in two steps. Firstly, 1 g of CTAB free MSNs was dispersed in 25 mL dried toluene and sonicated for 10 min. ICPTES (0.2 mL) was added to the mixture and heated at 120°C overnight. MSNs-ICP was separated and washed with dry toluene and DMF. Secondly, MSNs-ICP was suspended in 10 mL DMF and sonicated for 10 min.

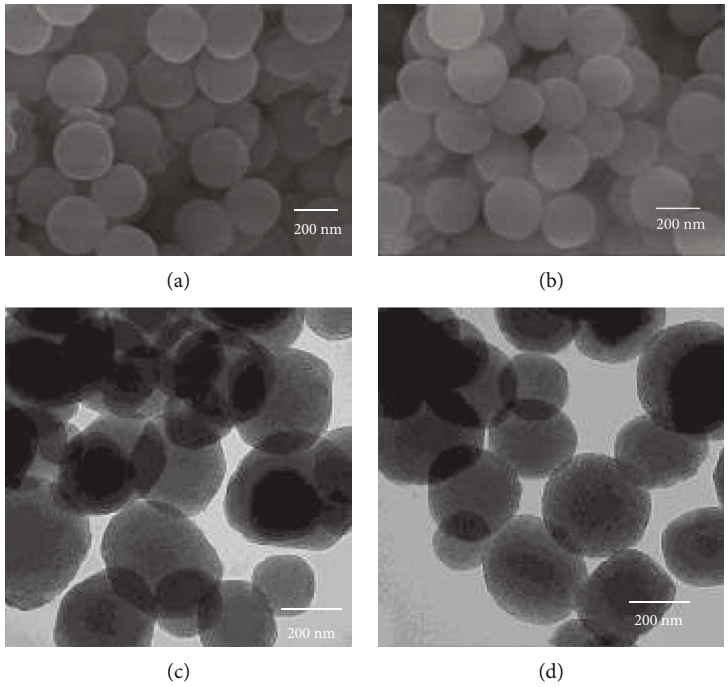

Figure 4: (a) and (b) SEM images of Asp-MSNs and Gly-MSNs, respectively. (c) and (d) TEM images of Asp-MSNs and Gly-MSNs, respectively.

To the suspension, 10 mL of DMF containing 200 mg of aspartic acid (or glycine) was added and sonicated for 10 min. The mixture was left under stirring at room temperature overnight. Asp-MSNs (or Gly-MSNs) were separated and washed with DW and methanol several times, and dried at 90°C for 3 h.

2.3. General Characterization. The structure and performance of the fabricated nanoadsorbents were characterized using several techniques. Scanning electron microscopy (SEM) images were obtained using JEOL instrument model JSM-6380 LA. Transmission electron microscopy (TEM) images were obtained using JEOL instrument model JEM-1230. The FTIR spectra measurements were mounted using Thermo Scientific Nicolet iS10 FT-IR spectrometer in KBr pellet at room temperature in a spectral range 4000–400 cm^{-1}. Shimadzu instrument model UV-2600 was used to acquire UV spectra of dye.

2.4. Adsorption Investigation

2.4.1. Batch Adsorption Experiments. Batch method experiments were performed using MB as probes to evaluate the adsorption performance of fabricated nanoadsorbents. The adsorption behavior was investigated at different pH values, initial concentration, and exposure time. The contaminated water samples were prepared by dissolving known amounts of MB in DW. The prepared adsorbent (10 mg) was placed in a sample tube containing 10 mL of different concentrations MB aqueous solution (20, 50, 80, 100, 200 mg·L) and then shaken at 150 r·min^{-1} for certain period time. The nanoadsorbents were separated by centrifugation and the concentration of MB after adsorption process was determined by UV–vis spectrophotometer. The removal efficiency and the amount of MB adsorbed onto nanoadsorbents were calculated using the following equations:

$$\begin{aligned} \text{Removal efficiency}(\%) &= C_0 - C_e/C_0 \times 100\%, \\ q_t &= (C_0 - C_t)V/m, \end{aligned} \tag{1}$$

where C_0 and C_e (mg·L) are the initial and equilibrium concentrations of MB, respectively. C_t (mg·L) is the concentration of MB at time t (min). q_t (mg·g^{-1}) is the amount of MB adsorbed per unit mass of the nanoadsorbents at time t. V (L) is the volume of the adsorbed solution. m (g) is the mass of the nanoadsorbents.

2.4.2. Adsorption Kinetics. The kinetics of MB adsorbed on the surface of the nanoadsorbents was explained by three adsorption models. Each equation model is expressed by:

(i) Pseudo-first-order model

$$l_g(q_e - q_t) = l_g q_e - k_1 t, \tag{2}$$

(ii) Pseudo-second-order model

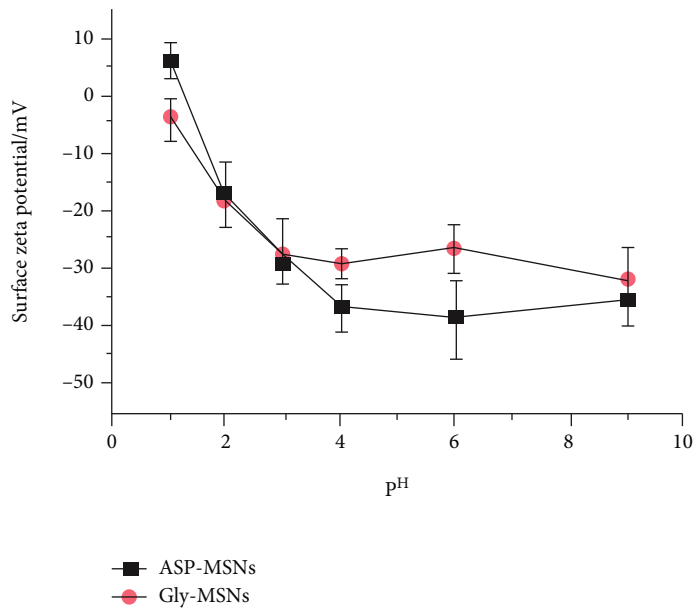

Figure 5: The electronic charges on the surface of Asp-MSNs and Gly-MSNs in aqueous solutions at different pH values.

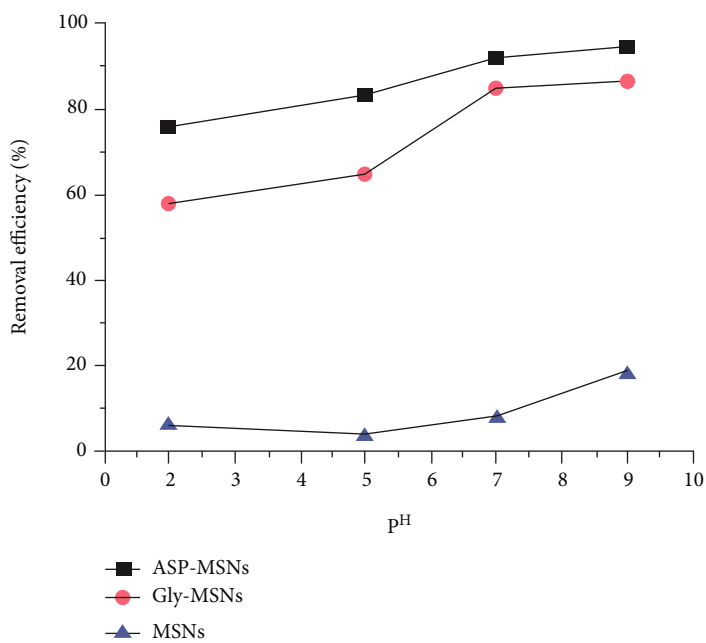

Figure 6: Effect of pH on adsorption behavior of MB by CTAB free MSNs, Asp-MSNs, and Gly-MSNs (C_0 = 50 mg·L, V =10 mL, T =298 K).

$$\frac{t}{q_t} = \frac{1}{k_2 q_e^2} + \frac{t}{q_e}, \quad (3)$$

(iii) Intraparticle diffusion model

$$q_t = k_{\text{dif}} t^{1/2} + C, \quad (4)$$

where q_e (mg·g^{-1}) is the amount of MB adsorbed onto the nanoadsorbents at equilibrium. q_t (mg·g^{-1}) is the amount of MB adsorbed onto the nanoadsorbents at time t (min). k_1 (mg·min·g^{-1}) is the pseudo-first-order rate constant. k_2 (mg·min·g^{-1}) is the pseudo-second-order rate constant. k_2 $q_e{}^2$ is the initial sorption rate (mg·g^{-1}·min^{-1}), revealing the movement rate of MB molecule. k_{dif} (mg·g^{-1}·min$^{-1/2}$) is the intraparticle diffusion rate constant.

2.4.3. Adsorption Isotherms. To understand the adsorption behavior of MB on the surface of nanoadsorbents, two isotherm equations were selected to model the adsorption

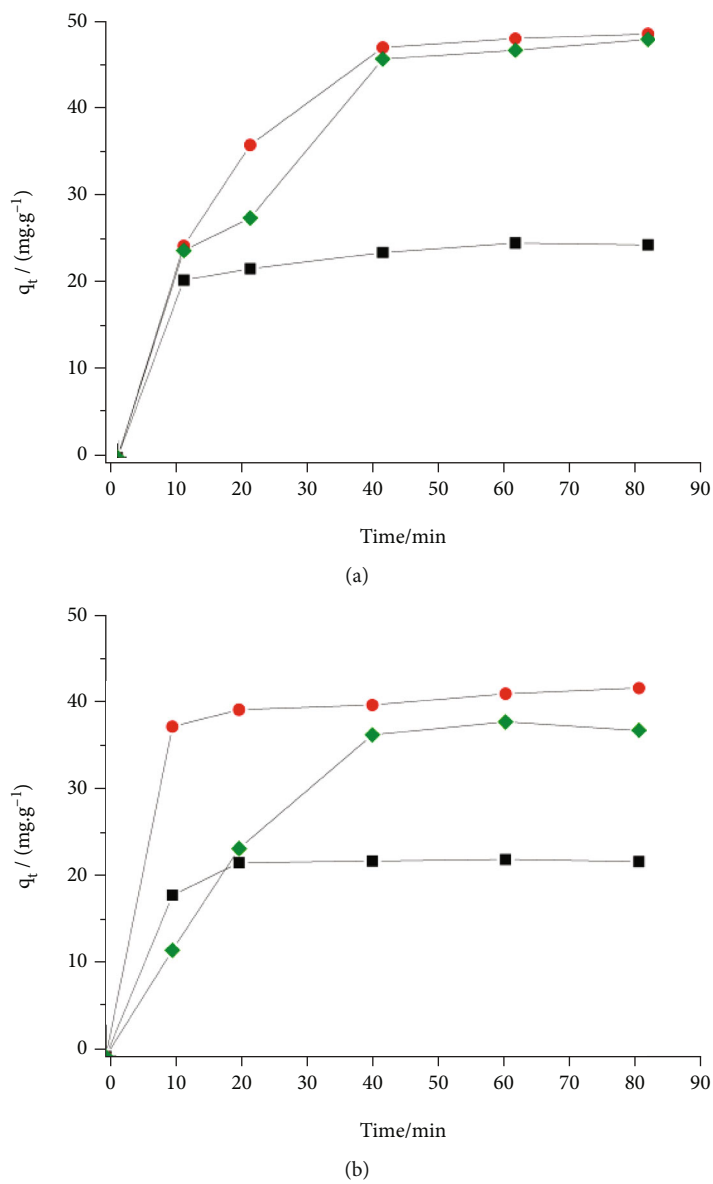

Figure 7: Effect of contact time and initial concentration (50 ppm (black), 100 ppm (green), and 200 ppm (red)) on adsorption behavior of MB by (a) Asp-MSNs and (b) Gly-MSNs (V =10 mL, T =298 K).

isotherm data. The Langmuir and Freundlich equation models are expressed by:

Langmuir equation:

$$\frac{C_e}{q_e} = \frac{1}{bq_m}\frac{C_e}{q_m}, \tag{5}$$

Freundlich equation:

$$\ln q_e = \ln K_f + \frac{1}{n} \ln C_e, \tag{6}$$

where q_m (mg·g^{-1}) is the maximum adsorption capacity. K_F is the constant related to the adsorption intensity. b (L·mg^{-1}) is the Langmuir constant which is related to the affinity of the binding site. A smaller value of $(1/n)$ suggests a more heterogeneous surface. However, when the value is equal or closer to one suggests that the adsorbent has relatively more homogeneous binding sites.

3. Results and Discussion

3.1. General Characterization. Asp-MSNs (or Gly-MSNs) were fabricated in four steps. In basic solution and presence of template (CTAB) and expander agent (hexane), condensation reaction of TEOS was carried out to obtain MSNs. CTAB was extracted by ion exchange process using a mixture of acetic acid and hydrogen peroxide, to have hydrophilic surface and allow reaction with inner surface. CTAB free MSNs were reacted with ICPTES through hydrolysis and condensation reactions between the silanol groups of MSNs and alkoxysilane groups of ICPTES to obtain isocyanato groups conveniently attached to MSNs surface. The primary amine groups in aspartic acid and glycine could

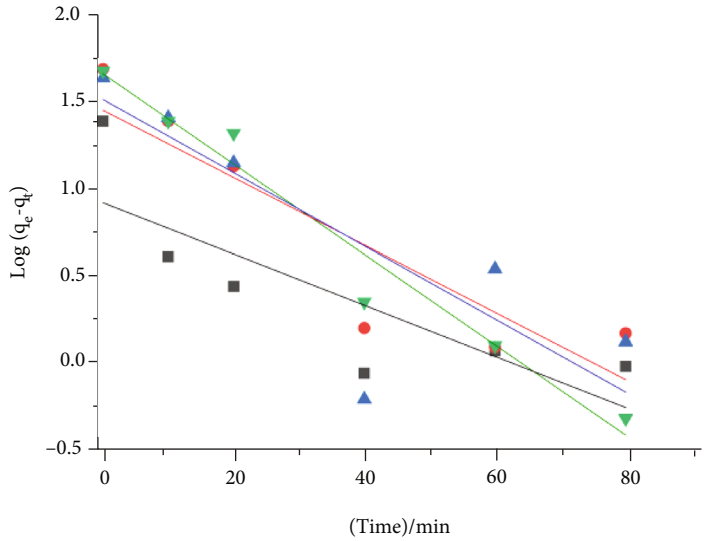

(a)

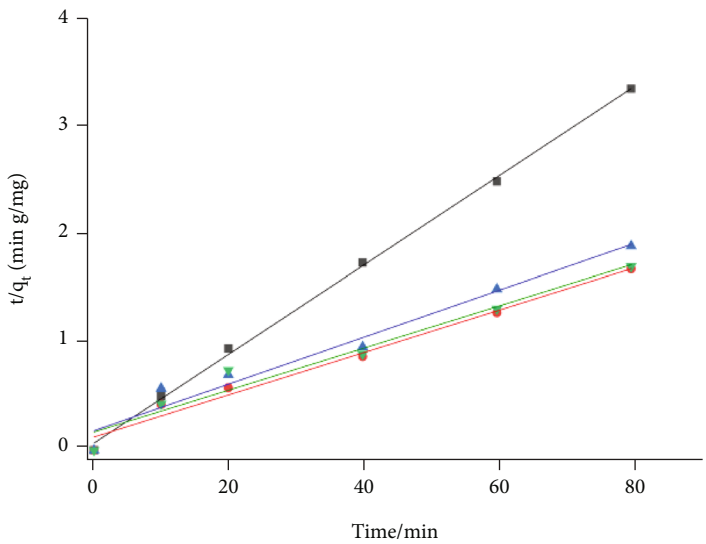

(b)

Figure 8: Continued.

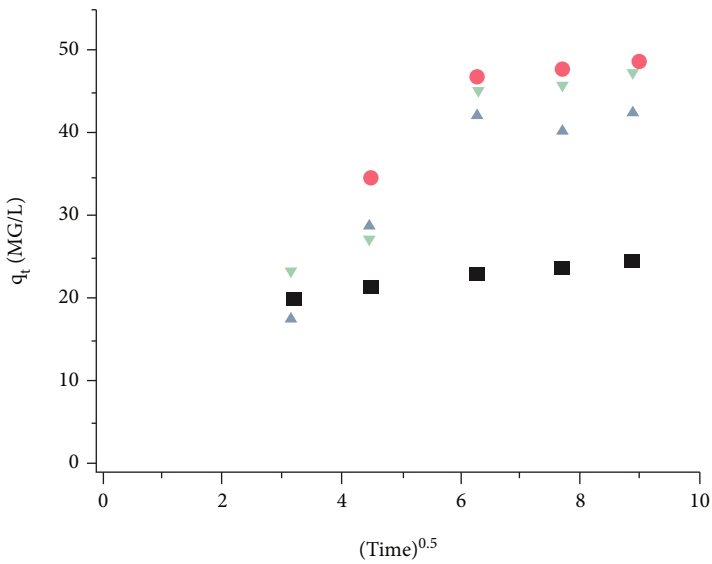

(c)

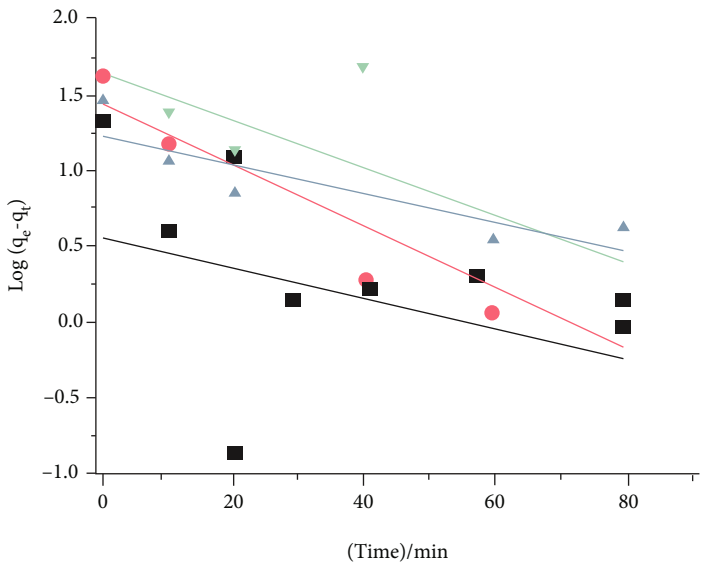

(d)

Figure 8: Continued.

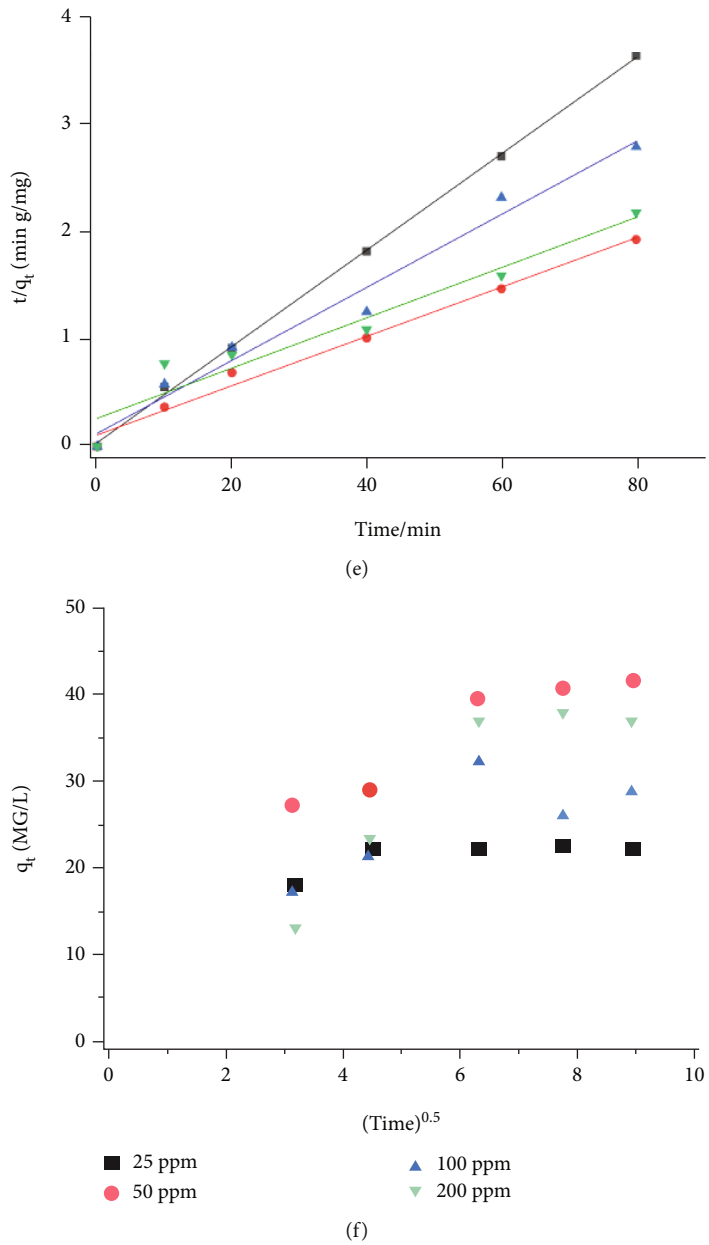

Figure 8: (a) Pseudo-first-order kinetics, (b) pseudo-second-order kinetics, and (c) intraparticle diffusion kinetics for adsorption of MB on Asp-MSNs. (d) Pseudo-first-order kinetics, (e) pseudo-second-order kinetics, and (f) intraparticle diffusion kinetics for adsorption of MB on Gly-MSNs (m =10 mg, V =10 mL, pH =7, and T =298 K).

react with isocyanato groups on the surface, producing Asp-MSNs (or Gly-MSNs).

The covalent functionalization of MSNs with aspartic acid and glycine was characterized by FTIR spectroscopy. Figure 1 shows the IR spectra for MSNs (with CTAB), CTAB free MSNs, MSNs-ICP, Asp-MSNs, and Gly-MSNs. Peaks at ~450 cm^{-1} (SiO_4, tetrahedron vibration) and ~800cm^{-1} (Si –O–Si, symmetric vibration) were noted. Peaks were observed between 1300 and 1000 cm^{-1}, ascribed to Si–O bands stretching of the silica network. A large band at 3400 cm^{-1} was observed for SiO–H. [33] Two bands located at ~2920 cm^{-1} and 2855 cm^{-1} due to $-CH_2-$ stretching vibrations of CTAB in MSNs (with CTAB) sample, which disappeared after solvent extraction process of CTAB, indicating the successful removal of the template from the pores of MSNs. [28, 29] In the MSNs-ICP spectrum, the peak appearing at ~2900 cm^{-1} and~1440 cm^{-1} corresponded to the C–H groups. In the Asp-MSNs and Gly-MSNs spectra, peak located at ~1720 cm^{-1} was observed, corresponding to the carbonyl (–CO–) presence in aspartic acid and glycine, which indicated the successful grafting of amino acids onto the MSNs surface.

In order to confirm the presence of aspartic acid and glycine components in Asp-MSNs and Gly-MSNs, elemental analysis was used to estimate the percentages of carbon, hydrogen, and nitrogen in CTAB free MSNs, MSNs-ICP,

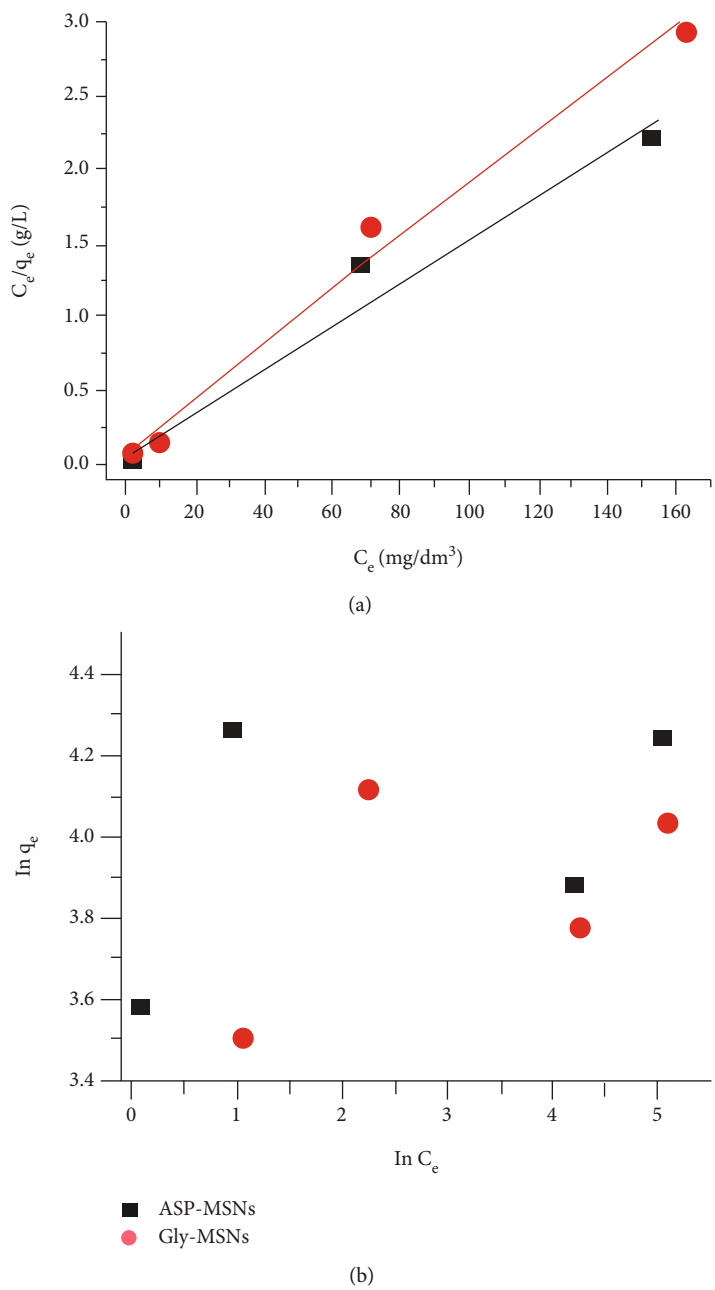

Figure 9: (a) Langmuir adsorption isotherm fit of MB onto Asp-MSNs and Gly-MSNs, and (b) Freundlich adsorption isotherm fit of MB onto Asp-MSNs and Gly-MSNs (m =10 mg, V =10 mL, pH =7, and T =298 K).

Asp-MSNs, and Gly-MSNs. As seen from Figure 2, there is an increase in amount of the C, H, and N elements at each step in the surface modification, which indicated the successful attachment of aspartic acid and glycine onto MSNs surfaces.

The texture properties of CTAB free MSNs, Gly-MSNs, and Asp-MSNs were studied by the N_2 adsorption-desorption isotherm. The BET surface area, total pore volume, and pore sizes were analyzed using Micromeritics Gemini 2375 instrument. It was observed that all the analyzed samples exhibited type IV isotherm with H_1 hysteresis loop, which is typical for mesoporous materials, as shown in Figure 3. This isotherm suggested the adsorption process on the surface of fabricated nanoparticles via multilayer adsorption followed by capillary condensation. Small different capillary condensation steps were found for modified nanoparticles (Gly-MSNs and Asp-MSNs) at higher relative pressures, compared with CTAB free MSNs. The presence of functional groups on MSNs surface reduced its effective silanol surface area. Moreover, the CTAB free MSNs pore diameter was smaller after surface modification due to the presence of functional groups on the internal and external pore surface, leading to the reduction in pore volume; the data are summarized in Table 1.

The SEM and TEM images were utilized to study the morphology of Asp-MSNs and Gly-MSNs. Representative images illustrated in Figures 4(a)–4(d) clearly showed that both Asp-MSNs and Gly-MSNs were almost spherical in shape particles with an average particles size of 290 nm. In addition, TEM images revealed that MSNs have well-ordered pores with an average pore size of 6 nm, which agreed with BET pore size.

The electronic charges on the surface of Asp-MSNs and Gly-MSNs in aqueous solutions at different pH values can be analyzed by zeta potentials. As shown in Figure 5, the result indicated that when the pH was higher than 2 (at pH above the pK_a of carboxylic acid), the surface charge of both nanoadsorbents was negatively charged due to the deprotonation of the carboxylic acid groups. Asp-MSNs and Gly-MSNs are expected to exhibit increased adsorption capacities at pH above the pK_a of carboxylic acid groups, since the electrostatic interactions usually dominate the adsorption process of cationic dyes.

3.2. Effect of pH on the Removal Efficiency. It has been reported that pH is an important parameter affecting the adsorption of organic dyes from contaminated water; [34, 35] therefore, a series of batch equilibrium experiments were conducted to study the effect of pH on the adsorption efficiency of MB by nanoadsorbents over a range of pH values. Figure 6 shows the removal efficiency of MB by CTAB free MSNs, Asp-MSNs, and Gly-MSNs as a function of the corresponding solution pH. According to the surface zeta potential obtained by DLS, as the pH of the solution increased, the surface zeta potential of Asp-MSNs and Gly-MSNs became more negative. Consequently, the adsorption capacities of adsorbents increased due to the electrostatic attractions between the surface of the nanoadsorbents and MB. When the pH of 50 ppm MB solution reached 9, the removal efficiency of MB by Asp-MSNs and Gly-MSNs was 95% and 87%, respectively, compared to 17% for CTAB free MSNs.

3.3. Effect of Contact Time and Initial Concentration on the Removal Efficiency. The contact time is an important parameter for evaluating the adsorption properties of nanoadsorbents. Figures 7(a) and 7(b) show the influence of the contact time and initial concentration on the adsorption capacities of MB by Asp-MSNs and Gly-MSNs. At all concentrations, the removal efficiency increased sharply within 10 min and reached equilibrium in 90 min. The adsorption sites on Asp-MSNs and Gly-MSNs for the MB were sufficient in the initial stage of the adsorption process. When the contact time increases, sufficient interactions can occur between the dye and the adsorption sites of nanoadsorbents. As time progressed, the number of adsorption sites was occupied by MB, and the adsorption capacities were eventually saturated. MB molecules have good mobility and reached equilibrium in a short time due to their low molecular weight and planar structure. [36]

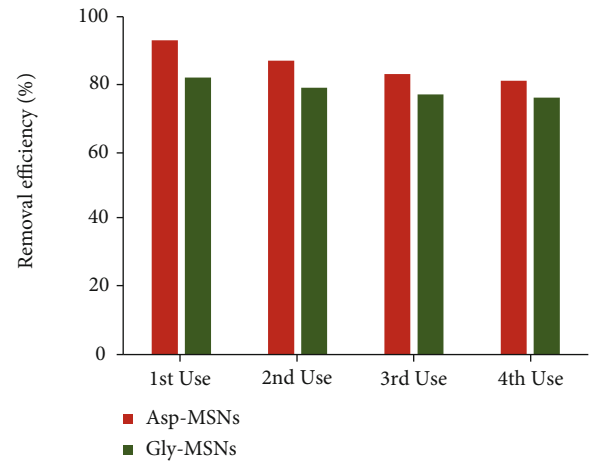

Figure 10: Adsorption efficiency of the fresh Asp-MSNs and Gly-MSNs (1st use) and that of the regenerated nanoadsorbents after two, three, and four uses in the removal of MB from contaminated water at $C_0 = 50$ mg·L, $V = 10$ mL, $T = 298$ K, and pH = 7.

3.4. Adsorption Kinetics. The kinetics of the MB adsorbed onto Asp-MSNs and Gly-MSNs were described by adsorption (equations (2), (3), and (4)). Figures 8(a)–8(c) show the linear fitting results of the kinetic data. The obtained experimental data fitted better with the pseudo-second-order kinetic model (MB on Asp-MSNs: $R^2 = 0.962$, MB on Gly-MSNs: $R^2 = 0.948$). These results suggested that the adsorption rate of MB on the nanoadsorbents was primarily controlled by chemisorption. Since there are electron-rich functional groups on the surface of the nanoadsorbent, then these groups provide attraction forces with dye. Furthermore, the calculated q_e from the pseudo-second order was 52.63 mg·g^{-1} for MB on Asp-MSNs, and 42.92 mg·g^{-1} for MB on Gly-MSNs, which were close to the experimental data (49.7 mg·g^{-1} for MB on Asp-MSNs, and 41.8 mg·g^{-1} for MB on Gly-MSNs).

3.5. Adsorption Isotherms. Two isotherm models, Langmuir and Freundlich, were selected to fit the adsorption isotherm data, to understand the adsorption behavior of nanoadsorbents. The fitted results of the selected isotherm models are presented in Figure 9. According to the correlation coefficients (R^2), the Langmuir model was found to be more suitable than the Freundlich model for describing the adsorption of MB onto Asp-MSNs and Gly-MSNs with correlation coefficients of 0.949 and 0.961, respectively. These results suggested that the surface of both Asp-MSNs and Gly-MSNs were coated by a monolayer of the dye. The maximum adsorption capacity of MB calculated from the Langmuir model was found to be 68.58 mg·g^{-1} and 55.11 mg·g^{-1} for Asp-MSNs and Gly-MSNs, respectively.

3.6. Nanoadsorbents Reusability. The spent nanoadsorbents after use under the optimal set of conditions ($C_0 = 50$ mg·L,

Table 2: The maximum adsorption capacities of different adsorbents for removing MB from aqueous solution, reported in the past literatures.

Adsorbents	q_e (mg·g^{-1})	Ref
Amine functionalized mesoporous silica	49	[37]
Mesoporous silica with cyclodextrin	60	[38]
Histidine modified mesoporous silica	60	[28]
Mesoporous silica functionalized with carboxylic groups	43	[39]
Mesoporous silica coated chitosan	43	[40]
Cysteine functionalized mesoporous silica	140	[27]
Aspartic acid-functionalized MSNs (Asp-MSNs)	55	In this study
Glycine-functionalized MSNs (Gly-MSNs)	43	In this study

V = 10 mL, T = 298 K, and pH = 7) were then washed with acidic solution and ethanol, and then reused under the same optimal conditions. The adsorption efficiencies obtained with successive reuse of the nanoadsorbents are shown in Figure 10. The adsorption efficiencies obtained after two, three, and four uses of Gly-MSNs 1.05-, 1.1-, and 1.13-fold lower than that for the unused Gly-MSNs, whereas the adsorption efficiencies obtained after two, three, and four uses of Asp-MSNs 1.04-, 1.06- and 1.1-fold lower than that for the unused Asp-MSNs.

To illustrate the adsorption performance of Asp-MSNs and Gly-MSNs, the maximum adsorption capacities of nanoadsorbents for MB were compared with those of other reported adsorbents. In general, the maximum adsorption capacities of the fabricated nanoadsorbents for MB were close to most of the other adsorbents, as reported in Table 2. Considering the convenient synthetic method and good adsorption performance, Asp-MSNs and Gly-MSNs are good absorbents for removing toxic cationic molecules from polluted water.

4. Conclusion

In this study, a simple and effective approach based on surface modification of mesoporous silica nanoparticles (MSNs) with amino acids was developed to obtain nanoadsorbents with good adsorption performances. Both Asp-MSNs and Gly-MSNs exhibited good removal properties of MB from aqueous solutions. The equilibrium adsorption capacity of Asp-MSNs was 55 mg·g^{-1}, whereas the equilibrium adsorption capacity of Gly-MSNs was 43 mg·g^{-1}, at 298 K. The experimental data from the adsorption kinetics and isotherm studies indicated that the adsorption of pollutant on both nanoadsorbents fitted well with the pseudo-second-order equation and Langmuir model, respectively. Based on the high efficiency and feasibility, Asp-MSNs and Gly-MSNs exhibited good potential for water treatment.

Data Availability

The data presented in this study are included in this article.

Conflicts of Interest

The authors declare no conflict of interest.

Acknowledgments

This project was supported by Researchers Supporting Project number RSP-2021/238, King Saud University, Riyadh, Saudi Arabia.

References

[1] K. Miksch, G. Cema, P. F.-X. Corvini et al., "R&D priorities in the field of sustainable remediation and purification of agro-industrial and municipal wastewater," *New Biotechnology*, vol. 32, no. 1, pp. 128–132, 2015.

[2] H. Zollinger, Ed., *Azo Dyes and Pigments, Colour Chemistry-Synthesis*, Properties and Applications of Organic Dyes and Pigments, New York, 1987.

[3] E. Forgacs, T. Cserháti, and G. Oros, "Removal of synthetic dyes from wastewaters: a review," *Environment International*, vol. 30, no. 7, pp. 953–971, 2004.

[4] A. Sintakindi and B. Ankamwar, "Fungal biosorption as an alternative for the treatment of dyes in waste waters: a review," *Environmental Technology Reviews*, vol. 10, no. 1, pp. 26–43, 2021.

[5] T. Ilame and A. Ghosh, "The Promising Applications of Nanoparticles for Synthetic Dyes Removal from Wastewater: Recent Review," *Management of Environmental Quality: An International Journal*, vol. 33, no. 2, pp. 451–477, 2022.

[6] A. Srivastava, R. M. Rani, D. S. Patle, and S. Kumar, "Emerging bioremediation technologies for the treatment of textile wastewater containing synthetic dyes: a comprehensive review," *Journal of Chemical Technology & Biotechnology*, vol. 97, no. 1, pp. 26–41, 2022.

[7] H. Chen, X. Wang, J. Li, and X. Wang, "Cotton derived carbonaceous aerogels for the efficient removal of organic pollutants and heavy metal ions," *Journal of Materials Chemistry A*, vol. 3, no. 11, pp. 6073–6081, 2015.

[8] M. Mariana, A. K. HPS, E. B. Yahya et al., "Recent trends and future prospects of nanostructured aerogels in water treatment applications," *Journal of Water Process Engineering*, vol. 45, p. 102481, 2022.

[9] A. Demirbas, "Agricultural based activated carbons for the removal of dyes from aqueous solutions: a review," *Journal of Hazardous Materials*, vol. 167, no. 1-3, pp. 1–9, 2009.

[10] S. B. Haderlein, K. W. Weissmahr, and R. P. Schwarzenbach, "Specific adsorption of nitroaromatic explosives and pesticides to clay minerals," *Environmental Science & Technology*, vol. 30, no. 2, pp. 612–622, 1996.

[11] S. Wang and Y. Peng, "Natural zeolites as effective adsorbents in water and wastewater treatment," *Chemical Engineering Journal*, vol. 156, no. 1, pp. 11–24, 2010.

[12] D. Vishnu, B. Dhandapani, S. Authilingam, and S. V. Sivakumar, "A comprehensive review of effective adsorbents used for the removal of dyes from wastewater," *Current Analytical Chemistry*, vol. 18, no. 3, pp. 255–268, 2022.

[13] A. K. Al-Buriahi, A. A. Al-Gheethi, P. S. Kumar et al., "Elimination of rhodamine B from textile wastewater using nanoparticle photocatalysts: a review for sustainable approaches," *Chemosphere*, vol. 287, p. 132162, 2022.

[14] M. Perwez, H. Fatima, M. Arshad, V. Meena, and B. Ahmad, "Magnetic iron oxide nanosorbents effective in dye removal," *International journal of Environmental Science and Technology*, 2022.

[15] B. Das, B. Das, N. S. Das, S. Sarkar, and K. K. Chattopadhyay, "Tailored mesoporous nanocrystalline Ga_2O_3 for dye-selective photocatalytic degradation," *Microporous and Mesoporous Materials*, vol. 288, p. 109600, 2019.

[16] Y. Wu, X. Du, Y. Kou, Y. Wang, and F. Teng, "Mesoporous SiO2 nanostructure: light-induced adsorption enhancement and its application in photocatalytic degradation of organic dye," *Ceramics International*, vol. 45, no. 18, pp. 24594–24600, 2019.

[17] H. Chaker, N. Ameur, K. Saidi-Bendahou, M. Djennas, and S. Fourmentin, "Modeling and Box-Behnken design optimization of photocatalytic parameters for efficient removal of dye by lanthanum-doped mesoporous TiO_2," *Journal of Environmental Chemical Engineering*, vol. 9, no. 1, p. 104584, 2021.

[18] Z. Yan, G. Li, L. Mu, and S. Tao, "Pyridine-functionalized mesoporous silica as an efficient adsorbent for the removal of acid dyestuffs," *Journal of Materials Chemistry*, vol. 16, no. 18, pp. 1717–1725, 2006.

[19] M. Anbia and S. Salehi, "Removal of acid dyes from aqueous media by adsorption onto amino- functionalized nanoporous silica SBA-3," *Dyes and Pigments*, vol. 94, no. 1, pp. 1–9, 2012.

[20] Y. Wu, M. Zhang, H. Zhao, S. Yang, and A. Arkin, "Functionalized mesoporous silica material and anionic dye adsorption: MCM-41 incorporated with amine groups for competitive adsorption of Acid Fuchsine and Acid Orange II," *RSC Advances*, vol. 4, no. 106, pp. 61256–61267, 2014.

[21] L. Adlnasab, M. Shabanian, M. Ezoddin, and A. Maghsodi, "Amine rich functionalized mesoporous silica for the effective removal of alizarin yellow and phenol red dyes from waste waters based on response surface methodology," *Materials Science and Engineering: B*, vol. 226, pp. 188–198, 2017.

[22] S. Shariati, A. Chinevari, and M. Ghorbani, "Simultaneous removal of four dye pollutants in mixture using amine functionalized Kit-6 silica mesoporous magnetic nanocomposite," *SILICON*, vol. 12, no. 8, pp. 1865–1878, 2020.

[23] J. R. Deka, Y.-H. Lin, and H.-M. Kao, "Ordered cubic mesoporous silica KIT-5 functionalized with carboxylic acid groups for dye removal," *RSC Advances*, vol. 4, no. 90, pp. 49061–49069, 2014.

[24] A. Feinle, F. Leichtfried, S. Straßer, and N. Hüsing, "Carboxylic acid-functionalized porous silica particles by a co-condensation approach," *Journal of Sol-Gel Science and Technology*, vol. 81, no. 1, pp. 138–146, 2017.

[25] J.-F. Lambert, "Adsorption and polymerization of amino acids on mineral surfaces: a review," *Origins of Life and Evolution of Biospheres*, vol. 38, no. 3, pp. 211–242, 2008.

[26] J. E. Rosen and F. X. Gu, "Surface functionalization of silica nanoparticles with cysteine: a low-fouling zwitterionic surface," *Langmuir*, vol. 27, no. 17, pp. 10507–10513, 2011.

[27] A. M. Beagan, "Investigating Methylene Blue removal from aqueous solution by cysteine-functionalized mesoporous silica," *Journal of Chemistry*, vol. 2021, Article ID 8839864, 12 pages, 2021.

[28] A. M. Alswieleh, "Remediation of cationic and anionic dyes from water by histidine modified mesoporous silica," *International Journal of Environmental Analytical Chemistry*, pp. 1–13, 2021.

[29] A. M. Alswieleh, "Cysteine-and glycine-functionalized mesoporous silica as adsorbents for removal of paracetamol from aqueous solution," *International Journal of Environmental Analytical Chemistry*, pp. 1–12, 2021.

[30] A. M. Alswieleh, H. Y. Albahar, A. M. Alfawaz et al., "Evaluation of the adsorption efficiency of glycine-, iminodiacetic acid-, and amino propyl-functionalized silica nanoparticles for the removal of potentially toxic elements from contaminated water solution," *Journal of Nanomaterials*, vol. 2021, Article ID 6664252, 12 pages, 2021.

[31] A. M. Alswieleh, M. M. Alshahrani, K. E. Alzahrani et al., "Surface modification of pH-responsive poly (2-(tert-butylamino) ethyl methacrylate) brushes grafted on mesoporous silica nanoparticles," *Designed Monomers and Polymers*, vol. 22, no. 1, pp. 226–235, 2019.

[32] A. M. Alswieleh, A. M. Beagan, B. M. Alsheheri, K. M. Alotaibi, M. D. Alharthi, and M. S. Almeataq, "Hybrid mesoporous silica nanoparticles grafted with 2-(tert-butylamino) ethyl methacrylate-b-poly (ethylene glycol) methyl ether methacrylate diblock brushes as drug nanocarrier," *Molecules*, vol. 25, no. 1, p. 195, 2020.

[33] C. Samart, S. Karnjanakom, C. Chaiya, P. Reubroycharoen, R. Sawangkeaw, and M. Charoenpanich, "Statistical optimization of biodiesel production from para rubber seed oil by SO_3H-MCM-41 catalyst," *Arabian Journal of Chemistry*, vol. 12, no. 8, pp. 2028–2036, 2019.

[34] K. M. Alotaibi, A. A. Almethen, A. M. Beagan et al., "Quaternization of poly (2-diethyl aminoethyl methacrylate) brush-grafted magnetic mesoporous nanoparticles using 2-Iodoethanol for removing anionic dyes," *Applied Sciences*, vol. 11, no. 21, p. 10451, 2021.

[35] K. M. Alotaibi, "Mesoporous silica nanoparticles modified with stimuli-responsive polymer brush as an efficient adsorbent for chlorophenoxy herbicides removal from contaminated water," *International Journal of Environmental Analytical Chemistry*, pp. 1–14, 2021.

[36] L. Hu, Z. Yang, Y. Wang et al., "Facile preparation of water-soluble hyperbranched polyamine functionalized multiwalled carbon nanotubes for high-efficiency organic dye removal from aqueous solution," *Scientific Reports*, vol. 7, no. 1, pp. 1–13, 2017.

[37] S. Ge, W. Geng, X. He et al., "Effect of framework structure, pore size and surface modification on the adsorption performance of methylene blue and Cu^{2+} in mesoporous silica," *Colloids and Surfaces A: Physicochemical and Engineering Aspects*, vol. 539, pp. 154–162, 2018.

[38] A. Ebadi and A. A. Rafati, "Preparation of silica mesoporous nanoparticles functionalized with β -cyclodextrin and its application for methylene blue removal," *Journal of Molecular Liquids*, vol. 209, pp. 239–245, 2015.

[39] Z. Jiaqi, D. Yimin, L. Danyang, W. Shengyun, Z. Liling, and Z. Yi, "Synthesis of carboxyl-functionalized magnetic nanoparticle for the removal of methylene blue," *Colloids and Surfaces A: Physicochemical and Engineering Aspects*, vol. 572, pp. 58–66, 2019.

[40] Y. Li, Y. Zhou, W. Nie, L. Song, and P. Chen, "Highly efficient methylene blue dyes removal from aqueous systems by chitosan coated magnetic mesoporous silica nanoparticles," *Journal of Porous Materials*, vol. 22, no. 5, pp. 1383–1392, 2015.